A Process Simulator for the Prediction and Optimization of the Operation of the Fuel Cycle of a Fusion Power Plant

Zur Erlangung des akademischen Grades eines

DOKTORS DER INGENIEURWISSENSCHAFTEN (DR.-ING.)

von der KIT-Fakultät für Chemieingenieurwesen und Verfahrenstechnik des Karlsruher Instituts für Technologie (KIT)
genehmigte

DISSERTATION

Von

M.Sc. Jonas Caspar Schwenzer

Aus Karlsruhe

Tag der mündlichen Prüfung: 13.09.2024

Erstgutachter: Prof. Dr.-Ing. Matthias Kind
Zweitgutachter: Prof. Dr. Rudolf Neu

Kurzfassung

Zukünftige Fusionskraftwerke erfordern den Betrieb mit einem geschlossenen Deuterium-Tritium Brennstoffkreislauf um ihren Betrieb aufrechtzuerhalten und radioaktives Tritium sicher einzuschließen. Im Rahmen eines solchen Kraftwerks erfüllt der Brennstoffkreislauf hierbei vier grundlegende Funktionen, welche seine Randbedingungen bilden. Zunächst sind seine Systeme dafür verantwortlich Brennstoff in der richtigen Zusammensetzung und Menge in die Brennkammer zu dosieren und das entstehende Abgas zu prozessieren. Dies erfordert als zweite Funktion auch den Erhalt des richtigen Isotopenverhältnisses von Deuterium zu Tritium sowie ein Gegenwirken etwaiger Kontamination durch Protium. Diese Funktionen, welche unmittelbar der Brennkammer zugeordnet sind und das Deuterium- Tritium Gemisch prozessieren bilden den inneren Brennstoffkreislauf. Darüber hinaus muss der Brennstoffkreislauf auch in der Lage sein, im Reaktor erbrütetes Tritium entgegenzunehmen und aufzubereiten, um es der Brennkammer zuführen zu können. Als letzte Funktion ist der Brennstoffkreislauf auch für die Prozessierung von Tritium verantwortlich, das bei der Detritierung von Kühlmedium und Gebäudevolumina anfällt. Diese beiden Funktionen, welche lediglich Tritium, jedoch kein Deuterium verarbeiten, bilden den äußeren Brennstoffkreislauf.

Der Brennstoffkreislauf des in Entwicklung befindlichen Europäischen Demonstrationsreaktors (EU-DEMO) implementiert diese Funktionen in einer dreigliedrigen Architektur. Beide Funktionen des inneren Brennstoffkreislaufs werden in eigenständigen Prozesspfaden umgesetzt, wohingegen die nötigen Prozessschritte für Funktionen des äußeren Brennstoffkreislaufs in kombinierten Systemen erfüllt werden. Der gepulste Reaktorbetrieb eines Tokamaks, wie für EU-DEMO vorgesehen, propagiert hierbei zwangsläufig auch zum Betrieb dieses Brennstoffkreislaufes, welcher durch abwechselnde Phasen mit hohen und niedrigen Durchsätzen charakterisiert ist. Das Design des Gesamtsystems erfordert hierbei also auch die Berücksichtigung dynamischer Effekte auf Auslegungskriterien, wie etwa die Verfügbarkeit und Zusammensetzung des Brennstoffgemischs oder Tritiumemissionen.

Aus diesem Grund wurde eine dynamische Prozesssimulation des gesamten geschlossenen Brennstoffkreislaufs entwickelt. Die Simulation erreicht ein detailgetreues Abbild des Prozesses, indem sowohl die übergeordnete Architektur des gesamten Kreislaufs als auch die Architektur der einzelnen Systeme auf einer Komponentenbasis wiedergegeben wird. Das dynamische Verhalten der Komponenten wird hierbei durch eine Reihe von Bilanzräumen, für welche dynamische Massen- und Speziesbilanzen formuliert wurden, berücksichtigt. Diese Architektur erfordert fünf einzigartige Trennaufgaben die durch sechs verschiedene Technologien umgesetzt werden. Für jede Kernkomponente dieser Technologien wurde ein dynamisches Modell basierend auf den zugrundeliegenden Stofftransportprozessen implementiert.

Solch eine geschlossene, allumfängliche Simulation eines Brennstoffkreislaufs mit physikalischen Modellen ist bislang in Umfang und Komplexität einzigartig. Um dennoch Glaubwürdigkeit der erzeugten Ergebnisse zu gewährleisten wurde das dynamische Verhalten der Ensembles aus Stofftransportmodellen und weiteren Komponenten eines jeden Systems im Freischnitt anhand ihrer Sprungantwort charakterisiert und auf physikalisches Verhalten überprüft.

Mit der entwickelten Simulation wurde zunächst der Betrieb des EU-DEMO Brennstoffkreislaufs für einen Referenzbetriebspunkt untersucht. Es konnte gezeigt werden, dass der Betriebspunkt alle Anforderungen erfüllt und dynamische Effekte keine Einschränkung in Brennstoffverfügbarkeit und -zusammensetzung verursachen. Ebenso treten nur schwache Schwankungen in der Tritiumkonzentration im Abgas auf und sowohl durchschnittliche als auch maximale Werte übertreffen alle Anforderungen an Emissionsvorgaben.

In einem zweiten Schritt wurde die Stabilität des Betriebspunkts auf Abweichungen in seinen Randbedingungen untersucht. In allen Fällen stellt sich ein neuer pseudostabiler Zustand ein, welcher linear proportional zur Abweichung ist. Es konnten keine selbstverstärkenden Prozesse identifiziert werden. Darüber hinaus konnte gezeigt werden, dass die Architektur effektiv zu einer Entkopplung zwischen innerem und äußerem Brennstoffkreislauf führt und so die Stabilität des Gesamtsystems verstärkt wird.

Abstract

Future fusion power plants will be required to operate with a closed deuterium - tritium fuel cycle to sustain self-sufficient operation and minimize tritium discharges. In view of supporting the operation of a power plant the fuel cycle has to provide four principal functionalities, constituting its boundary conditions. Firstly, the fuel cycle systems are responsible for supplying fuel to the reactor chamber and processing the resulting exhaust. As a second function this also requires to maintain the desired isotope ratio of deuterium and tritium and to counteract the build-up of protium. These functions that are directly associated with the management of the deuterium - tritium fuel form the inner fuel cycle. Furthermore, the fuel cycle has to be able to accept tritium bred in the reactor breeding blanket and make it available for fueling. Lastly, the fuel cycle is also tasked with processing tritium arising from tritium recovery and detritiation of coolants and building volumes. These functions that are associated with the sole processing of tritium form the outer fuel cycle.

The fuel cycle of the European demonstration reactor (EU-DEMO), which is currently in development, implements these functionalities in a three-loop architecture. Both functionalities of the inner fuel cycle are realized using dedicated loops whereas the outer fuel cycle uses combined systems for both. The pulsed operation of the Tokamak reactor foreseen for EU-DEMO directly propagates to the fuel cycle causing alternating phases of high and low throughputs. Thus, the design of the integral system also needs to consider dynamic effects on design criteria and figures of merit such as the fuel availability and composition as well as tritium discharges.

For this reason, a dynamic process simulation of the integral EU-DEMO fuel cycle has been developed. The simulation achieves a detailed replica of the fuel cycle by mirroring its overall system-block architecture as well as the component-based architecture of all individual systems. The dynamic behavior of components is considered by balance areas for which dynamic mass and species balances are specified. This architecture of the fuel cycle relies on five principal types of separations that are implemented using six different technologies. For each, physical models based on the underlying mass transfer processes have been implemented.

Such a closed loop dynamic simulation of a continuous fuel cycle is to date unique in scope and complexity. To nevertheless establish the trustworthiness of generated results, stand-alone versions of the developed system models have been characterized by their step-change response and verified to show physical behavior.

Using the developed simulation, the operation of the EU-DEMO fuel cycle has been investigated for a reference design point. It could be shown that the operation point satisfies all requirements and that dynamic effects do not impact the fuel availability and achievable composition. Furthermore, only minor oscillations in the tritium concentration of the discharged stream were found with both maximum and average values within acceptable limits.

In a second step, the stability of the operation point against deviation in the fuel cycle boundary conditions was characterized. In all investigated cases the fuel cycle converges to a new pseudo-steady state linearly proportional to the deviation and no positive gain factors were found. It could furthermore be shown that the inner and outer fuel cycle are effectively decoupled by the architecture, improving the stability of the overall system.

Table of Contents

Abbreviations and Symbols

Abbreviations

Abbreviation	Description
ALARA	As Low as Reasonably Achievable
ASDEX	Axisymmetric Divertor Experiment
BV	Buffer Vessel
CANDU	Canada Deuterium Uranium
CD	Cryogenic Distillation
CECE	Combined Electrolysis and Catalytic Exchange
CMSB	Cryogenic Molecular Sieve Bed
DEMO	Demonstration Fusion Power Plant
DIII-D	Doublet III
DIR	Direct Internal Recycling
DIRL	Direct Internal Recycling Loop
DTE	Deuterium Tritium Experiment
DTF	Distillate to Feed Ratio
EDS	Exhaust Detritiation System
EPS	Exhaust Processing System
EU-DEMO	European Demonstration Fusion Power Plant
GB	Glovebox
GB-DS	Glovebox Detritiation System
GLC	Gas Liquid Contacting
HCPB	Helium Cooled Pebble Bed
HETP	Height of a Theoretical Plate
HVAC	Heating Ventilation Air Conditioning
INTL	Inner Tritium Plant Loop
IRPR	Isotope Rebalancing and Protium Removal System
ISS	Isotope Separation System
JET	Joint European Torus
KALPUREX	Karlsruhe Liquid Metal Based Pumping Process for Fusion Reactor Exhaust Gases
LDP	Linear Diffusion Pump
LPCE	Liquid Phase Catalytic Exchange
MFP	Metal Foil Pump
NEG	Non Evaporable Getter
NIST	National Institute of Standards and Technology
OUTL	Outer Tritium Plant Loop
PEG	Plasma Enhancement Gas
RMSB	Reactive Molecular Sieve Bed
RR	Reflux Ratio
TBR	Tritium Breeding Ratio
TER	Tritium Extraction Ratio
TFTR	Tokamak Fusion Test Reactor
TSTA	Tritium System Test Assembly
WCLL	Water Cooled Lithium Lead
WDS	Water Detritiation System
WSC	Wet Scrubber Column

Symbols

Symbol	Description	Unit
A	Cross section or surface area	m^2
A_{ij}	Binary interaction parameter	$J.mol^{-1}$
B	Second virial coefficient	$cm^3.mol^{-1}$
c	Concentration	$mol.m^{-3}$
D	Diffusion coefficient	$m^2.s^{-1}$
d	Diameter	m
F	Molar flowrate	$mol.s^{-1}$
f_b	Fuel burn-up fraction	-
f_i^0	Standard fugacity	Pa
$\bar{G}_i^E$	Gibbs free energy of mixing	$J.mol^{-1}$
h	Length domain	m
J	Total angular momentum quantum number	-
j	Molar flux	$mol.s^{-1}m^{-2}$
K	Chemical equilibrium coefficient	-
K_s	Sievert's constant	$mol.m^{-3}Pa^{-0.5}$
k	Mass transfer rate coefficient	$mol.s^{-1}$ or $mol.s^{-1}m^{-3}$
k_c	Carman-Kozeny coefficient	$Pa.s.mol^{-1}m^{-1}$
l	Length	m
m	Mass	kg
$\dot{m}$	Mass flowrate	$kg.s^{-1}$
MW	Molecular weight	$g.mol^{-1}$
N	Molar amount or hold-up	mol
p	Pressure	Pa
Pe	Permeability	$mol.m^{-1}s^{-1}Pa^{-0.5}$
Q	Pressure-volume flow	$Pa.m^3s^{-1}$
q	Heat flux	$W.m^{-2}$
R	Fuel cycle boundary condition dimensionless number	-
R	Universal gas constant	$J.mol^{-1}K^{-1}$
S	Pumping speed	$m^3.s^{-1}$
s	Thickness	m
T	Temperature	K
t	Time	s
V	Volume	m^3
y	Vapor phase molar fraction	-
x	Liquid phase molar fraction	-
z	General molar fraction	-
Greek Letters		
α	Heat transfer coefficient	$W.m^{-2}K^{-1}$
α	Separation factor	-
γ	Activity coefficient	-
ε	Porosity	-
η	Efficiency	-
λ	Vapor to liquid ratio	-
κ	Molecular interaction parameter	-
τ	Residence time	s
φ	Relative humidity	-
Φ	Sink- and source terms	$mol.s^{-1}$
ϕ	Fugacity coefficient	-

Sub- and Superscripts, Modifiers	
$d\blacksquare$	Infinitesimal difference
$N\blacksquare$	At normal conditions
$\Delta\blacksquare$	Macroscopic difference
$\blacksquare^{*}$	In equilibrium
$\blacksquare^{0}$	Boundary or initial value
$\blacksquare^{g}$	Gas phase
$\blacksquare^{l}$	Liquid phase
$\blacksquare^{v}$	Vapor phase
$\blacksquare_{0}$	Reference state
$\blacksquare_{c}$	At critical point
$\blacksquare_{E}$	Tritium extraction
$\blacksquare_{f}$	Tritium fueling
$\blacksquare_{i}$	A species in a mixture
$\blacksquare_{p}$	Property of a particle
$\blacksquare_{R}$	Tritium recovery
$\blacksquare_{t}$	At triple point

1 Introduction

1.1 Fusion Reactor Fuel Cycle Simulator Development – Motivation and Context

Following the industrial revolution, the global per-capita energy demand has drastically increased alongside the total population. This has culminated in more primary energy usage in the last 70 years as in all of previous human history. With both population and individual energy demand still growing rapidly, clean and abundant sources of energy are urgently needed. The requirement to grow and simultaneously decarbonize the global energy market has reinvigorated the pursuit in fusion energy after its inception in the 1950s. In the recent past this has led to the development of a multitude of national and international programs pursuing the development of fusion power plants.

Following a report of the National Academy of Science the United States have formulated a "*Bold Decadal Vision for Commercial Fusion Energy*" at a 2022 White House Summit calling for an energy producing fusion reactor by the end of the decade [1].

In the United Kingdom the development of fusion energy has been adopted as an integral part of "*The ten-point plan for a green industrial revolution*" and in a corresponding whitepaper "*Towards Fusion Energy"* the goal "*For the UK to demonstrate the commercial viability of fusion by building a prototype fusion power plant in the UK that puts energy on the grid*" is defined [2][3].

The People's Republic of China has established a road map calling for "*Establishing a commercial fusion power plant*" [4]. Similarly, Japan and Korea are actively pursuing demonstration power plants [5][6].

In the European Union fusion research and development activities are housed in the framework of the "*European Research Roadmap to the Realization of Fusion Energy*", working against the "*the ultimate goal of achieving electricity from fusion energy*" [7].

Above programs all center around the construction of a prototype demonstration reactor, hereafter referred to as DEMO reactor, aiming to validate key physics and engineering principles and to provide the final stepping stone for a wider commercialization of fusion energy.

One of the principal challenges of any fusion power plant is to maintain suitable conditions, via so called confinement, at which nuclear fusion can occur in a controlled manner to allow the extraction of energy and ultimately the operation of a power plant. The EU, CN, JA, K, and UK programs are all based on magnetic confinement fusion while in the US also alternative concepts are pursued. To date, the most advanced magnetic confinement concept is that of the Tokamak, historically achieving conditions closest to those required for power plant applications. In a Tokamak fusion reactions are sustained in a torus shaped plasma confined in a magnetic field with closed flux surfaces. If the kinetic energy of the confined particles is sufficiently high fusion reactions occur. For the purpose of a fusion power plant the plasma also needs to achieve a burning

state, meaning that products of the fusion reactions must provide kinetic energy to the plasma, minimizing the amount of external heating required and providing a net-energy gain.

As DEMO reactors are commonly understood to be the last step towards commercial power plants they need to feature all relevant elements at scale and aim to demonstrate electricity production while employing only technologies that are viable for the use in future fusion power plants. In many ways, a fusion power plant will not differ from conventional large-scale power plants as the way of electricity generation, by exploiting a heat source that is then used to drive a power cycle, remains unaltered (Figure 1.1).

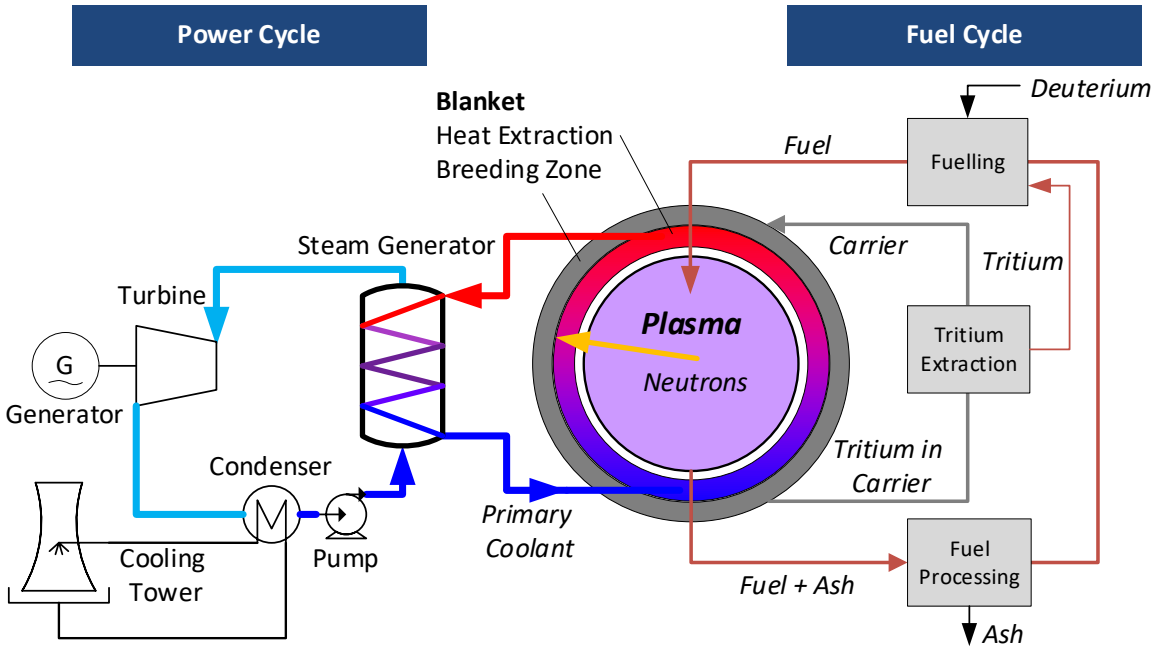

Figure 1-1.1: Schematic flow diagram of a tritium self-sufficient deuterium-tritium fusion power plant. The burning plasma is enveloped by a blanket utilizing the generated neutrons for heat extraction and tritium breeding. The fusion reaction is sustained by continuously fueling the plasma and exhausting unburned fuel and helium ash. The ash is removed from the exhaust and contained fuel recycled. Burned tritium is made up with tritium extracted from the blankets, burned deuterium is made up from external supply.

In a fusion power plant, the heat source is the sustained fusion reaction of which the most favorable, and thus pursued for DEMOs, is that of the hydrogen isotopes deuterium (^{2}H, or D) – tritium (^{3}H, or T) (equation 1) offering the highest reactivity of all viable fusion reactions in the lowest range of kinetic energies between 10^1 and 10^2 keV [8].

$$^3_1\mathrm{H} + {}^2_1\mathrm{H} \rightarrow {}^4_2\mathrm{He} + {}^1_0\mathrm{n} + 17.58 MeV \qquad (1.1)$$

The use of tritium in a fusion power plant has unique consequences for its design. Tritium is not naturally abundant as it undergoes β-decay with a half-live of 4500 ± 8 days (about 12.3 years) [9]. Therefore, only trace quantities are present in the earth's upper atmosphere and bodies of water as a result of cosmic radiation, estimated to a total inventory of 1.8 kg [10].

With equation 1.1 it immediately follows that natural abundancies are vastly insufficient to supply even one deuterium-tritium fusion power plant as every gigawatt of fusion power corresponds to

the consumption of 56 kg of tritium per year. Consequently, any viable fusion power plant needs to operate tritium self-sufficient by breeding tritium on site. The most commonly pursued tritium breeding mechanism are the (n,α) reactions of the natural abundant lithium isotopes ^{6}Li and ^{7}Li:

$$^{1}_{0}\mathrm{n} + {}^{7}_{3}\mathrm{Li} \rightarrow {}^{4}_{2}\mathrm{He} + {}^{3}_{1}\mathrm{H} + {}^{1}_{0}\mathrm{n} - 2.47\ MeV, \quad (1.2.a)$$

$$^{1}_{0}\mathrm{n} + {}^{6}_{3}\mathrm{Li} \rightarrow {}^{4}_{2}\mathrm{He} + {}^{3}_{1}\mathrm{H} + 4.78\ MeV. \quad (1.2.b)$$

While the ratio of neutrons generated by the fusion reaction and those consumed by the breeding reaction is unity – meaning that in theory one triton can be produced per triton consumed – additional neutron multiplication based on (n,2n) reactions is required for practical reasons as not every fusion neutron can be made to interact with a lithium atom. Both mechanisms ultimately rely on interactions with neutrons generated by fusion reactions in the plasma and good areal coverage around the plasma chamber is required. The plasma is therefore surrounded by an actively cooled blanket structure, allowing heat extraction as well as containing breeder materials and neutron multipliers.

A second requirement in order to maintain a burning plasma is in keeping its purity. As the fusion reaction continuously produces helium, which can be considered the fusion "ash", the accumulation thereof in the burning plasma has to be avoided in order to limit its dilution effects. This necessitates to continuously provide a fuel throughput to the plasma, exhausting a stream containing the helium ash and unburned fuel and introducing an equivalent amount of purified fuel. Due to the radioactivity and scarcity of contained tritium the unburnt fuel must not be discharged, rather it has to be reprocessed in a closed loop.

These tritium processing functionalities which, are required to operate the power plant, form its fuel cycle. This fuel cycle houses all systems needed for these tasks and as such forms an intricate processing plant in itself, integrating a multitude of different technologies into a continuous operating cycle supporting the operation of the plasma.

The adaption of a Tokamak architecture for a fusion power plant bears additional challenges for the fuel cycle. Tokamaks are operated in a pulsed mode of plasma discharges intermitted by dwell phases without plasma operation, during which the plasma chamber is evacuated in order to reset the machine into a defined initial state to restart a new discharge. This alternation between phases requiring active fuel throughput and phases with only evacuation of the plasma chamber leads to inherent transients in the processing systems of the fuel cycle. This directly affects the design and operation of the fuel cycle where a multitude of processing technologies have to interlink to form a continuous, closed system.

1.2 Objectives of this Work

In order to efficiently design and develop an optimized fuel cycle a clear understanding of its dynamic performance is a strict necessity. More precisely, a given fuel cycle design point synthesized from individual, and often steady state designs of individual processing systems, has to be validated with regards to its integral dynamic behavior. Furthermore, sensitivities towards deviation in its boundary conditions and performance of employed systems need to be characterized.

To address these issues, process modelling and simulation are an essential tool that can be employed cost effectively in early design stages. Any fuel cycle will feature a wide array of novel and diverse technologies purpose built for tritium processing while also having to accommodate species and molecules not readily available in common property databases. These unique requirements far exceed the scope of commercial process simulation suites and have prompted the primary objective of this work, the development of a dedicated process simulation tool aimed at predicting and optimizing the dynamic operation of a fusion fuel cycle. To accomplish this overarching goal it is broken down into a series of individual aspects that need to be mastered successfully:

- The context of the work requires a clear-cut understanding of the role of the fuel cycle in a fusion power plant. It is necessary to identify its boundary conditions as well as figures of merit and design drivers used in optimization to make well founded judgments on the performance of a fuel cycle design.
- The use of flow-sheet based modelling requires in-depth knowledge of the functional system block architecture and employed technologies in each system in order to allow their accurate representation.
- Identification of a steady state reference design point, optimally tailored to the fuel cycle boundary conditions and expected technology performance, is required to provide a basis of comparison for the dynamic operation.
- For each of the employed technologies state-of the art mass transfer models suitable for the present operation conditions need to be identified.
- The uses of physics based mass transfer models requires computational efficient formulation of thermodynamic property and equilibrium data for all relevant species and equilibrium systems present in the fuel cycle technologies.

Accomplishing all individual sub-goals enables the synthesis of dynamic models of the fuel cycle systems and of the holistic fuel cycle. The structured analysis of its dynamic behavior and performance then requires:

- Assessing the dynamic characteristic and performance of individual fuel cycle systems, demonstrating that they are able to achieve the specifications of the reference design point.
- Assessing the dynamic behavior of the integrated architecture in terms of the fuel cycles figures of merit, also demonstrating that the integrated operation of systems does not caused deviations in performance or unexpected feedback loops.
- Characterizing the robustness of the integrated fuel cycle design against deviations in its boundary conditions, demonstrating that a sufficiently large operational space is available to effectively support the operation of the fusion power plant.

This sequence is reflected in the structure of the work, following the necessary steps to achieve the individual and overarching goals.

1.3 Structure of this Work

Chapter 2 derives the principal functionalities of a DT fusion power plant fuel cycle and a set of universal metrics to quantify the tritium processing loads imposed on the fuel cycle by its plant boundary conditions. Following this, the applying constraints in order to achieve all required functionalities in a safe and economical manner are outlined in Chapter 2.2.

This understanding of the functionalities and constraints of a generic fuel cycle is then applied to the EU-DEMO fuel cycle in Chapter 3, breaking it down into its individual processing systems and interfaces. From the plant interfaces and global requirements the architecture of the EU-DEMO fuel cycle is developed, introducing also the technology selection and internal architecture of each system. By imposing a set of principal design targets for the performance of each systems onto this architecture, a reference design point of steady state tritium throughputs for the full fuel cycle is derived in Chapter 3.2. This design point then serves as a benchmark for later dynamic assessments.

Chapter 4 then develops the technical foundation for the simulation tool. First, the requirements for the tool in order to be able to simulate a continuous deuterium-tritium fuel cycle are derived in Chapter 4.1 and modelling techniques used to achieve these requirements are outlined. The physical foundation of employed property and equilibrium data is then described in Chapter 4.2. Chapter 4.3 then introduces the technology-specific mass transfer models that are employed as well as a collection of auxiliary component- and general purpose models needed to complete the model of the integral fuel cycle.

Chapter 5 then details the transfer of modelling techniques to the systems of the EU-DEMO fuel cycle and the construction of the process simulation tool. Chapter 5.1 discusses how the mathematical models are implemented into a simulation environment and computed. In Chapter 5.2 the models for individual fuel cycle systems, as constructed from technology and supplementary models, are introduced and their stand-alone behavior is characterized.

Chapter 6 focuses on the application of the developed tool to the holistic EU-DEMO fuel cycle, analyzing its integrated behavior first for the reference configuration and operation point and then testing it against deviations in its boundary conditions. In a final step, analyses investigating scenarios with deviating performance in central fuel cycle systems are performed.

2 The Fuel Cycle of a DT Fusion Power Plant

In the overall scope of a fusion power plant the fuel cycle is a service unit to provide all processing functionalities required to fuel and exhaust the machine as well as to condition and handle the fuel constituents. Simultaneously, the design of the fuel cycle has to match the global constraints of an economic power plant, such as safety and minimizing costs. Both, functionalities and constraints, thus mark the high-level requirements for the fuel cycle design and build the foundation to derive its architecture.

2.1 Boundary Conditions from Plant Operation

As tritium is the scarcest and most hazardous component in the fuel cycle, its overall design pivots around the unique processing requirements of tritium. In a DEMO reactor or fusion power plant, four principal tritium processing requirements can be identified, marking the fuel cycle boundary conditions.

First: The fuel cycle has to provide all necessary fueling contributions to the plasma and extract unburnt fuel and ash from the torus from which as much unused fuel as possible has to be recycled.

The amount of burned-up tritium is directly proportional to the achieved fusion power and the rate of fusion reactions occurring which defines the lower theoretical fueling limit. However, significantly more fuel has to be injected into the plasma in order to also keep the helium ash concentration in the plasma below a set threshold to limit its dilution effect. This is achieved by purposefully exhausting a larger than theoretically necessary fraction of the plasma's particles continuously. In order to maintain also a constant particle density, the exhausted matter has to be compensated by fueling. The ratio of total amount of fuel introduced into the plasma to the amount consumed in fusion reactions is referred to as the burn-up fraction f_b. Historically, no significant burn-up fractions have been achieved as no experimental machine using tritium, such as the Tokamak Fusion Test Reactor (TFTR) or Joint European Torus (JET), has achieved a steady state burning plasma with continuous plasma fueling. For the first experimental demonstration of a burning plasma in ITER, plasma burn-up fractions ranging from 0.9% to 1.9% are predicted [11].

Furthermore, not all fuel injected into the plasma chamber reaches the burning plasma core and considerable transport losses occur. Core-fueling by injecting pellets of frozen hydrogen fuel at high speeds is considered the most efficient way and has been adopted by all DEMO programs. The technology has been demonstrated with deuterium pellets at a number of experimental tokamaks such as ASDEX Upgrade [12], JET [13], and DIII-D [14]. From the production of the pellet to its final destination in the plasma core losses occur as evaporation and ablation of pellet mass on the flight path or at the boundary of the plasma (the so-called scrape off layer). Experimental investigations at machines operating at high plasma densities have shown pellet fueling efficiencies ranging from 20% to 60%, but extrapolation to a fusion power plant plasma scenario is challenging due to larger scales in almost all parameters such

as the spatial plasma dimensions, ion and electron temperatures, and plasma density [15][16].

In addition, fuel or individual fuel constituents are purposefully injected into other areas of the plasma chamber for control of the plasma stability or cooling of components. The total effective fueling efficiency η_f is therefore defined as the ratio of all fueling contributions to the machine versus those reaching the plasma core.

Combining above metrics directly establishes a link between the total fuel throughput of the plasma chamber with the fusion power of the machine, commonly referred to as the fuel conversion rate or tritium conversion rate R_F defined as

$$R_\mathrm{F} = \eta_\mathrm{f} \cdot f_\mathrm{b} \,. \tag{2.1}$$

Maintaining one gigawatt of fusion power requires $3.55{\cdot}10^{20}$ D-T fusion reactions per second. Assuming in first approximation a burn-up fraction of $f_\mathrm{b} = 1\%$ and a fueling efficiency of $\eta_\mathrm{f} = 50\%$ for a total $R_\mathrm{F} = 0.5\%$, an integral machine gas throughput of $F_\mathrm{fuel} = 0.118$ mol DT per second is required which corresponds to 0.36 $\mathrm{g.s^{-1}}$ of tritium and 0.24 $\mathrm{g.s^{-1}}$ of deuterium. Correspondingly, a helium molar fraction in the exhaust gas of 0.5% is obtained if only DT is fueled.

Second: The fuel cycle has to maintain the correct isotopic composition of the fuel.

The fusion reaction occurs in equal stoichiometric parts of its constituents deuterium and tritium and thus, the reactivity is a function of their density ratio in the plasma. While the exact relationship depends on machine parameters and particle transport processes during fueling and in the plasma core, it follows that a pre-determined D/T isotope ratio has to be maintained in the plasma core for optimization of the achieved fusion power. This requirement directly propagates to the provided fuel, albeit possibly with a different isotope ratio than that intended in the core if strong isotope effects occur.

Additionally, deuterium and tritium may not be the only hydrogen constituents in the fuel and exhaust gas stream. Protium (^{1}H) is naturally abundant and omnipresent dissolved in metals, leading to outgassing of protium from surfaces in vacuum. The plasma chamber of a Tokamak is characterised by large metal surfaces at vacuum conditions and at elevated temperatures during operation. Hence, a protium background in the circulated fuel is always present and unavoidable and also expected to change over the lifetime of the machine. Up to a certain limit the presence of protium in the fuel and plasma core does not pose a challenge for the operation of the plasma, it simply contributes to the dilution effect of helium ash and other species. It must, however, still be actively controlled to prevent build-up with time as it does not undergo fusion reactions.

In order to keep the desired isotope ratio and isotopic purity of the fuel at steady state, the same absolute amount of imbalance ΔF_i of any given isotope (i = H, D, T) from the circulating fuel stream F_fuel has to be removed. To this purpose, a fraction R_i of the circulating fuel has to be continuously removed and processed to re-establish the desired composition. If assuming an ideal processing efficiency this fraction is obtained from a species balance around the circulated fuel as

$$R_{\mathrm{i}} = \max\left(\frac{\Delta F_{\mathrm{i}}}{z_{\mathrm{i}} F_{\mathrm{fuel}} + \Delta F_{\mathrm{i}}}\right) \ (\mathrm{i} = \mathrm{H}, \mathrm{D}, \mathrm{T}). \tag{2.2}$$

Here z_{i} is the desired or maximum tolerable atomic fraction of one of its isotopic constituents.

This metric can be applied to all isotopic constituents of the fuel and the total amount of the machine fuel throughput that has to be processed is then given by the largest imbalance. Source terms for deuterium and tritium are inherently negative due to burn-up, meaning that some imbalance up to that limit can be tolerated and corrected for by the mandatory fuel make-up if pure or enriched constituents are available. Protium, on the other hand, is not burned while having a positive source term and, thus, needs to be controlled by stripping it from the processed stream.

Third: The fuel cycle has to process and incorporate tritium extracted from breeding blankets.

As the breeding blankets are located close to the plasma and inside the Tokamak, a tritium carrier stream is used to transport tritium out of the tokamak into a tritium extraction system, sending the resulting stream to the fuel cycle for further processing. While the overall composition and flowrate of the resulting streams is dependent on the tritium extraction technology, the overall rate at which tritium that has to be extracted F_{ext} is directly governed by the condition of tritium self-sufficiency. In theory, a ratio of extracted to burned tritium F_{burn} of unity is required to maintain the fuel balance.

$$R_{\mathrm{E}} = \frac{F_{\mathrm{ext}}}{F_{\mathrm{burn}}}. \tag{2.3}$$

This, however, does not guarantee true self-sufficiency, as tritium is also lost to decay or sequestration in structural materials and waste. For economical purposes the tritium extraction ratio thus has to exceed unity by a large enough margin to compensate for these effects, commonly excess tritium production in the range of 5% is considered to be required [17].

Fourth: The fuel cycle has to process all tritium that is recovered from secondary enclosures or media.

As a hydrogen isotope, tritium is highly mobile in its atomic form and able to permeate through structural materials. Breeding blankets offer favorable conditions due to elevated temperatures and large surface areas needed to facilitate efficient heat transfer, while at the same time harboring high tritium concentrations. Tritium is therefore prone to migrate from the breeding zone of the blanket into the coolant with which it is transported outside of the Tokamak, where it can potentially migrate further into secondary enclosures and building rooms. Similarly, the tritium extraction loop offers a pathway out of the tokamak from which tritium permeation into secondary enclosures can occur.

From a tritium balance perspective, all tritium that is lost from the primary fuel cycle has to be recovered. Ultimately this has to be achieved during decommissioning, or ideally at least partially during operation of the machine with a recovery rate F_{rec}. Active tritium recovery

is especially important to mitigate tritium build-up in the primary coolant, plasma facing components, and secondary enclosures, maintaining an equilibrium between the tritium loss rate and recovery rate.

If relating the rate at which tritium that can be recovered to the burn-up rate, equivalently as for the tritium extraction ratio, then the total effective Tritium Breeding Ratio (TBR) of the plant is given as the sum of directly extracted tritium and recovered tritium so that $TBR_{\mathrm{eff}} = R_{\mathrm{E}} + R_{\mathrm{R}}$, where

$$R_{\mathrm{R}} = \frac{F_{\mathrm{rec}}}{F_{\mathrm{burn}}}. \tag{2.4}$$

The layout and architecture of a fuel cycle providing these functionalities is a direct consequence of the requirement for processing tritium in different amounts and from different origins as illustrated in Figure 2-1.1. Fuel streams that interface the torus directly (fuel recycling and fuel rebalancing) mark the **inner fuel cycle**, whereas streams carrying tritium that is extracted from breeding and recovered from secondary volumes marks the **outer fuel cycle**. By using the developed metrics of equations 2.1 -2.4, the total tritium throughput in each stream is expressed directly in relation to the burn-up rate as a measure of the plant's fusion power.

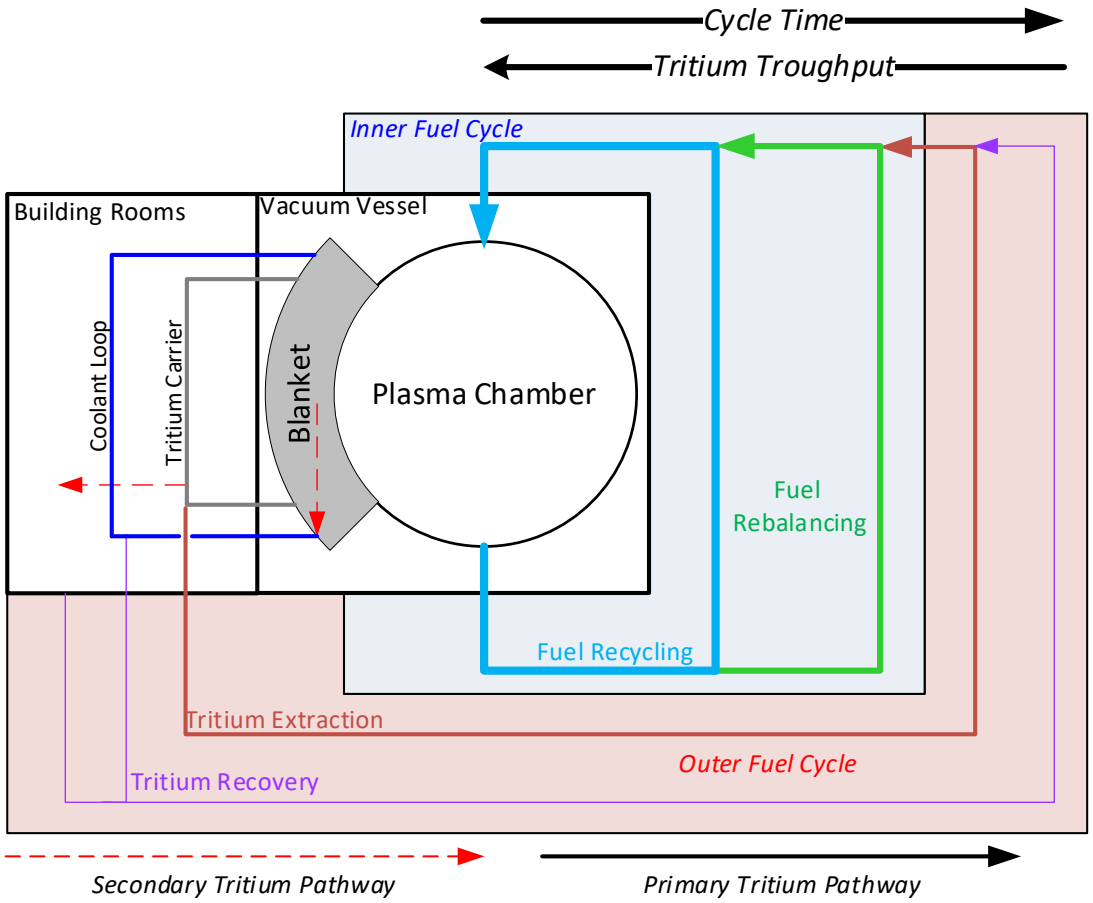

Figure 2-1.1: Principle layout of the tritium fuel cycle (colored boxes) and its interfaces (white boxes) of a fusion power plant. Deuterium-tritium fuel is circulated in the inner fuel cycle (cyan and green) and tritium extracted from breeding blankets and recovered from secondary volumes is processed in the outer fuel cycle (red and purple).

2.2 Design Drivers and Figures of Merit

As with any large scale process, a fuel cycle design formulated to achieve the outlined functionalities needs to be quantitatively assessed to allow its comparison to alternative concepts. The first and foremost figures of merit are those measuring the compliance with the plasma requirements in providing fuel in the specified composition at the requested time. Details thereof are pursuant to the specific fueling requirements corresponding to the employed plasma scenario and technology selections in each machine. This is discussed in greater detail for the EU-DEMO fuel cycle in Chapter 3.

Next to the achievement of its primary function, the fuel cycle design faces further requirements in the context of the integral fusion power plant. These are in many ways identical to any conventional power plant, nuclear or other, with safety and economic viability being the two most prevalent. Under these considerations the following requirements and constraints have to be applied in the design of a fuel cycle for a DT fusion power plant:

First: Minimization of hazardous, especially radiological, inventories.

From a safety perspective the control and minimization of hazardous mobilizable inventories is the most effective tool to assure the compliance with stringent regulatory criteria for the exposure of the general public in case of a release of radionuclides to the environment as a result of accidents. For radiological exposure, this commonly encompasses adherence to the absence of evacuation or shelter measures in case of worst case accidents as defined in regulatory frameworks. For example, in Germany dose limits of 100 mSv and 10 mSv, respectively must not be exceeded over a period of seven days following an emergency event [18].

In a fuel cycle, radiological inventories are dominated by the presence of tritium. Any processing equipment such as piping, vessels, and tanks containing tritium or tritiated species is characterized by a tritium inventory proportional to its volume and tritium concentration therein. As the upkeep of a defined tritium concentration in the fuel is the fuel cycle's primary function, these inventories are necessary and unavoidable. Such tritium inventories stemming from the fulfillment of a primary function of the fuel cycle are referred to as operational tritium inventories and their quantity is a fundamental figure of merit for the design of the fuel cycle and systems, bearing minimization wherever possible. These inventories may also be evaluated as a product of a system's residence time and tritium throughputs. The main avenues to minimize operational tritium inventories are therefore by means of reducing the overall tritium throughput, volumes, and concentrations where permissible while still fulfilling all necessary functions.

Tritium inventories can also accumulate as a result of adsorption onto or absorption into structural materials in contact with tritium. While these sequestered tritium inventories are often not as mobile in comparison to operational inventories their minimization is still beneficial under safety and economical aspects, as any sequestered tritium cannot contribute to the fueling of the machine and ultimately has to be recovered in the decommissioning phase. The build-up of such inventories can be limited or mitigated by operating equipment and piping at conditions unfavorable for permeation and absorption, typically at ambient temperatures or below, and limiting tritium partial pressures wherever possible.

Second: Minimization of chronic releases of hazardous, especially radioactive, species to the environment.

Next to releases of hazardous or radioactive substances to the environment as a consequence of accidents, their chronic releases via any stream that is discharged from the site also occurs and is to be strictly limited. Even though all primary tritium processing functionalities are operated in closed loops some secondary streams still have to be discharged from the plant and the fuel cycle. Characterizing and minimizing these discharges according to the "As Low as Reasonably Achievable (ALARA)" principle is a design focus of the fuel cycle and as such projected chronic emissions are a key figure of merit.

Third: Minimization of operational and investment cost.

While the fulfillment of the fuel cycles primary function and adherence to safety requirements are vital for the licensability of the plant, economic viability can still hamper the commercialization of a fusion power plant design. Detailed cost assessments can typically only be done in an advanced design state, but the impact of potentially prohibitive costs should nevertheless be considered as early as possible. This applies especially to operational costs where a significant contribution is the energy consumption of the processing systems employed in the fuel cycle. Any electric power consumed by the fuel cycle directly impacts the net electricity output of the plant and as such has to be accounted for. For this reason, identifying and characterizing clients with largest power consumption provides an additional metric in judging the merits of a fuel cycle design.

In summary, any given fuel cycle is characterized by metrics of how well it can achieve its intended purpose and at what cost in terms of tritium inventory, chronic releases, and power consumption. Predicting these cornerstones presents key information in the design process which must work to find an optimum of all aspects combined. While these concepts are applicable to any generic fuel cycle, be it demonstration reactor or full fletched fusion power plant, the detailed assessment thereof is however closely linked to the technical implementation of the architecture and processing systems unique to each machine. The remainder of this work therefore focuses exlusively on the fuel cycle of the European demonstration power plant.

3 Design of the EU DEMO Fuel Cycle

The European Demonstration Power Plant (hereafter EU-DEMO) is a fusion power plant in development, aimed at demonstrating electrical power output between 300 and 500 MW from a fusion reactor. As such it will feature a full scale fuel cycle. In 2021 the project has completed the pre-concept design phase including the first consolidated formulation of a fuel cycle design point co-developed by the author of the present monograph. A summary has been has been published in 2022 [19]. Since then the design and development activities have continued and as such no detailed and recent description of the EU-DEMO fuel cycle is available in literature. As a good understanding of the interfaces, architecture, and technologies is fundamental in order to simulate and analyze them, these aspects are developed in this chapter.

The first steps in designing a processing plant are to attain an understanding of the requirements and constraints and the subsequent quantification. Furthermore, it is also useful to be informed early on by comparable systems already in operation. However, as of now no tritium processing facilities on the same scale as for the EU-DEMO fuel cycle, with throughputs of the order of 10 kg tritium per day exist. The first fusion machine to operate with tritium was the Tokamak Fusion Test Reactor (TFTR) of the Princeton Plasma Physics Laboratory, with an overall on-site tritium inventory limit of 5 g [20]. It operated without a closed fuel cycle, rather receiving an external tritium supply and shipping tritiated water off-site for tritium recovery and processing. The TFTR exhaust was processed at the Tritium System Test Assembly (TSTA) in Los Alamos, marking the first non-laboratory scale tritium processing facility, handling up to 1000 g of tritium per day at a maximum site inventory of 130 g [21], but, without a direct interface to a fusion machine. Similarly, another non-fusion tritium processing system is that of the Karlsruhe Tritium Neutrino Experiment, processing 40 g of tritium per day in its inner loop [22]. To date the only fully closed and still operable fuel cycle and tritium processing plant of a fusion machine is the Active Gas Handling system of the Joint European Torus (JET), which processed up to 20 g of Tritium at a time in batch mode during its first full scale tritium campaign DTE1 [23].

While none of these systems is comparable in scale and functionality to the projected fuel cycle of a fusion power plant, they have established a wide knowledge and experience base from which best practices for technology selections, design, and modelling can be derived. One system that is not yet built and operated, but progressed further in its design is the fuel cycle of ITER [24]. The plasma fueling systems are designed to deliver a fueling rate in the same order of magnitude as for DEMO which amounts to 22 $kg.day^{-1}$ at highest throughput, and supporting the pulsed burn/dwell operation typical for Tokamaks, even if at drastically shorter pulse durations and longer dwell phases [25].

These tritium processing systems are all part of experimental facilities and as such designed and operated with a focus on versatility and flexibility, with the fuel cycle required to support a wide window of experimental conditions. In contrast, any fuel cycle of a fusion power plant will largely be needed to support a much narrower operational envelop of the reactor, and thus can itself be designed and optimized closely tailored to the reactor operation.

3.1 Architecture and System Block Requirements

The EU-DEMO fuel cycle can be conceived as a processing plant supporting the operation of the reactor. It takes in tritium carrying educt streams, transforming them into the desired products while adhering to the applying constraints. The principal educt streams arising from plant operation are:

1) The torus exhaust containing unburnt fuel, helium ash, any admixed gases, and impurities.
2) A stream containing the extracted tritium from tritium breeding.
3) A stream containing recovered tritium from coolant purification.
4) One or more streams of air or inert gases sent for detritiation.

These educts are received from interfaces of other plant systems and two products then have to be delivered by the fuel cycle to maintain operation of the plant:

1) A mixture of the hydrogen isotopes deuterium and tritium usable for fueling the reactor or storage.
2) Detritiated air and gases that can be safely discharged from the fuel cycle.

The processing operations required to accommodate the interfacing streams and produce the desired products, while at the same time aiming to minimize tritium inventories, directly lead to an architecture of the fuel cycle based on Direct Internal Recycling (DIR). This concept has been pioneered for the EU-DEMO fuel cycle [26] and calls for the removal of a large fraction of the exhausted unburnt hydrogens close to the torus before performing any other processing operations. Thereby, a reduction in the total throughput, size, and inventory of downstream systems is achieved. In combination with systems for fueling and composition control this marks the **Direct Internal Recycling Loop** (DIRL) closest to the torus. Further processing of the remaining exhaust and isotopic rebalancing of a fraction of the torus throughput are achieved in the **Inner Tritium Plant Loop** (INTL). These two loops only process constituents of the fuel, interfacing directly to the torus and as such make up the inner fuel cycle. The immediate handling of the machine gas throughput is then supplemented by the **Outer Tritium Plant Loop** (OUTL), housing all system required for handling of interface streams stemming from tritium extraction and recovery as well as discharges from the inner fuel cycle.

This architecture represents a trade-off between directly mirroring the principal processing functionalities by implementing individual systems and loops for each task, as well as combining similar processing tasks from different functionalities allowing a reduction of the total number of systems. In the inner fuel cycle, where tritium throughputs are highest, purpose built and optimized system designs are employed whereas in the outer fuel cycle, where the total throughputs are highest, systems are used according to the processing functionality they provide and designed to accommodate multiple clients in a wider operational window. Besides direct internal recycling, another trade-mark of this advanced fuel cycle is to only employ fully continuous or semi-continuous technologies in all systems, foregoing the use of any technologies that accumulate large tritium inventories over time (such as cryogenic pumps) and therefore also alleviating the associated batch wise processing of fuel “packets” after regeneration of such a pump. This fully continuous operation aims to allow operation of almost all systems in steady or pseudo steady state if the dynamic loads induced by the burn/dwell cycle of the tokamak can be successfully buffered or dampened. To this objective so called dwell bypass streams are employed maintaining a throughput in systems in cases where the primary load is temporarily not present.

A generalized block diagram of the primary tritium flows and processing blocks of the EU-DEMO fuel cycle is given in Figure 3-1.1. The tokamak is evacuated by the **Fuel Separation and Torus Vacuum** systems, where a fraction of the unburnt hydrogens is directly recycled and both resulting gas streams are compressed to the operating pressure of downstream systems. The remaining exhaust is routed to the **Exhaust Processing** system (EPS), where the remaining hydrogen is recovered. This stream is then routed through the **Isotope Rebalancing and Protium Removal** (IRPR) system performing the necessary isotope separations to keep the fuel balance. The pure hydrogen streams from fuel separation and isotope rebalancing are returned to the **Gas Distribution and Storage** (GDS) system. In this system the fuel mixture is prepared and also topped off with bred tritium and external deuterium to compensate for burn-up. The fuel is then sent to the **Fueling** systems and reinjected into the torus as pellets or gas. This completes the inner fuel cycle. The outer fuel cycle receives all tritium carrying streams from its plant interfaces as well as discharges from the inner fuel cycle. Helium ash and remaining impurities after the Exhaust Processing system are sent to the **Exhaust Detritiation** system (EDS) which also receives air and glove box atmosphere gases containing trace amounts of tritium for detritiation before discharging them from the fuel cycle. Any tritiated water arising in the fuel cycle as well as in the coolant purification systems is sent to the **Water Detritiation** system (WDS) where tritium bound in water is recovered and converted to hydrogen gas. Tritium recovered from water is routed to the **Isotope Separation** system (ISS) in a hydrogen stream where, with hydrogen streams from tritium extraction and conditioning, as well as the waste stream from Isotope Rebalancing and Protium Removal, any tritium is enriched up to fuel quality and sent to the inner fuel cycle.

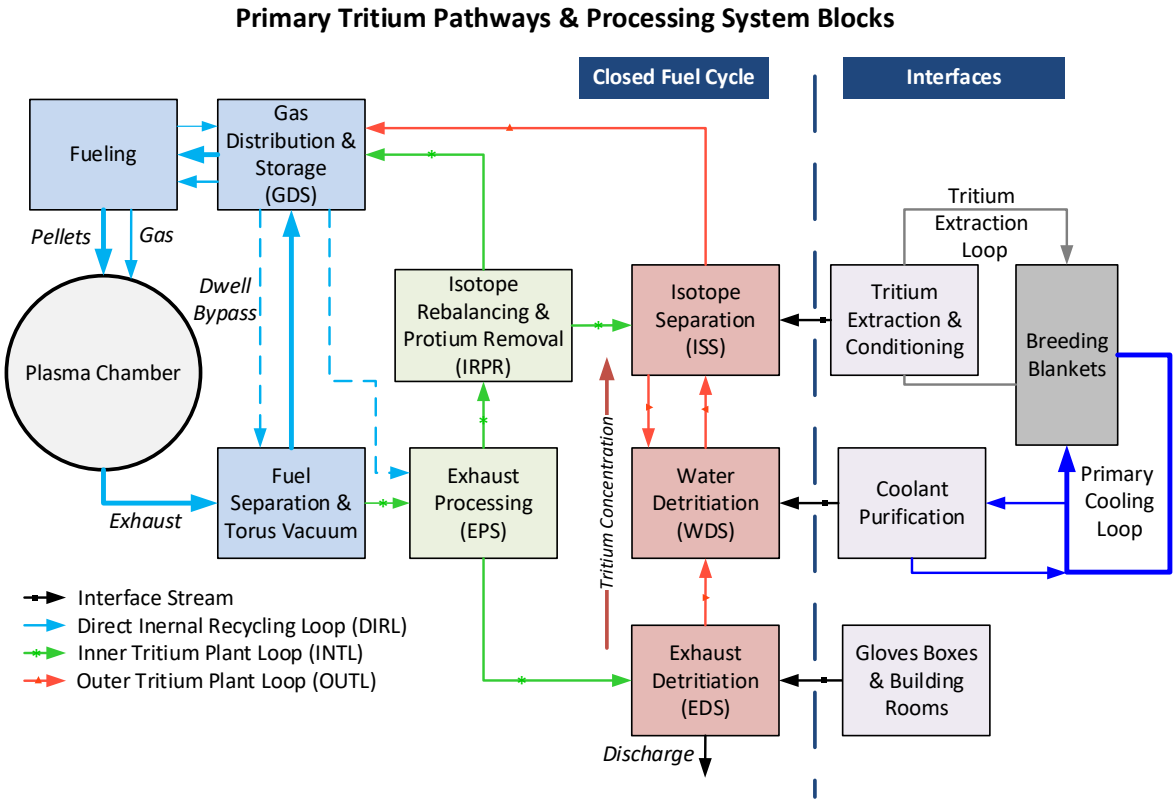

Figure 3-1.1: System block view of the EU-DEMO fuel cycle showing all systems involved in the processing of tritium. The systems are grouped in the Direct Internal Recycling Loop (blue) interfacing to the torus, the Inner Tritium Plant Loop (green), and the Outer Tritium Plant Loop (red) receiving all tritium streams from tritium extraction and recovery. Adapted from [19].

The technical implementation of this architecture requires five different types of separation operations to act on a tritium carrying stream in order to process all educts into the required products. These are:

- Separation of non-hydrogenic species from a flow of predominantly hydrogen (Fuel Separation, Exhaust Processing).
- Removal of hydrogen from a flow of primarily non-hydrogenic species (Exhaust Processing).
- Isotopic separation of hydrogen (Isotope Rebalancing and Protium Removal, Isotope Separation).
- Isotopic separation (removal of tritium) from liquid tritiated water (Water Detritiation).
- Removal of trace tritium from air and gas streams (Exhaust Detritiation).

These central separation processes in turn have to be supported by additional processing operations such as heating/cooling, compression, and pumping in order to operate them at the required conditions. The following sections describe the individual systems in detail, covering the employed technologies, operating conditions, and design goals. For interface streams their current reference values are developed whereas for integrated system part of closed fuel cycle a dedicated design point of steady state throughputs is derived in section 3.2.

3.1.1 Interfaces to the Fuel Cycle

3.1.1.1 Plasma Chamber

The primary interface to the fuel cycle and sole client for the inner fuel cycle is the plasma operation of the Tokamak that has to be supported by the fuel cycle. As such it directly dictates how much fuel is needed in what composition at what time. For the EU-DEMO no dedicated plasma scenario is yet developed, but a general understanding of the fueling requirements can nevertheless be developed from established plant parameters and general physics requirements [27]. Three different type of fueling contributions are installed as shown in Figure 3.2:

- Pellets of frozen DT admixed with xenon as Plasma Enhancement Gas (PEG) are injected at high speeds into the plasma.
- A gaseous hydrogen stream admixed with argon as plasma enhancement gas is injected at the divertor level.
- A gaseous stream of pure hydrogens is injected at the equitorial level.

Ultimately, any ion escaping the plasma confinement is transported along open magnetic field lines to the bottom of the plasma chamber where it is neutralized at solid plates forming the machine's divertor. From there it is transported towards the vacuum systems of the fuel cycle along with any other neutral gas such as pellet fueling losses or directly injected gas that is not ionized. Next to the fuel transport along these intended pathways, particles impinging from the plasma to the first wall may be implanted therein. From there they may outgass alongside protium dissolved in the structural material.

As a Tokamak, the EU-DEMO is intrinsically a pulsed machine, alternating between flat-top burn phases sustaining two gigawatt of fusion power over a minimum of 7200 seconds, and a dwell phase without plasma operation of about 600 seconds, in which the plasma chamber is evacuated and the central solenoid magnet is recharged to prepare the next discharge. The transient behaviour of the fuel contributions needed to support these operations and control of their actuators to achieve

the desired profiles of plasma density and fusion power is closely linked with the plasma scenario. Thus, by now no reference design point exists. Recent studies, however, point to an optimum ramp time of the central solenoid ranging from 100 – 200 s while the plasma power should be ramped up as fast as possible to maximize the time for operating at full fusion power. To mitigate the transient loads on the power conversion systems the use of thermal energy storage systems or auxiliary power is foreseen which enables ramps as fast as 100 seconds [28].

A conservative estimate for troughputs from a fuel cycle perspective is obtained if assuming the upper bounding case during the burn-phase as then the overall throughput and processing load of the fuel cycle is at a maximum.

During the flat-top burn phase the througput and composition of fuel is defined by Day et al. [19] by considering the helium ash limit in the plasma core and associated fueling efficencies for pellet fueling, as well as gas cooling requirements in the divertor which are indicated in Table 3.1. A total fueling rate of 430 Pa.m ^{3}s^{-1}[†] of hydrogen is obtained with a D/T ratio of unity and a maximum allowed protium contamination of the hydrogen of 1 mol%. Any plasma enhancement gas additions are then considered additively.

Table 3.1: Fueling contributions to the plasma chamber during the flat-top burn phase.

Fueling Contribution	**Flat-topQ_2 Fueling (Pa.m^{3}s^{-1})**	**D/T isotope ratio (-)**	**Protium contamination (mol%)**	**PEG addition (mol%)**
Pellets	380	1.0	1.0	0.045 Xenon
Gas Puffing	50	1.0	1.0	0.9 Argon
Gas Injection	0	1.0	1.0	none

During the dwell phase no fueling contributions are active to allow the evacuation of the plasma chamber. Ramp-up and ramp-down fueling are then modulated, enabling the transition between these phases in a technological feasible manner. This modulation must still respect the requirements of the plasma, which has to be operated in a way such that its stability is permanently assured and no loss of control or power spikes on in-vessel components are encountered [29].

Here, ramp-up and ramp-down durations of 100 seconds each are assumed, which are then supported by the fueling systems as follows:

- During ramp-up pure hydrogen in the isotopic composition of the fuel is injected into the machine to provide the initial plasma inventory (gas injection). For the remainder of the phase the flowrate is modulated as to always achieve a linear ramp in the combined total fueling input by all systems leading to the flat-top throughput of 430 Pa.m^{3}s^{-1} at the end of the ramp-up. The gas puffing throughput is increased linearly to its flat-top value over the full duration. The pellet throughput is increased linearly after a dead time of 50 seconds in order to avoid firing pellets into the initially empty vacuum chamber.
- During ramp-down pellets and gas puffing throughputs are decreased linearly over time, with pellets being fully disengaged after 50 seconds and gas puffing after 100 seconds.

[†] Throughout this document the unit for pressure · volume (pV) flowrates is given as Pa.m ^{3}s^{-1} using a reference temperature of T = 273.15 K.

Figure 3.3 shows the described time evolution of the fueling contributions over the burn-dwell-burn transition, starting after 7200 seconds of flat-top operation, with 100 second ramp durations and 600 seconds of dwell phase. This sequence of events occurring over a total of 8000 seconds marks the reference pulse as considered in this work.

If in a first approximation implantation and outgassing contributions are neglected, the total amount of gas exhausted from the machine has to equal all fueling contributions, and the composition will establish as a mixture of all species. This yields:

- 2.68 $Pa.m^3s^{-1}$ of ^4He, corresponding to $3.55 \cdot 10^{20}$ fusion reactions per second, providing 2 GW of fusion power,
- 430 – 2.68 = 427.3 $Pa.m^3s^{-1}$ of primarily deuterium and tritium, containing 4.30 $Pa.m^3s^{-1}$ of protium,
- 0.17 $Pa.m^3s^{-1}$ of xenon and 0.45 $Pa.m^3s^{-1}$ of argon.

Small deviations may be caused by implantation and outgassing effects, their impact is however not directly quantifiable and depends on the plasma chamber configuration, plasma scenario, and machine history.

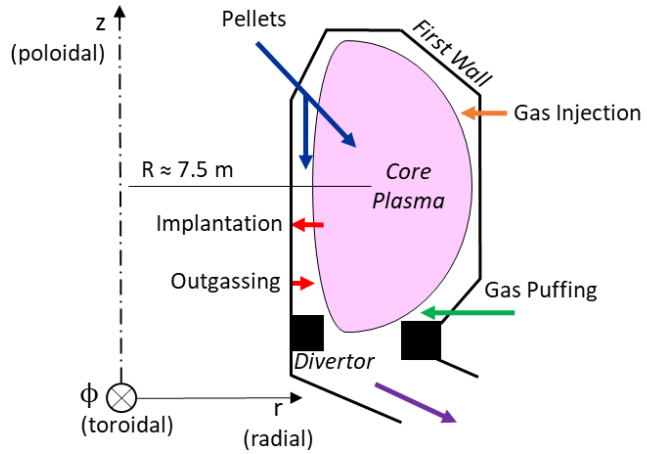

Figure 3.2: Toroidal cross-section of a Tokamak plasma chamber and fuel transport pathways therein.

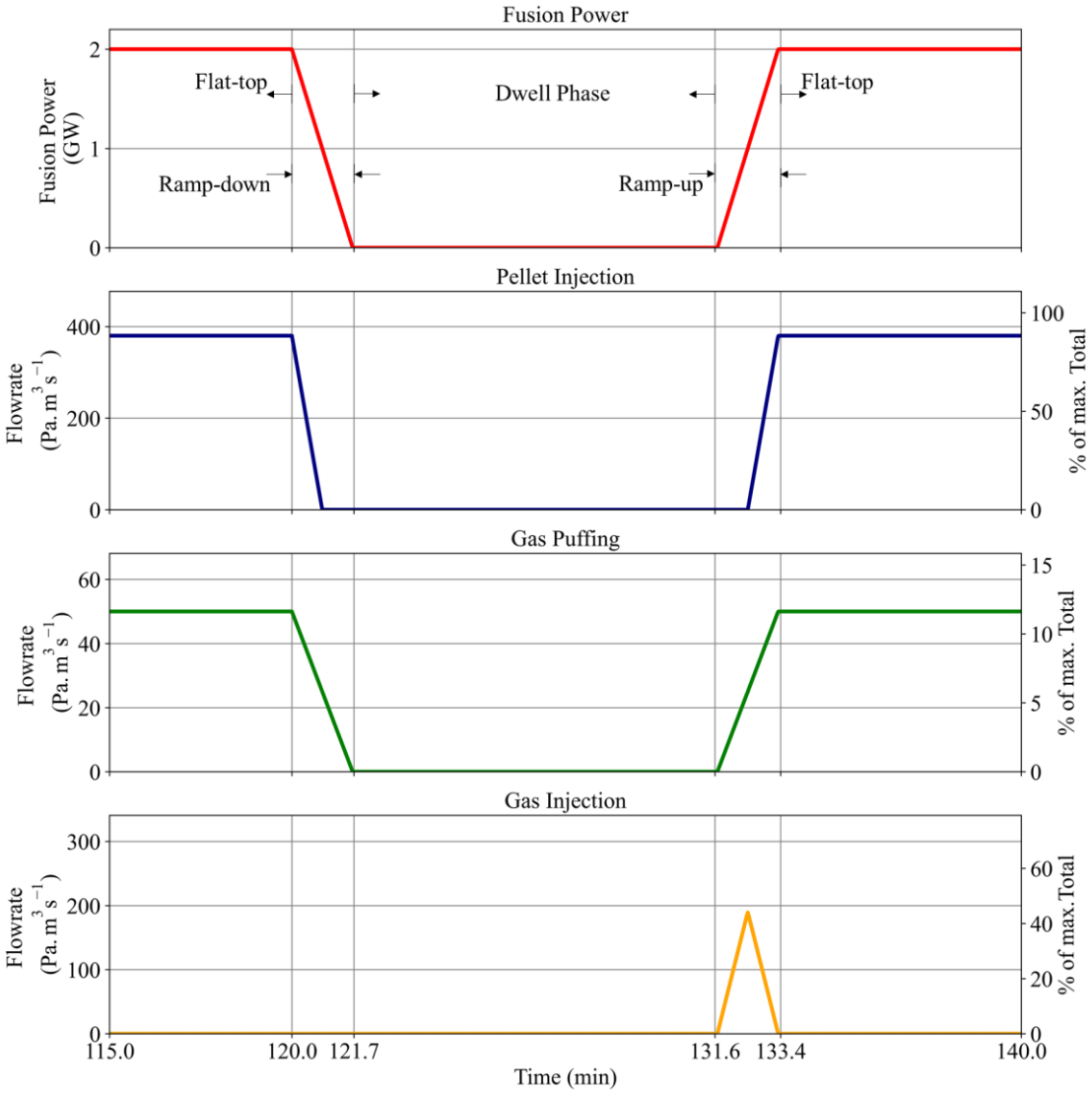

Figure 3.3: Idealized time profiles of the fusion power (top) and fueling contributions (bottom three) during the burn – dwell – burn transition. The fusion power is ramped up and down over a duration of 100 seconds. Pellet fueling is disengaged faster and ramped up after a dead time whereas gas puffing follows the fusion power profile directly. During ramp-up the fueling contributions are supplemented by puffing in additional gas in order to raise the pressure in the vessel.

3.1.1.2 Tritium Extraction

Currently two different types of breeding blanket concepts are under development for the European DEMO. The blankets differ in the employed coolant, either water or helium, as well as the tritium breeding and neutron multiplier materials. For the water cooled variant an eutectic lithium-lead alloy serves as breeder and multiplier, whereas lithium-ceramics as breeder and beryllium as neutron multiplier is foreseen for the helium cooled variant. The resulting blanket concepts are referred to as the Water Cooled Lithium Lead (WCLL) breeding blanket [30] and the Helium Cooled Pebble Bed (HCPB) breeding blanket [31], which will be down selected later in the project timeline [32].

Technologies used for tritium extraction are unique to each breeding blanket type. Hence, two different interface streams need to be accommodated by the fuel cycle depending on the blanket type installed.

Helium Cooled Pebble Bed

The Helium Cooled Pebble Bed breeding blanket features breeding zone compartments housing the breeder materials Li_4SiO_4 and Li_2TiO_3, with the lithium enriched to 60 at% ^6Li fraction as well as a neutron multiplier of $TiBe_{12}$ [33]. The breeding zone is purged by continuous flow of helium containing 0.1 mol% protium and trace amounts of steam with a total combined flowrate of 10 000 Nm^3h^{-1} for all breeding zones [34]. After leaving the breeding zone this flow is routed over a Reactive Molecular Sieve Beds (RMSB), adsorbing the contained humidity. Afterwards, the flow is routed over a Cryogenic Molecular Sieve Bed (CMSB), adsorbing the remaining hydrogens. At least two beds are always operated in parallel to allow for cycling between an active bed and a bed in regeneration.

Once saturated, the RMSB is regenerated by passing a stream of pure protium over it. Hydrogen undergoes isotope exchange with the adsorbed tritiated water reducing its tritium content. Afterwards the water is released by heating up the bed. The CMSB is regenerated by depressurizing and raising its temperature. As a consequence of these regeneration operations the following streams that are sent to the fuel cycle are obtained:

- The hydrogen flowrate used for isotope exchange in the RMSB,
- The hydrogen regenerated from the CMSB,
- Liquid water from the regeneration of the RMSB.

The hydrogen streams are combined and sent for isotope separation, while the tritiated water is transferred to water detritiation. The actual operation schemes and scheduling of the different bed regeneration cycles are still subject to design and optimization and no reference design is available. However, time averaged values and compositions can be calculated from the purge gas stream compositions using the following assumptions:

- A total amount of tritium corresponding to the plants design value for the tritium extraction ratio is extracted. This tritium is split between hydrogen and steam according to their ratio in the purge gas.
- The total activity of liquid water sent to the fuel cycle may not exceed 500 $Ci.kg^{-1}$. All excess tritium contained in the adsorbed water is removed in the isotope exchange phase.
- A time averaged isotope exchange flowrate of 3 Nm^3h^{-1} of protium is used.
- All tritium is present as HT or HTO due to the excess of protium.

During the switchover of the beds, some helium from the purge gas stream is inevitably contained in the bed and routed to the fuel cycle during the regeneration. In order to obtain a pure hydrogen stream that can be sent for isotope separation, the gaseous exhaust is passed through palladium silver permeators, retaining any helium present.

Assuming a TER = 1.05 as well as a steam content in the purge gas of $2.5 \cdot 10^{-3}$ mol% the time averaged flowrates and composition in the interface streams as listed in Table 3.2 are obtained.

Table 3.2: Estimated time averaged flowrates and composition of streams sent to the fuel cycle as a consequence of tritium extraction from the helium cooled pebble bed blanket.

Stream	Flowrate	Composition (mol%)	
Hydrogen	13 Nm^3h^{-1} 580.00 $mol.h^{-1}$	99.66 H_2	0.34 HT
Water	0.2 $kg.h^{-1}$ 11.1 $mol.h^{-1}$	99.97 H_2O	$3.09 \cdot 10^{-4}$ HTO

Water Cooled Lithium Lead

In the water cooled lithium lead breeding blanket tritium is bred in a eutectic alloy of PbLi where lead provides the neutron multiplication functionality and lithium undergoes the breeding reaction. The liquid metal stream is circulated through the breeding blanket and tritium extraction can therefore be done outside of the breeding blanket. The current reference technologies for tritium extraction from lithium lead are Gas Liquid Contacting (GLC) or Permeation Against Vacuum (PAV) [33]. From a fuel cycle perspective the former marks the more demanding solution, as here larger flowrates have to be processed. In this process the liquid metal is introduced at the top of a stripping column and purged in counterflow with helium containing 0.1 – 0.5% protium with a total upper case flowrate of up to 3500 Nm^3h^{-1}. This helium stream is then further processed to separate hydrogens and helium, routing hydrogens to the fuel cycle and returning helium.

For *TER* = 1.05 and the highest protium addition the time averaged flowrate and composition of hydrogen to the fuel cycle as given in Table 3.3 is obtained. This assumes that all tritium is present in the form of HT due to the overabundance of protium.

Table 3.3: Estimated time averaged flowrates and composition of streams sent to the fuel cycle as a consequence of tritium extraction from the water cooled lithium lead blanket.

Stream	Flowrate	H_2 content (mol%)	HT content (mol%)
Hydrogen	17.50 Nm^3h^{-1} 780.76 $mol.h^{-1}$	99.75	0.25

3.1.1.3 Coolant Purification

Coolant purification aims to control the concentration of tritium in the primary coolant to a specified limit by continuously detritiating a bleed stream. Tritium ingress into the coolant occurs in the breeding blankets where high tritium concentrations and large surface areas at elevated temperatures provide conditions favorable for permeation. A steady state is achieved if tritium can be extracted from the bleed stream at the same rate as the permeation rate. The permeation characteristics and technologies employed for coolant purification are dependent on the coolant, helium or water.

Helium Coolant

The helium coolant is detritiated by routing the bleed stream over a packed bed of copper oxide pellets where any contained hydrogen is oxidized forming water vapor. The resulting stream of helium and tritiated water vapor is then cooled down to room temperature and passed over a bed of zeolite molecular sieves on which water is adsorbed. The stream is then reheated against the incoming stream in an economizer and routed back to the coolant loop. Once the molecular sieve

bed is saturated it is decoupled from the loops, depressurized and purged with a stream of hot helium. This releases the adsorbed water which is collected in a condenser and the helium purge gas is recycled through the bed.

From tritium transport modelling of the breeding blankets a total maximum tritium permeation rate of 0.74 $g.day^{-1}$ from the tritium extraction purge gas to the primary coolant is predicted [35]. Next to permeating tritium the intentional addition of protium and steam to the coolant is also foreseen up to a partial pressures of 1000 Pa and 50 Pa respectively. Meanwhile, the upper limit for the partial pressure of HT is limited to 0.04 Pa [19]. In order to achieve a steady state between the amount of tritium removed from the system as liquid water via the condenser and the tritium permeation rate, a total of 4.83 $kg.h^{-1}$ of water must be extracted from the system for the highest case of steam and protium addition, which is considered as reference case. The liquid stream molar fraction of HTO is then $x_{HTO} = 3.81 \cdot 10^{-5}$ (corresponding to a specific activity of 61.6 $Ci.kg^{-1}$) if assuming all tritium to be present in the form of HTO.

Water Coolant

Significantly larger permeation rates are predicted for the water cooled breeding blanket which are projected to reach up to 43 $g.day^{-1}$ in an unmitigated case and as such considered unfeasible. Permeation reduction measures such as surface treatment or permeation barriers are therefore imposed to achieve a reduction of the permeation flux by at least two orders of magnitude. The upper tritium permeation rates that can then be identified are 0.43 $g.day^{-1}$ to the breeding zone coolant and 0.009 $g.day^{-1}$ to the first wall coolant [35].

In total, 0.44 $g.day^{-1}$ of tritium are expected to have to be continuously removed from the coolant to counteract the build-up of tritium therin. This can only be achieved by treating a large enough fraction of the primary coolant that carries the required amount of tritium and the total rate thus depends on the allowable tritium concentration in the coolant. A common reference point is the typical tritium concentration in Canadian CANDU fission reactors primary coolant loops, which is about 2 $Ci.kg^{-1}$ [36]. At this concentration 88.5 $kg.h^{-1}$ of primary coolant have to be continuously removed from the system and processed in the fuel cycle.

In order to reduce the overall processing load and to better integrate the stream in terms of its tritium concentration a coolant purification system based on water distillation is foreseen to provide a pre-enrichment and corresponding volume reduction of the tritium containing stream. The same absolute amount of tritium has to be routed to the fuel cycle, now at elevated tritium concentration and inversely reduced overall flowrates. With feasible enrichments up to 100 $Ci.kg^{-1}$ (corresponding HTO molfraction of $x_{HTO} = 6.19 \cdot 10^{-5}$) the overall flowrate to the fuel cycle reduces by a factor of 50 to 1.76 $kg.h^{-1}$ [37].

3.1.1.4 Air and Glove Box Detritiation

The interface of air and inert gases that are sent to the fuel cycle is determined by the confinement strategy employed for the nuclear classified buildings on site. Details of its implementation are subject to the applicable regulatory framework in the host country of the plant site. Until the plant site is selected the confinement strategy assumed is based on best practice and according to ISO 17873 and features two major concepts that impact the fuel cycle [38]:

- Active confinement is established by maintaining a pressure cascade from the environment to the rooms with the highest contamination levels with depressurization increasing with

contamination. This ensures that any airborne contamination is always carried towards areas of higher contamination.

- Tritium processing equipment is housed in secondary confinement structures with inertized atmosphere and served by a detritiation system (commonly referred to as Glove Boxes (GB) with a Glove Box Detritiation System (GB-DS)).

The upkeep of depressurization levels requires to counteract any in-leakage of air by continuously removing at least the same amount. Simultaneously, a set air change rate in a room may be enforced by taking in conditioned air from the plant's Heating, Ventilation and Air Conditioning (HVAC) systems which then also contributes to the rate with which air has to be exhausted from a room. The HVAC system is also required to maintain nominal conditions in terms of temperature and humidity.

Glove boxes are the final element in the depressurization cascade, illustrated in Figure 3.4, and their inert atmosphere is continuously circulated through a glove box detritiation system. In addition to its depressurization, glove boxes also need to maintain their inertization by continuously replacing a portion of its atmosphere, which is then also exhausted to the plants exhaust detritiation system.

In consequence, the total flowrates and conditions of the streams routed to the exhaust detritiation system depends on the air circulation rate and air leak rate, which depends on the room volumes and depressurization levels. These can ultimately only be evaluated for an established building layout not yet available for EU-DEMO. Instead, the exhaust detriatiation system is designed and sized against an upper bounding case which is defined as:

- A maximum total flowrate accepted by the EDS of 12 000 Nm^3h^{-1} [19].
- A maximum temperature and relative humidity of T_{gas} = 25°C and φ = 65%.
- A concentration of airborne tritium of $1 \cdot 10^8$ $Bq.m^{-3}$.

This confinement strategy is backed up by additional standby detritiation systems in place to provide additional capacity either to support maintenance operations or following a release of tritium into building volumes. However, their operation is decoupled from the continuous operation of the fuel cycle and not considered here. The flowrate and composition of the combined interface flowrate is then as listed in Table 3.4, which assumes all tritium to be present in the form of HTO.

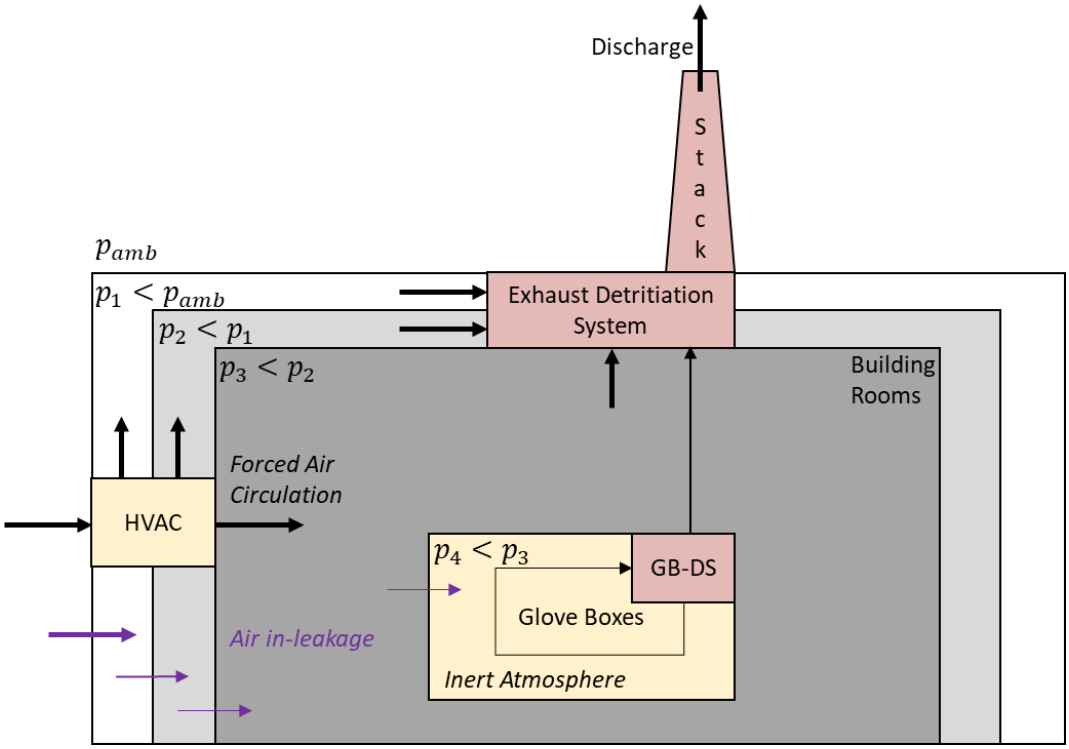

Figure 3.4: Pressure cascade and air-flows between the environment and tritium containing systems and potentially contaminated rooms. In order to maintain the required depressurization levels any ingressing air is discharged via the exhaust detritiation system connected to the stack.

Table 3.4: Considered combined flowrate and composition of streams sent to the fuel cycle arising from air and gas detritiation.

	Flowrate	**Composition (mol%)**
Total	12 000 $Nm^3.h^{-1}$ $5.35 \cdot 10^5$ $mol.h^{-1}$	100
Dry air / gases	11 773 $Nm^3.h^{-1}$ $5.25 \cdot 10^5$ $mol.h^{-1}$	98.11
H_2O	226.65 $Nm^3.h^{-1}$ 10.11 $mol.h^{-1}$	1.89
HTO	$2.74 \cdot 10^{-5}$ $Nm^3.h^{-1}$ $1.22 \cdot 10^{-3}$ $mol.h^{-1}$	$2.28 \cdot 10^{-7}$

3.1.2 Gas Distribution and Storage

The gas distribution & storage system is the central hub of the fuel cycle, receiving all fuel product streams from the individual loops and producing fuel mixtures which are supplied to the fueling systems.

The system architecture is based around multiple gas vessels and storage beds of depleted uranium in which hydrogen can be safely stored in hydride form below ambient pressure. However, as one requirement of the direct internal recycling based fuel cycle is that it should work fully continuous, no such hydride storage beds are employed for the inner fuel cycle product streams. The outer fuel cycle product is received by hydride beds in the gas storage section of the system. The overall layout of the system is shown in Figure 3.5.

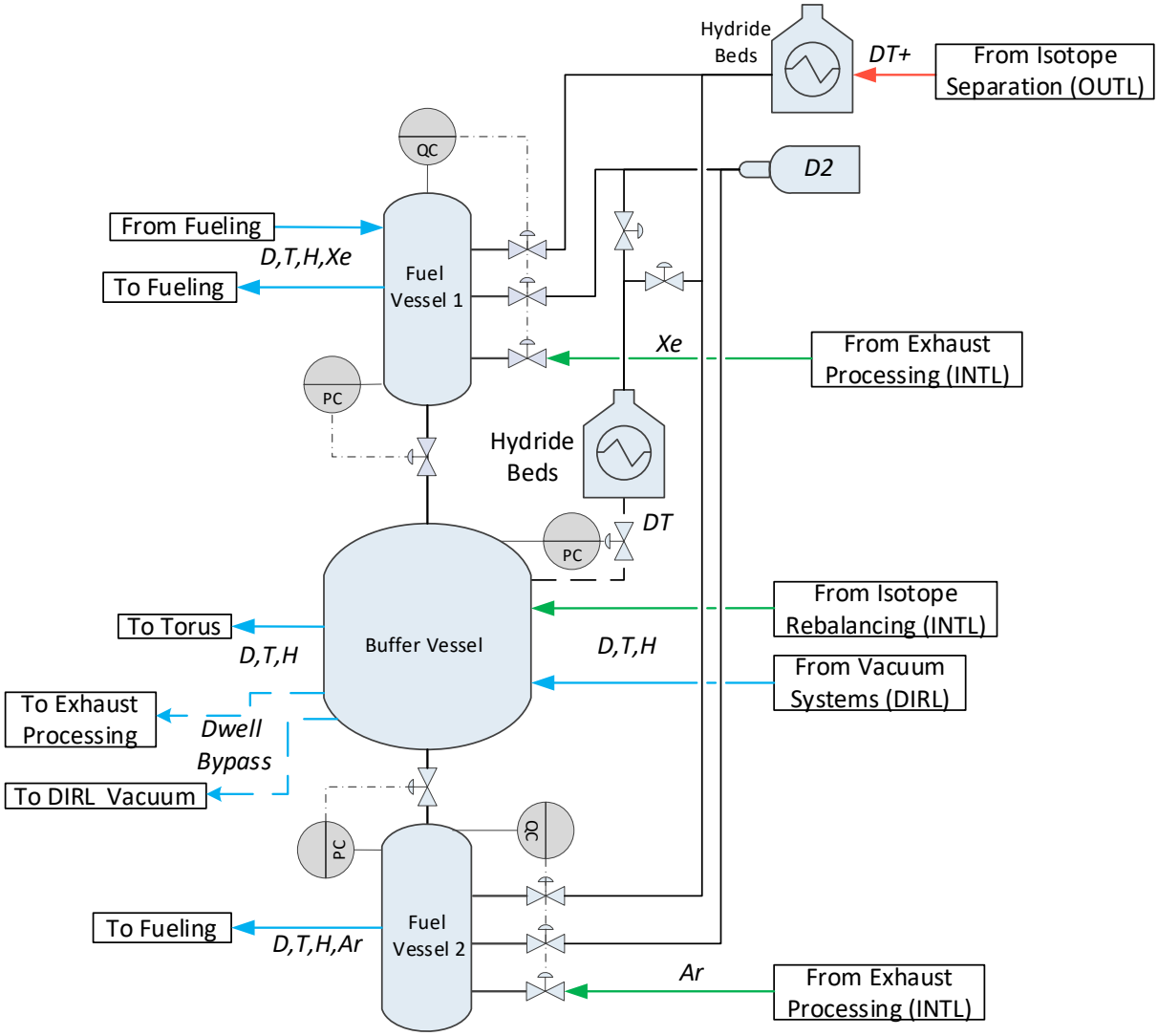

Figure 3.5: Architecture of the Gas Distribution and Storage System. Hydrogen flows from the DIRL and INTL are received in a buffer vessel and distributed to two mixing vessels where the desired fuel composition is established. The product of the OUTL is received in hydride getter beds from where it can be requested for composition control or fuel make-up alongside bottled deuterium. (PC: Pressure Control, QC: Composition Control).

The hydrogen gas streams from the torus vacuum system (DIRL) and isotope rebalancing system (INTL) are collected in a central *Buffer Vessel* (BV). This buffer vessel is connected to two smaller

fuel vessels in which the fuel composition required for pellet fueling and gas puffing is continuously monitored and can be corrected if needed by drawing on supplies of a tritium rich hydrogen mixture (DT+) supplied from isotope separation (OUTL). Pure deuterium is supplied from external imports and plasma enhancement gases are received from exhaust processing. Any fuel required for gas injection is directly extracted from the buffer vessel. The buffer vessel also connects to the DIRL vacuum system and exhaust processing system to provide dwell bypass streams. The fuel vessels are controlled to constant pressure, drawing required make-up from the buffer vessel. The fuel vessel serving the pellet injection system also receives a return stream therefrom.

The buffer vessel is also connected to hydride storage beds containing deuterium and tritium in the isotopic ratio of the fuel. This connection is used to replenish burned up deuterium and tritium in intervals once a lower pressure threshold is encountered as well as for discharging of excess inventory if an upper pressure threshold is exceeded. During normal operation only the former case is expected to occur if the buffer vessel is sized appropriately and pressure thresholds are set accordingly. The system does not employ any pumps or blowers, rather, flow is driven by a pressure cascade from the buffer vessel towards the fueling systems. The control system of the fuel vessels therefore requires the specification of a pressure set-point at a lower value than the buffer vessel minimum threshold, as well as specification of the desired isotope ratio and plasma enhancement gas content.

3.1.3 Torus Fueling

The plasma operation of the machine needs to be supported by fueling via gas puffing, gas injection, and pellet injection. The first two constitute no significant processing operations, as prepared gas mixtures are supplied to the torus directly. For pellet injection additional steps are needed in order to prepare the frozen pellet and inject it into the torus. Figure 3.6 shows the architecture of the employed system.

A fuel supply is drawn from the gas distribution system in amounts needed to control for constant pressure in the *liquefier*. There, the incoming gas is continuously liquefied at approximately 14 – 20 K, close to the mixtures triple point temperature. The liquid stream is passed to a *twin screw extruder* where it is solidified and continuously extruded into a rod that is cut into cylindrical pellets which then are accelerated by a *centrifuge* and injected into the torus via a *guide tube*. As the pellet fueling system needs to modulate the fueling rate to achieve pre-determined fueling patterns, precise control over the rate of pellets injected into the torus is needed. This is achieved by adjusting the rotation rate of the extruder to control the extrusion rate. However, this is expected to be slow and lacking in precision due to the thermal inertia of the system. Additionally, the extruder is best operated at a minimum non-zero rate. In order to achieve zero injection rate and to provide fine control over the fueling rate, the *pellet chopper* is therefore supported by a selection mechanism, forwarding pellets either to the centrifuge and torus or towards an *evaporator*. There, the pellet is thawed and the resulting gas internally recycled to the liquefier inlet. This allows for arbitrary modulation of the fueling rate between the maximum extruder output and zero, discretized by the size and frequency of the pellets. Following the selector unit the centrifuge is evacuated in order to minimize drag and the guide tube is then open ended towards the torus and maintained at the same pressure levels.

Under these conditions pellet losses occur due to sublimation or mechanical ablation in the guide tube. Both areas are therefore served by vacuum systems to maintain the necessary vacuum. The

exhaust from the centrifuge is refluxed to the liquefier, whereas the guide tube exhaust is routed back to the corresponding fuel vessel in the gas distribution system. Any losses of the pellet mass that are captured in this way and do not reach the plasma chamber is referred to as recoverable pellet losses.

Depending on the required spatial distribution of fuel injection locations multiple identical systems can be distributed circumferentially around the torus.

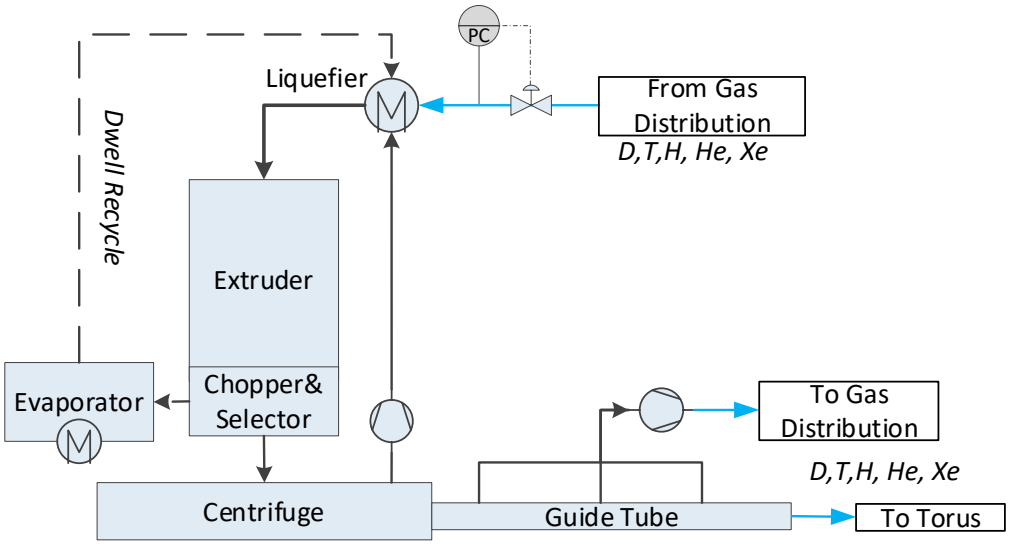

Figure 3.6: Architecture of one Pellet Injection System. The fuel mixture is introduced into a liquefier where it is cooled down and passed to an extruder. There it is solidified and formed into a thin rod which is cut into pellets. These are then either selected for injection into the machine or rejected if they are not needed. Rejected pellets are evaporated again and the gas is refluxed to the condenser. Pellets to be injected are accelerated in a centrifuge and shot into the guide tube towards the plasma chamber. The centrifuge and guide tube are evacuated and the exhaust is recycled.

3.1.4 Fuel Separation and Torus Vacuum

The fuel separation and torus vacuum system combines the separation task needed to implement direct internal recycling and the first stage of the torus evacuation functionality needed to maintain the machine gas throughput and to provide evacuation of the plasma chamber during dwell phases. The plasma chamber is exhausted via circumferentially distributed ports in the lower section of the vacuum vessel, with ten of sixteen available ports employed for vacuum pumping [39]. Figure 3.7 shows the architecture of the system for the installation at one port.

As a first stage in the pumping system a series of *Metal Foil Pumps* (MFP) housed in rectangular casks directly located in the port duct are installed. Each cask is foreseen to house 6 tubular metal foil pumps in parallel. As a result of their operating principle, based on super permeation through a metal foil (c.f. [40]), only pure hydrogen is able to cross the metal foil and can be compressed and separated from the exhaust stream forming a permeate stream. The remaining gas (retentate) is compressed by means of mercury driven *Linear Diffusion Pumps* (LDP) connected to the outlet of the metal foil pumps. Both outlet streams are discharged into individual *ring lines* spanning the circumference of the machine and collecting gas from all pumping ports. The ring lines are connected to *booster pumping* stages of mercury jet pumps further compressing the gases to allow them to be handled by the rough vacuum pumping system comprised of *liquid*

ring pumps also operated with mercury [19][41]. A total of six sequential stages, each with multiple parallel pumps, is used to compress from rough vacuum pressures to slightly below ambient pressure at which gas is discharged from the system. The exact number of parallel pumps depends on the achievable pumping speed of a single pump and desired pressure levels between pumping stages. The overall system is an implementation of the KALPUREX process, alleviating the need for non-continuous cryogenic pumps and only using tritium compatible mercury as operating fluid [42].

In view of the overall fuel cycle, the performance of this system is characterized by the total effective pumping speed applied to the torus as well as the achievable separation performance of the metal foil pump. This separation performance is measured as the fraction of hydrogen in the exhaust stream that can be directly recycled, referred to as Direct Internal Recycling ratio, (DIR-ratio). During the dwell phase the DIR-ratio becomes zero as the collisional plasma source of the metal foil pump cannot operate at pressures lower than approximately one Pascal. Consequently, the effective pumping speed of the overall system reduces as well and no gas enters in the DIR loop. In order to still maintain a steady state of the subsequent pumping system a dwell bypass connected to the DT buffer vessel in the gas distribution system is engaged, maintaining a set minimum pressure in the ring line.

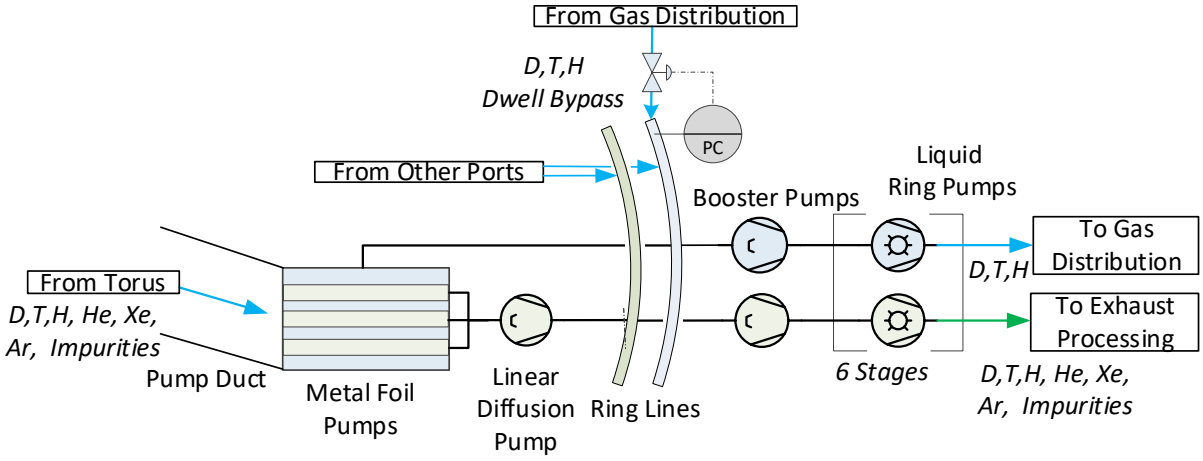

Figure 3.7: Architecture of one vacuum pumping train of the fuel separation and torus vacuums system. The system interfaces to the torus via a set of metal foil pumps arranged in a cask in the lower pump duct. Their retentate and permeate streams are passed into ring lines spanning the circumference of the torus and collecting gas from all pump ducts. The ring lines are then evacuated by a series of mercury vapor booster pumps and liquid ring pumps providing further compression.

3.1.5 Exhaust Processing

The exhaust processing system receives the torus exhaust that is not directly recycled which is a mixture of unburnt hydrogen, helium ash, plasma enhancement gases, and any impurities that may be formed. The system then has to fulfill the following functions:

- Separation of hydrogen from the exhaust stream.
- Recovery of hydrogen bound in impurities from the exhaust stream.
- Separation of plasma enhancement gases from the exhaust stream.

The remaining exhaust of the system is discharged towards the exhaust detritiation system and crosses the boundary between the inner and outer fuel cycle. This system needs to be designed and operated under the constraint of retaining as much tritium as possible in the inner fuel cycle.

Figure 3.8 shows the layout of the system. The feed stream received from the torus vacuum system is further compressed and routed to a first stage of tubular palladium-silver *permeators* which are able to selectively permeate hydrogen towards a reservoir of lower partial pressure and thus achieve a sharp separation between hydrogen and non-hydrogen species. Recovery of hydrogen from impurities is then achieved by a series of catalytic reactors (*low temperature* and *high temperature recombiner)* promoting water gas shift reactions and cracking of hydrocarbons, liberating bound hydrogen in the process. A second stage of permeators is then used to separate out remaining and liberated hydrogen. In order to further reduce the content of tritium in the remaining retentate stream it is passed through a packed bed of Non Evaporable *Getter* (NEG) where hydrogen is absorbed. Two beds are operated in parallel, one absorbing and the second one being regenerated by evacuation. The regenerated hydrogen is also passed through a third permeator to guarantee the absence of inert species and impurities. All three permeator stages are connected to a central vacuum system which provides the necessary depressurization to drive the permeation process as well as compression of the now purely hydrogenic permeate stream which is sent to isotope rebalancing and protium removal. The remaining exhaust after the getter bed stage is then passed to a *PEG removal system*, separating out and retaining xenon and argon and discharging the fusion ash towards exhaust detritiation.

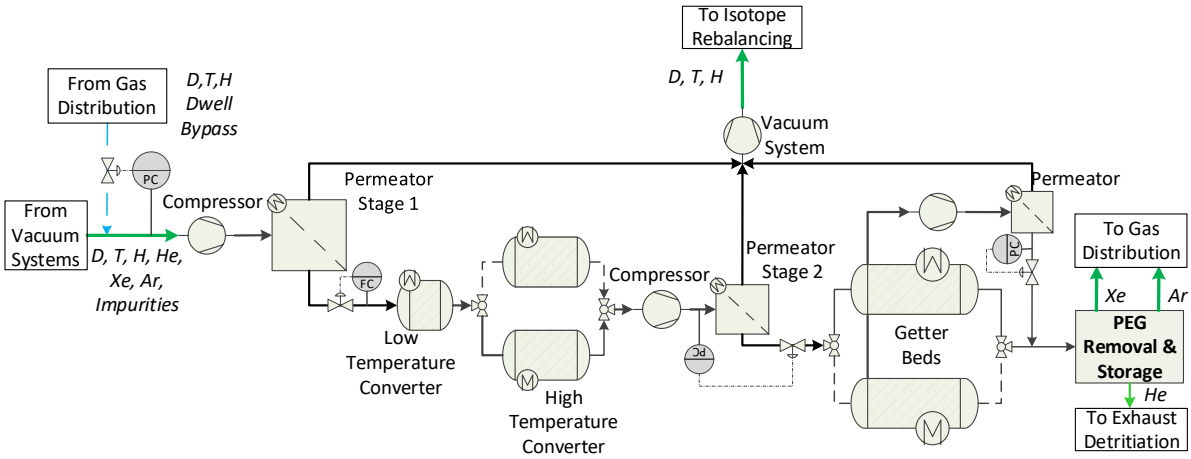

Figure 3.8: Architecture of the Exhaust Processing System. Incoming gas is compressed and routed to a set of Pd-Ag permeators. The retentate is then passed over a series of low and high temperature converters and passed to a second permerator stage. The permeate of both stages is re-compressed by a vacuum system and discharged from the system. The retentate of the second stage is passed over a pair of getter beds before being sent for PEG-removal as final processing step. Once a bed is saturated it is disengaged and evacuated for regeneration. The regenerated stream is passed through a third permeator set and joined to the other permeate streams. PC: Pressure Control, FC: Flow Control.

The operation of the system relies on the use of active control loops in order to guarantee stable operation conditions during dwell phases. As the feed stream from the torus diminishes during dwell phases the inlet of the system is controlled to a minimum pressure by means of a dwell bypass flowrate from the DT buffer vessel in the gas distribution systems. Additionally, the bleed

flowrates of the two main permeator stages are controlled. In the first stage to a constant throughput, and in the second stage to retain a constant feed side pressure.

Despite the considerable complexity of the employed architecture, technologies, and controls, the primary performance metrics from an integral fuel cycle perspective are the fraction of tritium that can be recovered and the amount of tritium that is discharged from the inner fuel cycle.

3.1.6 Isotope Rebalancing and Protium Removal

The control of the isotopic fuel composition relies on the availability of streams enriched in tritium that can then be supplemented with deuterium from external supplies. Simultaneously, protium has to be removed from the inner fuel cycle in order to counteract build-up and dilution of the fuel.

The required isotope separation functionality in the inner fuel cycle is provided by a temperature swing absorption system, operating semi-continuously, shown in Figure 3.9. A feed stream of pure hydrogens received from exhaust processing is collected in a *feed tank* building up pressure over time. From there it is fed at intervals to one of two absorption *columns* depressurizing the tank. Any gas not required to be processed in the system (the difference between the DIR-ratio and $R_{\mathrm{H/D/T}}$, see section 2.1) is bypassed and routed to gas distribution directly.

The columns are packed with active metal materials into which hydrogens absorbs, forming hydrides. If the employed materials in each column preferentially absorb different isotopes, their separation can be achieved by thermally cycling the gas inventory between the columns using alternate (phase shifted) heating and cooling, promoting absorption in one column and desorption in the other. This flow cycling leads to the formation of concentration profiles in the cycled gas, with light and heavy fractions each moving towards the end of different columns where they are extracted during the desorption phase. The light isotope fraction containing protium is discharged to the isotope separation system of the outer fuel cycle and the heavy isotope fraction enriched in tritium and stripped of protium is sent to the gas distribution system.

In addition to the integral, time averaged flowrate routed through the columns, the system performance is determined by the split factor between the two extracted streams as well as their respective composition.

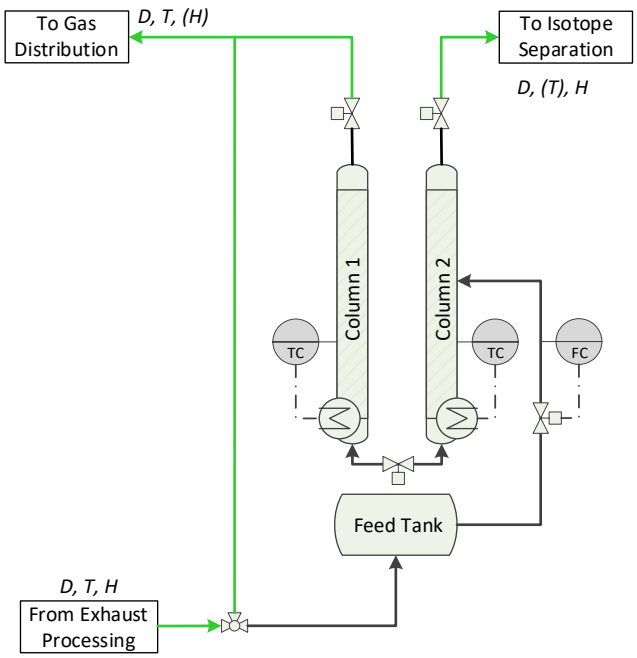

Figure 3.9: Architecture of the Isotope Rebalancing and Protium Removal System. The system feed stream is collected in a buffer tank from where it is routed periodically to one of two absorption columns. The gas is cycled thermally between the columns and periodically a product stream enriched in heavy isotopologues is extracted from column 1 and a product stream enriched in light isotopes is extracted from column 2. TC: Temperature Control, FC: Flow Control.

3.1.7 Exhaust Detritiation

The exhaust detritiation system is the first system part of the outer fuel cycle and constitutes the only interface of the fuel cycle towards the environment. As such the system receives the final discharge from the inner fuel cycle exhaust processing system, consisting primarily of helium and not recovered hydrogen and plasma enhancement gases, as well as large volumetric flow rates of air and air like species arising from building rooms and glove boxes in potentially contaminated areas to be detritiated before being discharged from the plant. The system is based on the use of wet scrubber columns fixing tritium into liquid water and modularized into parallel trains, each providing the same capacity.

Figure 3.10 shows the layout of one train of the system. The incoming stream is chilled down in a *condenser* to lower its dew point and remove some humidity from the stream to avoid condensation at cold spots in the process. Afterwards the gas is passed over a series of two catalytic *recombiner* reactors burning all remaining trace hydrogen species to water, utilizing oxygen contained in the stream. These are operated at 150 and 450 °C and are interconnected by *economizer* heat exchangers to recover heat. In order to then detritiate the gas any tritiated vapor must be removed. This is done in so called *wet scrubber columns*. In a packed column the gas stream is scrubbed in counter flow with purified water. Tritium is then transferred chemically (by isotope exchange reaction) and physically (by vapor-liquid interaction) to the liquid phase traveling down the column. At the bottom of the column a *saturator* is employed in order to establish a saturated gas stream in the column (preventing dry out) at the column operating conditions. The tritiated water at the exit of the saturator and condenser is collected and routed to water detritiation. The gas

flow through the system is driven by a blower at the outlet of the wet-scrubber column, prefaced by another condenser lowering the dew-point of the discharged stream.

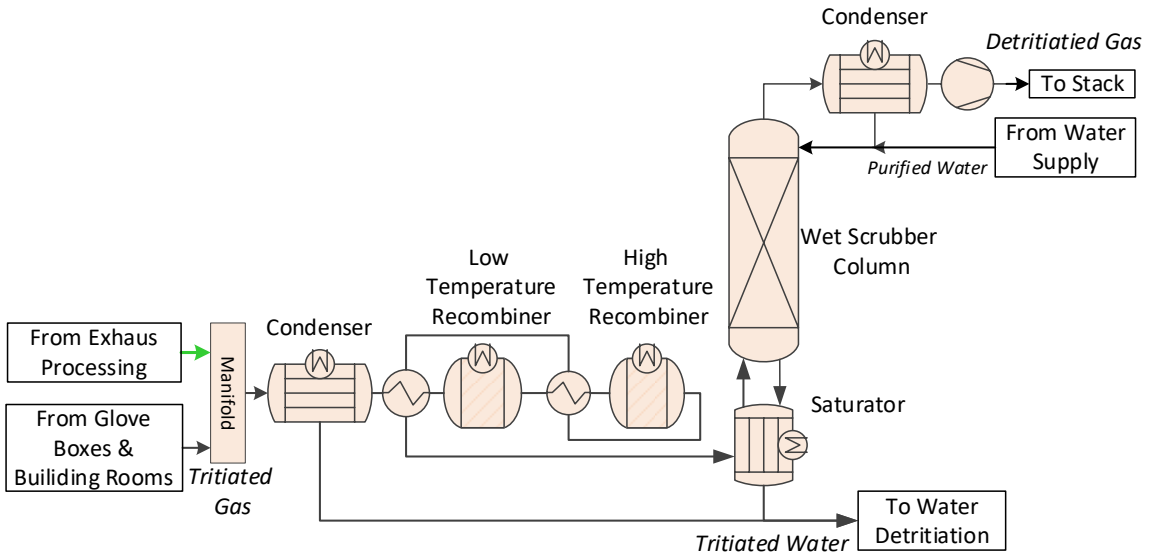

Figure 3.10: Architecture of one train of the exhaust detritiation system. All gas sent for detritiation is collected in a manifold and distributed between a number of parallel trains. Each train features first a condenser followed by a series of catalytic reactors operating at elevated temperatures. The gas stream is cooled down again, saturated with water vapor and introduced into a wet scrubber column. All gas is moved through the system by a blower, prefaced by a condenser, and finally sent to the stack for discharge.

The system is characterized by its achievable detritiation factor, which is calculated as the ratio of tritium in the feed and in the discharged stream. In order to also determine the liquid output of the system, the vapor to liquid ratio is used to relate the rate at which purified water is introduced at the top of the column to the vapor stream traveling up the column.

3.1.8 Water Detritiation

Any liquid tritiated water arising in the fuel cycle or interfacing plant systems is sent to the water detritiation system, illustrated in Figure 3.11, where it is collected in a *feed tank*. The system employs the Combined Electrolysis and Catalytic Exchange (CECE) process to generate streams of detritiated protium and oxygen as well as a hydrogen gas stream enriched in tritium. The process exploits the affinity of tritium towards the liquid water phase, stripping it out of a humid hydrogen gas stream in a counter current *Liquid Phase Catalytic Exchange (LPCE)* column. The tritiated water is introduced along the column height, traveling down the column in the so-called enrichment section, after which it is collected in an *electrolyzer*. The generated hydrogen is sent up the column and oxygen is treated in an adjacent *oxygen detritiation* system, returning any tritiated water back to the electrolyzer. As the tritium concentration is highest in the electrolyzer a side stream of the generated hydrogen is drawn off at this location and sent towards the isotope separation system after having passed through a *permeator* to guarantee a pure hydrogen stream. In order to establish a saturated feed stream for the column inlet the hydrogen stream entering the column is passed through a *saturator*. In order to also provide detritiation of the hydrogen stream the column is extended up from the feed location and purified water is introduced at the top, forming a stripping section. This section also receives a return stream of hydrogen containing trace amounts of tritium

from the isotope separation system which is further purified. The detritiated hydrogen at the top of the column is passed through a *condenser* to reduce its humidity content and sent for storage or reuse. Even though the generated hydrogen and oxygen are not released to the environment, they are detritiated to a level which allows their handling in inactive areas of the plant.

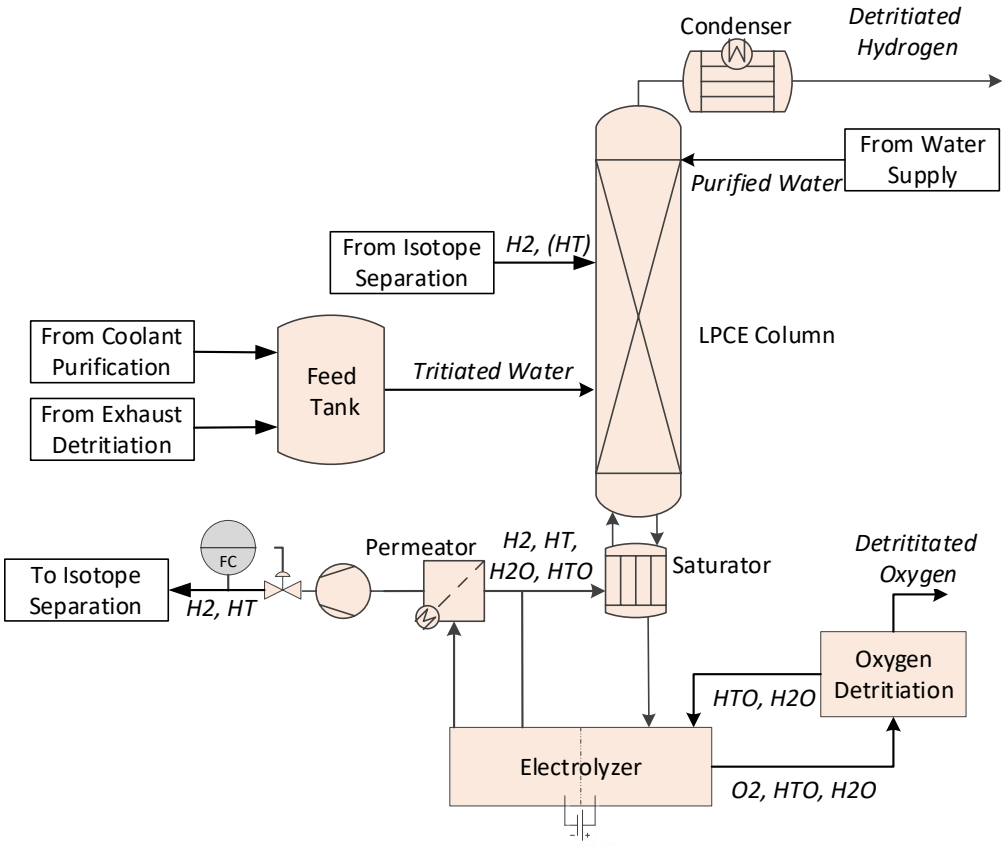

Figure 3.11: Architecture of the water detritiation system based on the Combined Electrolysis and Catalytic Exchange process. Tritiated water is collected in a feed tank and introduced along the length of a Liquid Phase Catalytic Exchange (LPCE) Column.

Any tritium being sent to the system therefore has to be extracted from the system by the side stream sent towards isotope separation. This flowrate is thus set so that a steady state tritium concentration in the electrolyzer is achieved. Similarly to the wet scrubber columns in the exhaust detritiation system, the purified water flowrate is set by specifying a vapor to liquid ratio for the top most section of the column.

3.1.9 Isotope Separation

The outer fuel cycle features a more universal isotope separation system than the isotope rebalancing and protium removal system in the inner fuel cycle. The system receives all tritium containing hydrogen streams which arise from water detritiation, tritium extraction, and isotope rebalancing. These are processed to a product stream enriched in tritium and depleted in protium which is sent to the gas distribution system where it is made available for fueling. The second product is then a stream of hydrogen depleted in tritium that is returned to the water detritiation system for final scrubbing before being sent to storage.

The isotope separation system is based on cryogenic distillation, exploiting vapor pressure differences between the molecular hydrogenic species to achieve their separation. As the streams from water detritiation and tritium extraction are comprised primarily of protium, the majority of contained tritium is present in the molecular form of HT. This poses an innate problem for the recovery of tritium, which at the same time requires the removal of protium, as further atomic separation cannot be achieved by distillation. In order to be able to recover pure isotopes, especially tritium from heterogeneous isotopologues (HD, HT DT) so called *equilibrators* are employed. These are catalytic reactors promoting the re-establishment of the chemical equilibrium between hydrogen istotopologues. For example, pure HT will with time re-equilibrate to a mixture of H_2, HT, and T_2, with the distribution dependent on temperature and converging towards a purely statistical distribution of 25% of each homogenous isotopologue and 50% of the remaining heterogeneous isotopologue at high temperatures (see section 4.2.2). While this process is ever-occurring for any mixture containing at least two hydrogen isotopes, reaction rates inside the distillation columns are negligible small due to the cryogenic temperatures close to 20 Kelvin. For that reason, dedicated equilibrator units operated at ambient temperature are used in locations between distillation columns with high concentrations of heterogeneous isotopologues, allowing the further recovery of tritium in subsequent columns.

Figure 3.12 depicts the architecture of the system which is arranged as a cascade of three cryogenic distillation columns in series of increasing tritium concentration. The *first column* essentially serves as a pre-enrichment step, directly interfacing to water detritiation bringing up the tritium concentration and reducing the volume of the flow to be processed in the subsequent columns. The *second column* receives a feed stream from tritium extraction, providing separation between H2 and HT and returning the lighter fraction to the first column. This pattern is repeated between the second and *third column* with the key selected to reflux all protium containing molecules (H_2, HD, HT) and to provide the heavy fraction (T_2, DT, D_2) as a product. This third column also receives the intermittent waste stream from isotope rebalancing in a buffer vessel from which a constant flowrate is extracted to allow steady operation of the columns

The columns are operated at a pressure cascade in the direction of tritium enrichment in order to drive the flow in that direction. This requires the use of blowers in the reflux streams. Equilibrators are then employed in streams between columns. As they are operated at higher temperatures than the cryogenic columns *economizer* heat exchangers are used to recover some of the energy required.

While relying on a complex internal architecture in order to achieve the necessary separations, the overall system performance is only determined by the flowrates and atomic composition of the two product streams. The system has to provide a tritium rich stream with a protium concentration below the allowable limit in the fuel as well as a protium rich stream with a maximum tritium concentration to be able to be further detritiated in the LPCE column of the water detritiation sytem.

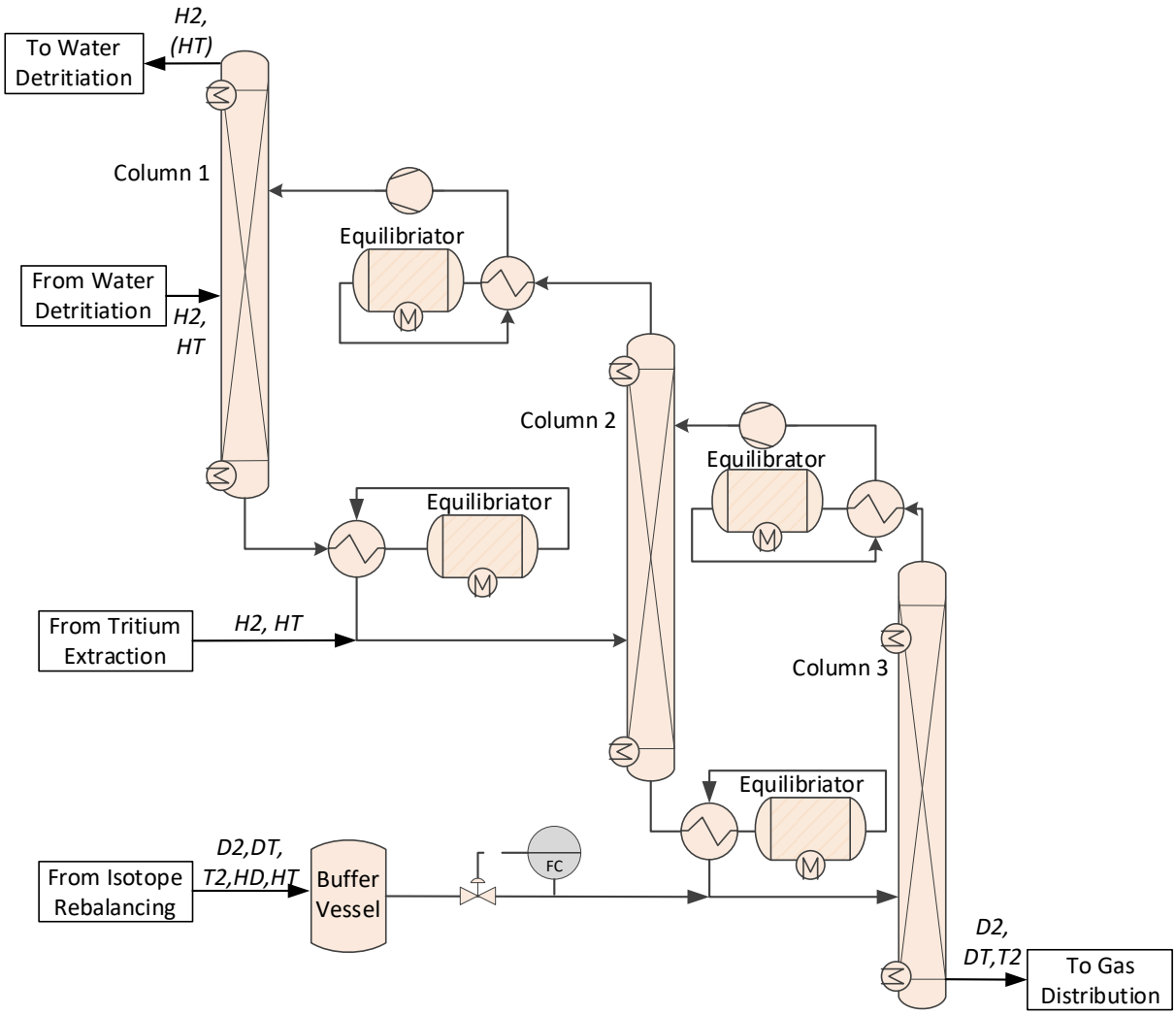

Figure 3.12: Architecture of the isotope separation system based on cryogenic distillation and isotopic equilibrators. Three columns form a cascade in increasing tritium concentration and reducing protium content with feed streams introduced at the appropriate locations. Isotopic equilibrators are used in-between columns, promoting the formation of homogenous isotopologues. Flow through the system is driven by a cascade in operating pressures, requiring the use of blowers in the reflux stream off the top of columns two and three.

3.2 Reference Operating Point

A reference point for the throughputs of the fuel cycle can be obtained from the available interface information (section 3.1.1) and by specifying targets for the performance of each systems characteristic as outlined in sections 3.1.2 to 3.1.9. Assuming steady state operation a set of material and components balances around all systems providing separation functionalities can be used to obtain a first evaluation of the throughputs and composition of the streams between all systems. This serves as an important first cornerstone in developing a quantitative understanding of the fuel cycles processing loops by providing an assessment of how much tritium is routed through each system block.

Wherever possible, performance targets have been selected to retain the pre-concept design status of the system as reported in [19], where none were available they have been selected to achieve an operation point of the fuel cycle satisfying all boundary conditions. This design and operating point has been holistically optimized with regards to the fuel cycle figures of merit when compared to earlier iterations of the EU-DEMO fuel cycle (e.g. reported by Hörstensmeyer in [43]) that were largely based on ITER fuel cycle extrapolation. Priority is given to minimum tritium inventories and discharges. The following performance specifications yield a design point that achieves all goals regarding the fuel availability, fuel composition and tritium discharges:

- The fuel separation system directly recycles 80% of all hydrogen contained in the torus exhaust.

This requirement is a trade-off between the achievable performance and number of the installed metal foil pumps, and load on downstream systems. While ideally as much hydrogen as possible should be separated, this is limited by the available space and achievable performance of the metal foil pump. A hydrogen separation efficiency of 80% is considered achievable with the available number of vacuum pumping ports and space therein [39]. In terms of the fuel recycling boundary condition R_F this means that all hydrogen not recovered by the fuel separation system has to be recovered by the exhaust processing system, or the full OUTL process path.

- The first two permeation stages in the exhaust processing system each recover 95% of the contained hydrogen in their feed stream.
- The getter bed stage achieves an integral recovery of 90% of the contained hydrogen in its feed stream.

These requirement on the exhaust processing system are tailored to the maximum demonstrated achievable performance with the employed technologies [44] [45]. Maximizing these requirements aims to retain as much tritium as possible in the inner fuel cycle. Any tritium not recovered in the inner fuel cycle has to be recovered by the much larger OUTL systems, increasing their tritium inventories and stack discharges.

- The isotope rebalancing and protium removal system processes 2.5% of the total torus gas throughput.
- 15% of that processing stream is then routed to the isotope separation system.
- 90% of the total contained protium is sent to the isotope separation system.
- No more than 10% of the total tritium contained in the feed stream is discharged to the isotope separations system.

In combination these requirements on the IRPR system are conservatively selected to match the projected performance of temperature swing absorption system which is still in development [46]. The total processing fraction remains a free parameter that can be adapted according to the fuel rebalancing plant boundary condition $R_{H/D/T}$ with the current selection driven by protium excess and aimed at ensuring a fuel protium limit of 1%. Improvements in the system performance potentially allow for further reduction of the flow fraction and tritium content of the stream that is routed to isotope separation in the OUTL.

- The exhaust detritiation system achieves a detritiation factor of $DF = 1000$.
- The exhaust detritiation system is operated at $p = 1.01$ bar and $T = 30$°C with a vapor to liquid ratio of unity.

The overall detritiation factor is based on conservative, experimentally demonstrated values achievable with technical feasible column heights at the process conditions employed [47]. A vapor to liquid ratio not exceeding unity aims to minimize the generation of tritiated water, only producing the same amount as initially contained as humidity in the stream.

- The tritium atom fraction in the hydrogen stream sent from WDS to ISS is $z_T = 1 \cdot 10^{-5}$.
- The tritium atom fraction in the protium product of WDS may not exceed $z_T = 1 \cdot 10^{-10}$.
- The LPCE column is operated at $p = 1.20$ bar and $T = 50$°C.

The specification of the water detritiation system is limited to an overall five order of magnitude detritiation factor, achievable by technical scale systems [48]. The tritium fraction of the high concentration tritium stream is then limited to the given value in order to ensure liquid water activities of less than 100 Ci.kg^{-1} in the system electrolyzer. Allowing for an increased tritium concentration in this stream can lower the total flowrate sent to isotope separation at the cost of a more challenging operation environment for the employed electrolyzer. The operating conditions are set at typical values.

- The tritium atom fraction in the stream from ISS to WDS may not exceed $x_T = 1 \cdot 10^{-8}$.
- The ISS product may at least be 70% tritium with a maximum protium contamination of 0.1%.

The tritium fraction of the return stream to WDS is selected as an interim value between WDS and ISS enrichment levels in order to allow the stream to integrated along the length of the LPCE column of the water detritation system. The specification of the fueling product is a trade-off between limiting the tritium inventory in the last cryogenic distillation column of the isotope separation system, while still maintaining high enough tritium fractions in the fueling product to be suitable to correct any deuterium excess of the fuel mixture in the composition control system.

Based on these specifications Table 3.5 reports the throughput of deuterium and tritium between systems of the inner fuel cycle as a fraction of the total amount fueled to the plasma chamber during flat-top operation, amounting to 0.57 g.s^{-1} of tritium and 0.38 g.s^{-1} of deuterium. Figure 3.13 then shows a graphical representation of the tritium throughput (a) and resulting volumetric flows (b). While tritium throughputs in the inner fuel cycle are highest, the outer fuel cycle processes significantly higher volumetric flows, with the exception of vacuum lines, at lower tritium concentrations.

Table 3.5: Evaluated tritium and deuterium throughputs (as % of the nominal Torus input) of the inner fuel cycle during steady state operation for the reference design point. Bold entries indicate the total product stream of a fuel cycle loop.

From	To	T as % of Torus input	D as % of Torus input
Pellet Injection	Torus	88.4%	88.4%
Gas Injection	Torus	0.0%	0.0%
Gas Puffing	Torus	11.6%	11.6%
Torus	Fuel Separation	99.4%	99.4%
Fuel Separation	**Gas Distribution**	**79.5%**	**79.5%**
Fuel Separation	Exhaust Processing	19.9%	19.9%
Exhaust Processing	**Exhaust Detritiation**	**0.005%**	**0.005%**
Exhaust Processing	Isotope Rebalancing	19.9%	19.9%
Isotope Rebalancing	Isotope Separation	0.2%	0.5%
Isotope Rebalancing	**Gas Distribution**	**19.6%**	**19.4%**

Next to the individual atomic component balances, the outer fuel cycle also requires the consideration of humidity in air and gas streams. As only lightly tritiated water is routed between systems, negligible impact of the HTO content on the humidity vapor pressure is assumed and the NIST formulation of the Antoine equation with parameters of Stull [49] for the vapor pressure of water has been used to calculate water vapor fractions at the indicated pressures and temperatures. Table 3.6 reports the tritium throughput in streams in either hydrogen or water form, related to the flat-top burn up-rate of ($3.56 \cdot 10^{-3}$ $g.s^{-1}$, 2.68 $Pa.m^3s^{-1}$ DT or 1.34 $Pa.m^3s^{-1}$ T_2). Values are time-averaged over the burn-dwell behavior of the machine, which leads to the sum of all bred tritium not reaching 100% of the flat-top burn up. While the inner fuel cycle is independent of the employed breeding blanket in the outer fuel cycle both variants have to be considered individually.

Table 3.6: Calculated tritium throughputs of the outer fuel cycle (time averaged over burn-dwell cycling) as percentage of the flat-top burn up, assuming technology performance parameter as specified in section 3.2.

From	To	T as % of burn-up (WCLL)	(HCPB)
Tritium as Hydrogen (time averaged)			
Tritium Extraction	Isotope Separation	92.2%	92.1%
Water Detritiation	Isotope Separation	0.97%	1.37%
Isotope Separation	Water Detritiation	0.001%	0.002%
Isotope Separation	*Gas Distribution*	*132.9%*	*133.2%*
Tritium as Humidity/Water (time averaged)			
Coolant Purification	Water Detritiation	0.146%	0.464%
Exhaust Detritiation	Water Detritiation	0.82%	0.82%
Tritium Extraction	Water Detritiation	-	0.081%
Rooms	Exhaust Detritiation	0.03%	0.03%

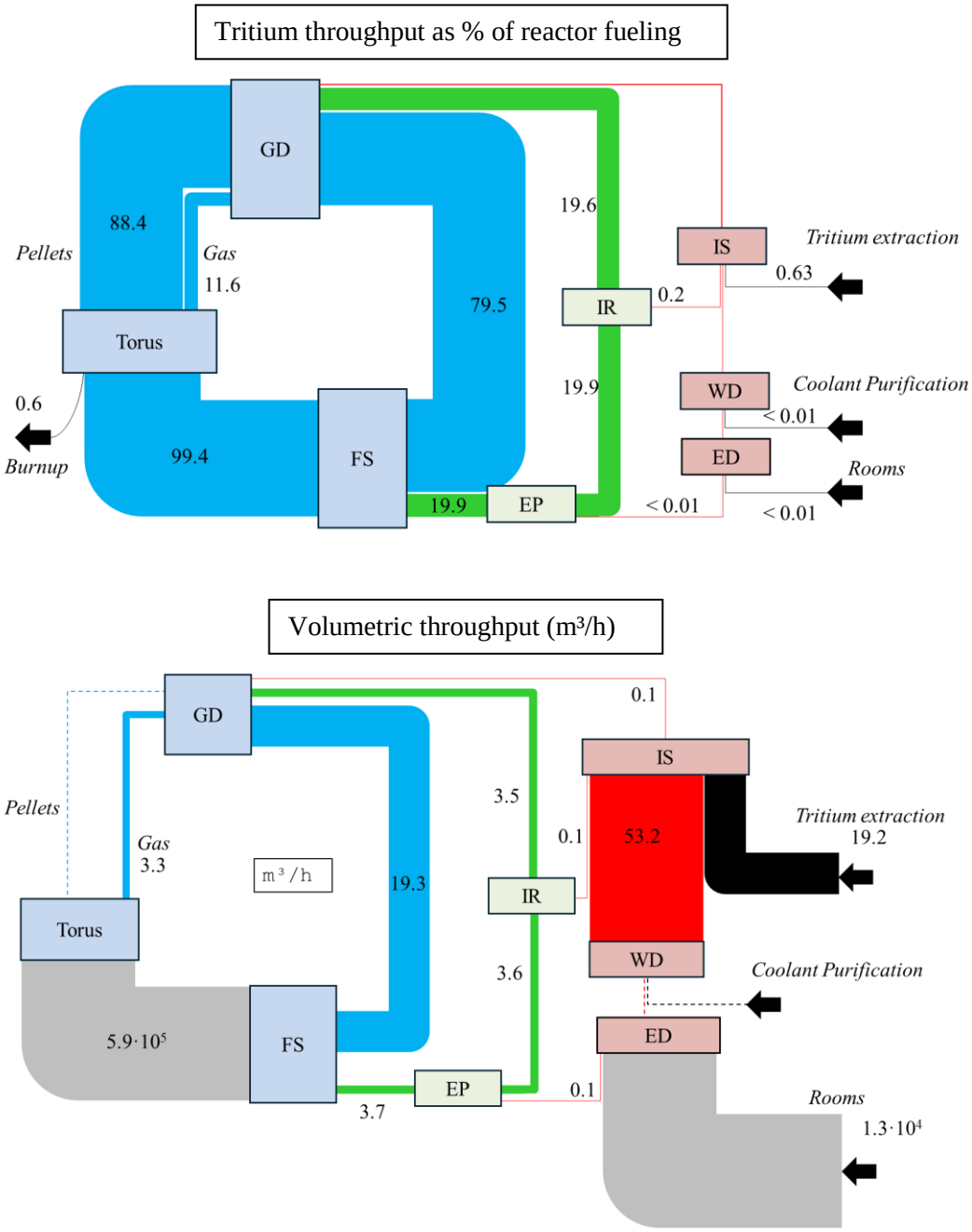

Figure 3.13 a) (Top): Weighted representation of the fuel cycle tritium throughputs as percentage of the total reactor input. b) (Bottom): Weighted representation of the volumetric throughput in m³/h. dashed lines indicate solid or liquid flowrates. Grey lines had to be limited to the maximum line weight and are not represented to scale.

In terms of the global plant boundary conditions this design point corresponds to:

- A tritium conversion rate of $R_F = 0.0063$, based on the hydrogen fueling rate of 430 Pa.m³s^{-1} containing 1% protium and burn-up rate of 2.68 Pa.m³s^{-1} DT.
- An isotopic rebalancing fraction of $R_{H/D/T} = 0.025$ which is obtained as a direct consequence of the specification of the feed rate of the isotope rebalancing and protium removal system. In the limiting case of a protium fuel imbalance a maximum source term of $\Delta F_H = 0.1$ Pa.m³s^{-1} should therefore not be exceeded in order to obtain long term steady state operation with an allowable maximum fuel protium fraction of 1%.

- The tritium processing load received from the tritium extraction interface corresponds to a tritium extraction ratio of $R_{\mathrm{E}} = 1.05$.
- The tritium processing load for recovery from interfaces corresponds to a tritium recovery ratio of $R_{\mathrm{R}} = 0.011$ (WCLL) and $R_{\mathrm{R}} = 0.015$ (HCPB), taking also into account tritium discharged to the EDS from the inner fuel cycle.

The 3-loop fuel cycle architecture provides a clear separation between inner and outer fuel cycle managing to effectively establish two areas of tritium flow. One is the inner fuel cycle where large throughputs of deuterium and tritium are being processed with a focus on purification and maintaining their isotopic balance, and the other is the outer fuel cycle where mainly tritium admixed with protium is being processed with the focus of obtaining a tritium stream in fuel quality.

The inner fuel cycle is tapered off along the DIRL and INTL loops, gradually reducing the processing load in each system and acting as barriers towards the OUTL. In total the inner fuel cycle injects 48.8 kg tritium per full power day into the plasma chamber of which 99.74% of the unburnt fuel are then recovered in the DIRL and INTL. Of then non recovered tritium (124 g.day^{-1}) only 2% are sent to exhaust detritiation, with the remainder directly sent towards isotope separation. This configuration also requires the make-up of 230 g deuterium per full power day, of which 204 g.day^{-1} are due to burn-up.

The total amount of tritium to be processed in the outer fuel cycle is 416 g.day^{-1} with the largest individual tritium flow extracted from the breeding blankets at 290 g.day^{-1} (time averaged over burn and dwell). Of this tritium only 0.92 g.year^{-1} are discharged from the stack via exhaust detritiation, complying with a discharge limit of less than one gram tritium per year. Additionaly, 0.06 g.year^{-1} are contained in the detritiated hydrogen generated by WDS which is reused internally. All other tritium is then ultimately enriched to fuel quality (adjusting the H and D content) in the isotope separation system. Compared to the first design point reported in [43], predicting stack discharges of 1.6 g.year^{-1}, this marks a 58% reduction in chronic radiological releases while processing the same tritium fueling rate.

While such a steady state assessment is crucial in developing a first quantitative understanding of the fuel cycle operation point, it is unable to address questions arising from its transient operation. First and foremost is the issue of fuel availability. While the steady state mass balances indicate sufficient supply of fuel and an excess of tritium due to breeding, it has also to be demonstrated that it is available when needed, and that the on demand supply is not impeded by transient effects. This is closely linked with the need to demonstrate that operational tritium inventories in systems do not fluctuate excessively, temporarily building up in undesirable system parts and posing a potential safety hazard. Additionally, even if sufficient fuel is available, no transient deviations in its isotopic ratio should occur that exceed the capabilities of the composition control system. This can lead to the supply of fuel to the plasma with the D/T isotope ratio or protium content out of specification, potentially threatening its stability or reducing the fusion power. Lastly, while time averaged environmental discharges are acceptable it also has to be ensured that regulatory limits are also not temporarily exceeded.

All of these effects are strongly related to the performance of the processing and separation technologies experiencing transient loads and operating in a closed loop. In order to judge the validity of a fuel cycle design and to be able to alleviate the raised concerns, a rigorous dynamic simulation of the integral fuel cycle using physics based models has been developed.

4 Process Engineering Models of Fuel Cycle Components

Process modelling and simulation is a common tool in the design, engineering and evaluation of chemical process plants with a wide variety of commercial tools available, such as Aspen Plus [50], HYSYS [51], gPROMS [52], or DWSIM [53]. For these commercial applications dynamic process simulation, however, is often not a primary functionality as production plants are designed and operated in steady state and transients ideally only occur in commissioning or shut-down phases during which typically no product is obtained. The fuel cycle of a Tokamak fusion power plant on the contrary is always in a transient state because of its pulsed operation mode or to support other operation phases (e.g. maintenance) of the plant. At the same time the fuel cycle uses a variety of technologies and systems not typically employed in commercial production plants. As such, commercial tools cannot simply be transferred to the fuel cycle.

With respect to fusion there is a history of custom codes for full scale fuel cycle simulation in literature, predominantly focused on the ITER fuel cycle. This is most notably the work of Busigin [54] and the code CFTSIM [55] which has later been progressed into TRIMO [56]. These codes all are dynamic simulations of the ITER fuel cycle, largely relying on the user specification of individual system performances and target compositions with only the ITER isotope separation system being modelled on a physics basis in TRIMO. Simultaneously, there also exists a large body of work in literature for the detailed modelling and simulation of individual technologies specific to fuel cycle applications and tritium processing that can be exploited. A quantitative, steady state assessment of the first EU-DEMO fuel cycle iteration has been performed in a predecessor work by Hörstensmeyer using a series of such models and is reported in [43].

4.1 Simulation Requirements and Modelling Techniques

If aiming to build a fully closed loop, dynamic, and physics based simulation framework for a continuous DT fuel cycle, a first step is in identifying the core functionalities required. These should enable to fully investigate the transient behavior and performance of the fuel cycle and ultimately demonstrate the achievement of its requirements and performance goals. The integral fuel cycle design is primarily concerned with the transport of tritium through its systems to derive time dependent inventories, quantifying potential releases to the environment, and confirming the availability of tritium in the specified purity for fueling under transient operation. These directly relate to a set of requirements that a simulation tool needs to match.

- **All tritium carrying streams** part of the closed fuel have to be included in the simulation domain to obtain fully closed tritium mass balances at each point of the simulation.

  In a dynamic system, closed mass balances are only achieved if the **transient behavior** of all hold-ups in composition and total inventory in each relevant location can be evaluated in the necessary temporal resolution. The relevant time scales hereby are directly derived from the transients introduced from the interface of the plasma chamber, with the plasma being operated in flat-top for two hours, and transitioning in and out of the ten minute dwell state by ramp-down and ramp-up phases occurring over 100 – 200 seconds. Simultaneously, the

upper simulation horizon needs to cover not only the characteristic time of single components, but also that of the resulting process chain of interlinked systems.

- **Any mass transfer processes** employed in each system associated with a separation of tritium into multiple streams is modelled physics based where possible to enable a consistent representation of the separation behavior and performance with dynamic boundary conditions. This necessitates the use of detailed models for all technologies providing a principal separation functionality. The usage of physics based models incorporating the adoption of **all relevant species** besides tritium that offer physical or chemical interactions therewith.

- Next to these internal requirements the simulation tool must offer usability in the wider context of the fuel cycle design by being **able to interface with system design tools** and common dimensioning methods. While the tool itself is aimed at evaluating a single given fuel cycle design at a time, parity between the system in the fuel cycle simulator and their design has to be achieved to allow synchronization. The simulator thus has to allow for easy implementation and adaption of relevant design data and parameter.

- All of these requirements lead to a complex simulation, combining detailed physics models for individual technologies with the vast architectural scope of the integral fuel cycle. The tool nevertheless needs to be **efficient and maintainable**. As such, simplifications are employed wherever possible to reduce the overall intricacy of the tool thus keeping its further application and continued development feasible.

- Finally, being a first of its kind tool, the **reliability and trustworthiness** of results has to be established. Next to correct representation of underlying physical processes in individual systems and process chains, this also requires the correct application of numerical methods using adequate temporal and spatial resolution.

In order to adhere to the above requirements on the simulation, a number of established techniques and best practices documented in literature are used in building the simulation tool and models.

Technique one: The simulation is built to mirror the fuel cycle architecture on all levels. The overall system block architecture is reproduced as well as the component based sub-system level. For every sub-system each component that provides a major processing functionality is included. In order to still obtain a manageable and lean tool, minor auxiliary components such as filters, pumps, pressurizer, and heaters that are only used to achieve a given set-point of major equipment are not included. Instead, the set-point of the component is specified directly assuming that all auxiliary equipment is sized adequate as to achieve the required conditions.

Technique two: Components and equipment models are connected by material streams which represent the physical flow of matter through the fuel cycle. Depending on the area of the fuel cycle, a stream may contain different species. The species a stream can carry are:

- All molecular hydrogen isotopologues of the atomic constituents protium (H), deuterium (D), and tritium (T), giving the molecules H_2, HD, HT, D_2, DT, T_2.
- All water molecules with isotopic hydrogen constituents, H_2O, HDO, HTO, D_2O, DTO, T_2O.

- Other gases, helium-3 (^{3}He), helium-4 (^{4}He), argon (Ar), xenon (Xe), oxygen (O_2), nitrogen (N_2).
- Gaseous impurities containing carbon collectively modelled as CD_2T_2, representing carbon based impurities in the inner fuel cycle.

In order to limit the numerical complexity, models only include and compute species expected to be present in the system.

Technique three: Conservation of mass is used for all areas of hold-up for total mass and individual species by specifying dynamic conservation equations of the form

$$\frac{dN}{dt} = \Delta F + \Delta \Phi. \tag{4.1}$$

The left hand side represents the transient change of a molar hold-up N which is acted upon by the right hand side which marks the total difference (Δ) of all of molar flows F in or out of the balance volume as well as any sinks or sources occurring within the volume denoted by Φ.

This conservation cannot only be applied to the total hold-up of matter in a balance area but also the hold-up of individual species i in a mixture with a molar fraction in the mixture of z_i, giving

$$\frac{d(z_\mathrm{i} N)}{dt} = \Delta(z_\mathrm{i} F) + \Delta \Phi_\mathrm{i}. \tag{4.2}$$

Above equations are the principal foundation for each dynamic component model by specifying at least one balance area. If only one balance area is specified the volume of the component is assumed to be ideally mixed with volume averaged properties and compositions applying in all locations of the balance area. The continuous integration of these balances and computation of the time evolution then requires the specification of a known initial state providing values for the total hold-up $N(t = 0)$ and composition $z_i(t = 0)$. Hold-ups are directly linked to the physical dimension of the respective element. Two different types of hold-up are common in the system of the fuel cycle, namely gaseous and liquid hold-up. The former may be evaluated from the volume of the unit using the ideal gas law, whereas liquid hold-ups are derived from the liquid occupied volume and molar density of the fluid.

By applying these equations to each unit model they effectively govern the dynamic behavior of each unit and system, as well as the integral fuel cycle model by linking the instationary state of each model ($N(t), z_i(t)$) to the occurring flows and mass transfer processes in each unit. Their application to the individual unit models is further described in section 4.3.

Conservation of Energy

Similar to the conservation of mass, energy conservation may be modelled by specifying a dynamic energy balance, tracking the change in the internal energy of a volume element by accounting the incoming and outgoing energy streams. For a fluid element this is typically convective transport via flows and their specific enthalpy h, as well as heat sink or source terms Q via convection or radiation. As dynamic energy balances are typically used to obtain information on the temperature evolution of a system they are commonly expressed using temperature as the only time variant variable by assuming non-temperature dependent fluid properties, giving

$$Nc_{p,m}\frac{dT}{dt} = \Delta(Fh) + \Delta Q, \tag{4.3}$$

where $c_{p,m}$ is the molar heat capacity of the system.

For the modelling of the fuel cycle and its technologies this approach is however only used in select applications and models where energy balances are required for the description of the relevant physical processes, or transient temperature evolutions are expected or required by the operating principle of the modelled technology. These cases are detailed in the respective sections of Chapter 4.3. For the majority of the systems and components their operation is assumed isothermal ($dT/dt = 0$) for a variety of reasons. By design, all systems that do not require a specified operating temperature are maintained close to ambient temperature to limit tritium permeation, which is facilitated by elevated temperatures. This is implemented by employing active cooling on pumps and compressors, as well as temperature control of secondary confinements. Equipment that requires elevated or a specific set-point temperature is required to be equipped with temperature control in order to ensure its specified operation point can be maintained. In these cases isothermal models are implemented, allowing the parametric specification of the operating temperature to simplify the obtained equation system and reduce the numerical complexity.

Technique four: Mass transfer is modelled using either an equilibrium stage or rate based mass transfer model in up to one spatial dimension.

The formulation of equations (4.1) and (4.2) does not allow for the description of gradients within a single volume. If a gradient within a component is essential to its function (e.g. a concentration profile along a distillation column) the component is modelled by a series of balance areas or volume elements in the direction of the gradient adding a spatial dimension to the model. Such gradients typically establish as a result of mass transfer processes or chemical reactions and are the fundamental operating principle in many separation technologies. Two principal methods to model them are employed in the simulator.

Most fundamentally such processes can be described by considering the total rate of mass transfer or reactions taking place and calculating it as sink or source terms Φ_i in each volume element dV. The driving force for such a mass transfer is the offset from a state with minimal thermodynamic potential, commonly referred to as equilibrium state. A generic formulation of this rate is given by

$$\Phi_i = k \cdot dV \cdot (z_i - z_i^*)^n, \tag{4.4}$$

where k is the rate coefficient, dV the volume element, n is the order of the process involved, and $*$ is used to indicate the value corresponding to an equilibrium state of an offset property (in this case composition). A more detailed description of employed rates is given in the subsequent chapters relevant to each technology model where rate based mass transfer models are used.

An alternative description of such mass transfer processes and reactions is obtained if the overall rate is fast compared to the ratio of throughput and hold-up of the volume (also referred to as residence time τ). Under these conditions the composition in the balance area converges to the equilibrium state such that $z_\mathrm{i} = z_\mathrm{i}^*$ for outgoing flows, yielding a theoretical equilibrium stage. Figure 4.1 shows a sketch of the numerical domain for both model types in a two-phase counter current arrangement, indicating all transport pathways. The molar fractions of phase A have been

labeled *y*, commonly used to refer to a vapor fraction, and molar fractions of phase B have been labeled *x*, typically used to refer to a liquid fraction.

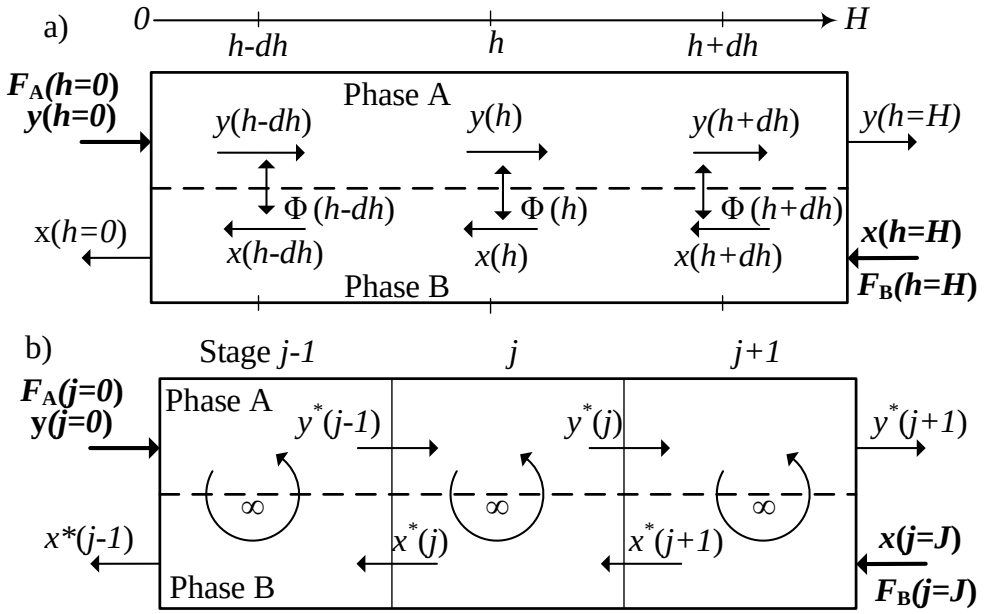

Figure 4.1: Mass transfer models in the fuel cycle simulator. Rate based models (a), top) rigorously calculate the rate of transfer of each species between two phases in a spatial dimension. Equilibrium models (b), bottom) assume that the residence time in a discretized volume element is large enough to establish thermodynamic equilibrium conditions. Bold labels indicate variable values that have to be specified as boundary condition.

The total number of discretization elements for both models is determined differently. For rate based models a sufficiently large number of elements has to be specified to achieve grid independence and not impact the results. In the case of the equilibrium model the number of elements is directly linked to the physical dimension of the component, determined by the volume needed for each element to satisfy the equilibrium condition. Consequently the total number of elements affects the separation performance.

Both models can then be solved numerically by computing the total and species balances (eq. 4.1 and 4.2) for each element and phase using the applying equilibrium conditions or mass transfer rates and integrating the obtained equation system with time. Next to initial conditions for hold-ups of each individual species, boundary conditions must also be specified. These are typically provided in the form of fixed value (in each time-step) on one stream on each opposing end, as well as zero-gradient on the corresponding other end. These two model types serve as the basis for each separation technology model for which they are adapted according the types and number of phases present.

Technique five: The trustworthiness of generated results is derived from validated literature models and verification of their correct implementation.

Since the decommissioning of the Tritium System Test Assembly in 2001, no integrated tritium test facility or large scale tritium processing facility has been in operation, disallowing the direct comparison of the integrated simulation to experimental results [57]. Instead, the following indirect approach is used:

- The simulation is built on the use of state-of the art validated literature mass transfer models previously successfully employed in relevant areas of tritium processing. Selected models and their sources are presented in section 4.3.
- The physical correct linkage of mass transfer models into larger process chains is ensured by strictly maintaining numerical validity criteria for all transport properties by assuring time and space discretization adhere to the Courant–Friedrichs–Lewy (CFL) condition, grid independence is achieved in 1-D models, and sufficiently small solver tolerances are selected. The numerical implementation into a simulation environment is discussed in section 5.1 and an exemplary sensitivity study of these parameters is provided in section 5.2.
- As the dissemination of dynamic responses, if receiving multiple transient inputs or superposition thereof, in multiple variables is often ambiguous, the correct implementation of mass transfer and auxiliary models in a dynamic environment is verified by testing each system assembly of models in a controlled stand-alone environment and applying single-variable step changes, allowing the verification of physical behavior in the system response.

In combination these three aspects yield the best validation status achievable with the current availability of integrated experimental results.

4.2 Thermodynamic Principles Used in Component Models

Evident by the conservation equations, the dynamic characteristics of each component model are a function of the total flowrates and mass transfer or reaction rates. While total flowrates are determined by forced or controlled flow, mass transfer rates depend on the equilibrium state and achievable mass transfer coefficient. Here, the thermodynamic basis of the fuel cycle simulator is introduced starting with a collection of pure component data of relevant species and then developing mathematical formulations for the different types of equilibria exploited in the technologies of the fuel cycle systems.

The in-depth study of single component and mixture properties is a field in and on itself and has led to the complete characterization of countless substances with great accuracy which are collected in property databases such as the NIST Standard Reference Database [58], REFPROP [59], CODATA [60], and Dortmund Data Bank [61]. However, if isotopic constituents are involved and especially in the case of tritium, relevant compounds are often not at all or only partially featured. As any mass transfer model in the fuel cycle simulator is foremost focused on the transport of hydrogen isotopes and their molecules, their property data and thermodynamic behavior is an essential building block of each model. The required formulation of property data and equilibrium descriptions involving hydrogen isotopes is therefore taken directly from primary sources in literature, often in narrow ranges relevant to the application at hand and reported in the following.

Treatment of hydrogen spin-isomer states

Hydrogen molecules are known to form nuclear spin isomers with either parallel spin states (odd quantum number of minimum J = 1), or with anti-parallel spin states (even quantum numbers of minimum J = 0). At room temperature hydrogen is present as a mixture of molecules with both spin states, referred to as normal hydrogen. The mixture ratio is temperature dependent and tends towards lower energy states at lower temperatures (ultimately towards minimum energy at J = 0). However, the equilibrium composition of homogenous isotopologues (H_2, D_2, T_2) is meta-stable

and any complete deexiatation on cooling down proceeds only spontaneously and may take hours to days [62].

For the purpose of this work all property & equilibrium data is reported and used for normal hydrogen for homogenous molecules and for equilibrium hydrogen for heterogeneous molecules.

4.2.1 Pure Component Property Data

Constant Properties

Any component is most fundamentally characterized by its molecular mass, triple point and critical point which are not dependent on external conditions such as pressure and temperature of the system. For common species and molecules these can be obtained from the aforementioned databases. For the isotopologues of hydrogen they are reported in Table 4.1.

Table 4.1: Constant properties of hydrogen isotopologues. Data from [63].

Species	**H_2**	**HD**	**HT**	**D_2**	**DT**	**T_2**
Molecular Weight MW (g.mol^{-1})	2.016	3.022	4.024	4.028	5.030	6.032
Critical Temperature T_c (K)	33.24	35.91	37.13	38.35	39.42	40.44
Triple Point Temperature T_t (K)	13.97	16.60	17.70	18.69	19.79	20.62
Critical Pressure p_c (bar)	12.93	14.84	15.71	16.5	17.73	18.50
Triple Point Pressure p_t (Pa)	7200	12370	14580	17150	20080	21600

Vapor Pressure

Water

Several streams in the fuel cycle carry humid gases, and the exhaust detritiation and water detritiation systems require the presence of humidity as part of their operating principle. The vapor pressure p^*_{H2O} of ordinary water is calculated from the NIST reference formulation of the Antoine equation with parameters of Stull [49]

$$\frac{p^*_{H2O}}{Pa} \cdot 10^{-5} = 10^{A-\frac{B}{C+T}}. \tag{4.5}$$

In which T denotes temperature and A, B, C mark species dependent parameters.

The vapor pressures for other water isotopologues p^*_{Q2O} can then be calculated via their vapor pressure isotope effect relative to H_2O as given by van Hook [64]:

$$\frac{p^*_{H2O}}{p^*_{Q2O}} = \exp\left(\frac{A_{Q2O}}{T^2} + \frac{B_{Q2O}}{T} + C_{Q2O}\right). \tag{4.6}$$

Parameter for use in equation (4.5) and (4.6) are given in Table B.1 in the Appendix and Figure 4.2 shows a plot of the isotope effect and resulting vapor pressures as a function of temperature. For a given temperature, vapor pressures decrease monotonically with molecular mass, with the strongest isotope effect observed for T_2O. The effect grows more pronounced towards lower temperatures.

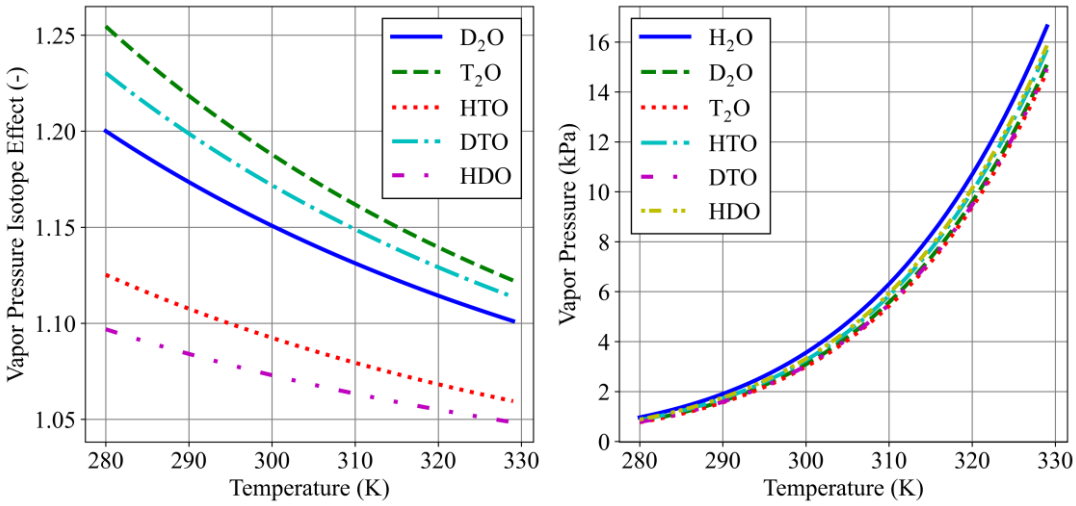

Figure 4.2: Left: relative vapor pressure isotope effect of water isotopologues as a function of temperature when compared to pure H_2O [64]. Right: Resulting absolute temperature dependent saturation vapor pressures using the NIST reference H_2O vapor pressure [49].

Hydrogen

Numerous vapor pressure correlations based on experimental investigations are available in literature, however most are only derived from measurements of an incomplete set of isotopologues often excluding tritiated molecules. The primary sources for tritiated species are the work of Grilly (1951) [65], Souers (1979, 1986) [63],[66] and Sherwood (1989) [67]. Here the equation of Souers is used as it provides as consistent expression for all six isotopologues with parameters as given in Table B.2 in the Appendix. Figure 4.3 then shows the hydrogen isotopologues vapor pressure from 15 to 25 K. At atmospheric pressure the resulting boiling point spans a range from 20.4 K to 25.0 K between H_2 and T_2, exhibiting the largest vapor pressure isotope effect of any substance.

$$\frac{p_i^*}{Pa} = \exp\left(C_1 + \frac{-C_2}{T} + C_3 \ln\left(\frac{T}{K}\right)\right) \tag{4.7}$$

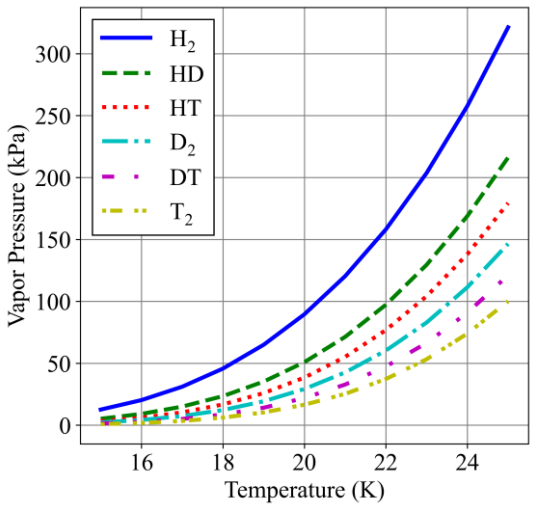

Figure 4.3: Vapor pressure of hydrogen isotopologues computed from the correlation of Souers [63].

4.2.2 Equilibrium States

A system is considered in thermodynamic equilibrium if it is simultaneously in mechanical equilibrium (homogenous pressure), thermal equilibrium (homogenous temperature) and chemical equilibrium (homogenous chemical potential). The following equilibria are used in the mass transfer models of the fuel cycle simulator.

Hydrogen Single Phase Isotopic Equilibrium

The three hydrogen isotopes protium (H), deuterium (D) and tritium (T) are able to form six corresponding binary molecules (isotopologues) of H_2, HD, HT, D_2, DT, T_2 which always co-exist given the presence of all isotopic constituents and naturally tend towards a chemical equilibrium composition which can be expressed by formulating isotope exchange reactions and the corresponding law of mass action. In theory any isotope exchange reaction between two hydrogen molecules of arbitrary constituents is possible, giving the following reaction pathways:

$$\begin{aligned} Q'Q' + Q^{\circ}Q^{\circ} &\leftrightharpoons Q^{\circ}Q' + Q'Q^{\circ} && \text{(a)} \\ PQ + QP &\leftrightharpoons QP + PQ && \text{(b)} \\ PP + QQ &\leftrightharpoons PQ + PQ && \text{(c)} \\ PP + QR &\leftrightharpoons PQ + PR. && \text{(d)} \end{aligned} \tag{4.8}$$

Here Q, P, and R refer to an arbitrary but always unique isotope of hydrogen.

The first reaction represent the spontaneous exchange of a hydrogen atom of the same isotope between two homogenous isotopologues. Even though this process is ever occurring it has no practical relevance on the total molar balance of that species within a system and is thus not further considered. The second reaction represent the same process now between two of the same heterogenous isotopologues. This reaction is also not further considered for the same reason as reaction one. Reaction three then marks the isotope exchange between two different homogenous isotopologues forming two of the resulting heterogenous isotopologues. This reaction leads to a change in hold-up of each reactant and as such the corresponding equilibrium composition is of considerable importance. Reaction four may be similarly considered. However, a system of all three hydrogen isotopes is fully determined by the equilibrium composition of the six isotopologues which can be derived from three equilibrium constants and atomic balances for each of the three constituents. Both can already be formulated for reaction (4.8) (c) yielding the required six equations. In the following reaction (4.8) (d) is therefore not further considered due to its higher complexity.

The equilibrium constant for reaction (4.6) (c) is then given by

$$K_{\mathrm{QP}} = \frac{[PQ]^2}{[PP][QQ]} = \mathrm{A_{QP}} \cdot \exp\left(-\frac{\mathrm{B_{QP}}}{T}\right). \tag{4.9}$$

With values for the parameters A, B for each reaction fitted by Peters [68] to the data of Urey [69] as given in Table B.3 in the Appendix.

Figure 4.4 shows a plot of the temperature dependent equilibrium constants for all three possible reactions. As can be seen the equilibrium tends towards favourable presence of the homogenous isotopologues at lower temperatures which exhibit a theoretical 100% abundancy at 0 Kelvin.

Towards higher temperatures the equilibrium shifts towards a purely stochastic distribution which, for an equimolar binary system, leads to the presence of 50% of the homogenous and heterogenous isotopologues, with the latter again equimolar distributed. As a consequence all possible isotopologues are always expected to be present in a system containing at least two different isotopes.

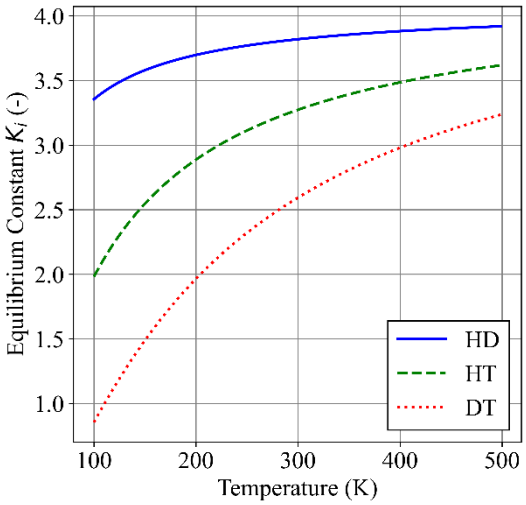

Figure 4.4: Temperature dependent equilibrium constants of the isotopic equilibrium for heterogeneous isotopologues. At lower temperatures homogenous isotopologues are energetically preferred, reflected in lower values of equilibrium constants for mixed isotoplogues. At high temperatures the distribution approaches the statistical limit with K_i converging to four.

Hydrogen – Water Isotopic Equilibrium

Next to isotope exchange between pure hydrogen molecules, hydrogen can also isotopically exchange with hydrogen in other molecules by the same mechanism. Within the scope of technologies employed in the fuel cycle this is especially of interest for the exchange between hydrogen and water. The system has a total of twelve constituents and is thus fully determined by six species balances and the reactions and associated equilibrium constants as given in Table 4.2. Correlations for the temperature dependence fitted to the data of Urey [69] are given in Table B.4 in the Appendix.

Table 4.2: Reactions between isotopic water and hydrogen isotopologues as well as the formulation for the associated equilibrium constant.

#	Reaction	Equilibrium
1	$H_2O + HD \rightleftharpoons HDO + H_2$	$K_1 = \frac{[HDO][H_2]}{[H_2O][HD]}$
2	$HDO + D_2 \rightleftharpoons D2O + HD$	$K_2 = \frac{[D_2O][HD]}{[HDO][D_2]}$
3	$H_2O + HT \rightleftharpoons HTO + H_2$	$K_3 = \frac{[H_2O][HT]}{[HTO][H_2]}$
4	$HTO + T_2 \rightleftharpoons T_2O + HT$	$K_4 = \frac{[T_2O][HT]}{[HTO][T_2]}$
5	$D_2O + DT \rightleftharpoons DTO + D_2$	$K_5 = \frac{[DTO][D_2]}{[D_2O][DT]}$
6	$DTO + T_2 \rightleftharpoons T_2O + DT$	$K_6 = \frac{[T_2O][DT]}{[DTO][T_2]}$

Figure 4.5 shows the resulting equilibrium lines for the exchange of hydrogen-tritide and hydrogen-deuteride with pure water (reaction 1 and 3 of Table 4.2). Both reactions show a preference for the heavier isotope towards the oxide form which is more pronounced for tritium and growing stronger towards lower temperatures.

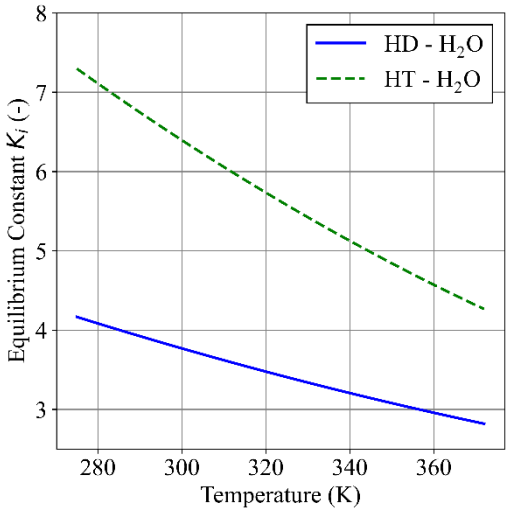

Figure 4.5: Temperature dependent equilibrium constants for the isotopic equilibrium between deuterated and tritiated hydrogen and water. The isotope effect is larger for larger mass differences between the constituents as well as at lower temperatures.

Vapor – Liquid Equilibrium

For the employed technologies in the processing systems of the fuel cycle two vapor liquid equilibria are of interest, namely that of hydrogen isotopes, as employed in cryogenic distillation in the isotope separation system, and that of water with different hydrogen isotopic composition at all interfaces between a gas and liquid stream such as in the exhaust detritiation system and water detritiation system.

Water

Isotopic mixtures generally form ideal mixtures and at pressures and temperatures relevant for the presence of water in liquid and vapor phases ideal gas behaviour is valid. For such an ideal system the vapor liquid equilibrium can then be described by Raoult-Daltons' law:

$$p y_\mathrm{i} = x_\mathrm{i} p_\mathrm{i}^*, \tag{4.10}$$

where p is the total pressure, y the molar fraction of species i in the vapor phase, x the molar fraction of species i in the liquid and and p_i^* is the saturation vapor pressure calculated using the formulation as given in section 4.2.1.

Hydrogen

The assumption of ideal mixture and ideal gas behaviour is no longer valid for the hydrogen system at cryogenic temperatures. A comprehensive model for the vapor liquid equilibrium has been developed by Sherwood and Souers [70] expanding the ideal Raoult-Dalton relationship by the use of fugacity and activity coefficients which then reads:

$$\phi_\mathrm{i} p y_\mathrm{i} = \gamma_\mathrm{i} x_\mathrm{i} f_\mathrm{i}^0. \tag{4.11}$$

Here, ϕ_i is the fugacity coefficient of species i, γ_i is the activity coefficient of species i and, f_i^0 its standard fugacity. For the vapor phase non-ideality the fugacity coefficient may be calculated from the second virial coefficient B, representing the deviation from the ideal gas behavior, as

$$\phi_\mathrm{i} = \exp\left(\frac{B_\mathrm{i} p}{RT}\right), \tag{4.12}$$

using an empirical correlation for $B_\mathrm{i} = B_{0,\mathrm{i}} \left(\frac{T}{20K}\right)^{-b}$ with parameter as given in Table B.5 in the Appendix. In this model the standard fugacity for species i is defined as

$$f_\mathrm{i}^0 = p_\mathrm{i}^* \exp\left(\frac{B_\mathrm{i} p_\mathrm{i}^*}{RT}\right), \tag{4.13}$$

using the pure component vapor pressure p_i^*as given in section 4.2.1. The activity coefficient γ_i can be evaluated from the Gibbs Free Energy of Mixing ($\bar{G}_\mathrm{i}^E$)

$$\gamma_\mathrm{i} = \exp\left(\frac{\bar{G}_\mathrm{i}^E}{RT}\right), \tag{4.14}$$

which in turn is calculated from the binary interaction parameter (A_ij)

$$\bar{G}_\mathrm{i}^E = \sum_j y_\mathrm{j} A_\mathrm{ij} - \frac{1}{2} \sum_i \sum_j y_\mathrm{i} y A_\mathrm{ij}\,. \tag{4.15}$$

A_ij is fitted to experimental data obtained from enthalpy of mixing measurements using equation 4.16. The parameter κ for each hydrogen isotopologue is given in Table B.6 in the Appendix.

$$A_\mathrm{ij} = 12.1 \frac{J}{mol} \left(\kappa_\mathrm{i}^2 - \kappa_\mathrm{j}^2\right)^{1.6} \cdot \exp[\left(\frac{14.74K}{T}\right)^6]. \tag{4.16}$$

From these relationships a temperature dependence for the liquid phase as well as a pressure and temperature dependence for the gas phase is observed. For atmospheric pressure as well as a mixture of equimolar parts of all six hydrogen isotopologues the observed non-idealities, represented by ϕ_i for the gas phase and γ_i for the liquid phase, are plotted in Figure 4.6. The fugacity coefficient for the gas phase is less than unity, with strongest deviations for the heavy isotopologues, meaning that the vapor pressure of the mixture is over predicted by the ideal method by approx. 10% at 20 Kelvin, whereas the liquid phase activity coefficient is larger than unity in all cases with the strongest non ideality observed for H_2 and T_2 (deviating the most from the mixture average molecular mass of 4) and lowest for HT and D_2. Equations (4.12) to (4.15) are derived ab inito from statistical thermodynamics and are thus exact, only the binary interaction parameter and virial coefficient have been determined empirically by Sherwood and Souers, who indicate deviations less than 5% for the overall model [70].

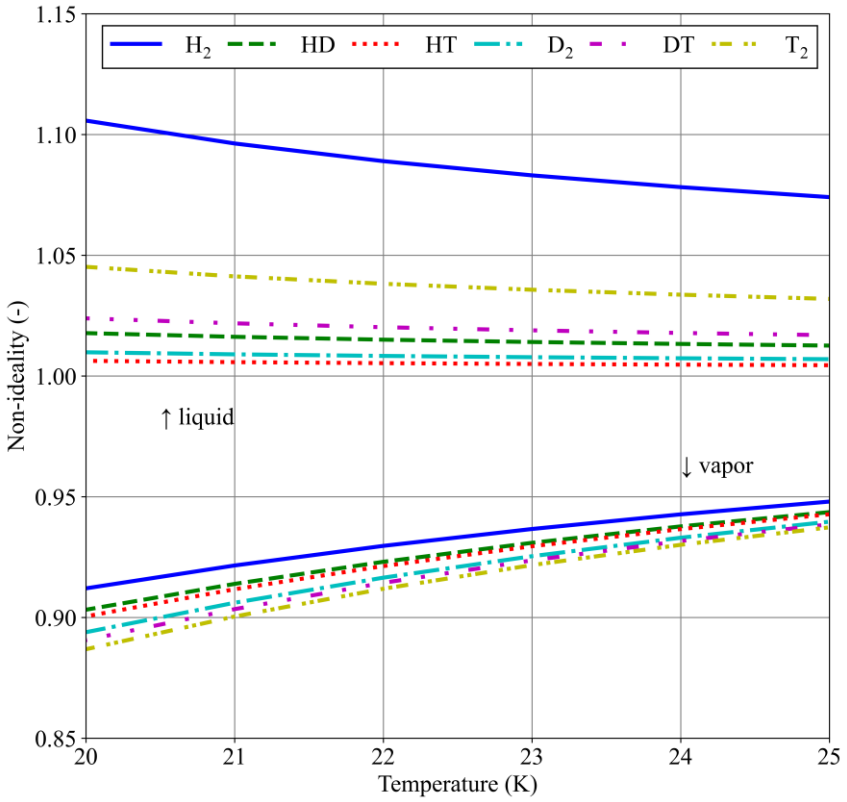

Figure 4.6: Calculated fugacity and activity coefficients as a metric for the non-ideality of the gas and liquid phase for an equimolar mixture of hydrogen isotopologues. The gas phase shows a negative deviation whereas that of the liquid phase is positive. Both effects are more pronounced at lower temperatures.

Hydrogen Metal Equilibrium

Several interactions of hydrogen with metal compounds are exploited in the fuel cycle and considered in the fuel cycle simulator. These follow essentially two different mechanisms. At low concentrations hydrogen molecules can adsorb on the surface where they disassociate and dissolve in the metal lattice, forming a so-called *alpha* phase. If hydrogen concentrations in the metal lattice exceed the solubility limit it begins to chemically bind to metal atoms forming a metal hydride or so called *beta* phase. The transition between the two phases is characterized by the coexistence of both, forming an *alpha-beta* phase.

Adsorption and solution

The adsorption equilibrium is commonly described by Sieverts' law which links a metal concentration of hydrogen (c_{Q}) to a corresponding gas phase equilibrium partial pressure (p_{Q2}) taking into account that the molecular form in the gas phase and atomic state in the metal leading to a square root dependence given as

$$c_{\mathrm{Q}} = K_{\mathrm{s}} p_{\mathrm{Q_2}}^{0.5}. \tag{4.17}$$

Here, K_{s} is the equilibrium – or Sieverts´ – constant (in units of mol.m^{-3}Pa$^{-0.5}$). As the disassociation of hydrogen is an activated process the temperature dependency of this process follows an Arrhenius type behaviour with the activation energy and proportionality dependent on the involved metal and hydrogen isotope. Metals and alloys employed in the fuel cycle featuring the adsorption of hydrogen are:

- A foil of Pd-Ag alloy for permerator tubes in the exhaust processing system,
- a foil of V or Nb in the metal foil pump in the fuel separation system,
- a Zr-V-Ti-Al alloy (ZAO) alloy for gettering of hydrogen in the exhaust processing system.

The accurate determination of relevant parameters is challenging and heavily influenced by the experimental set-up, sample surface characteristic and material history. The body of literature work commonly features spreads exceeding one order of magnitude. For the relevant systems in the fuel cycle and fuel cycle simulation, reference literature values for systems as close as possible to the intended application are used, given in Table B.7 in the Appendix.

Absorption

For application in temperature swing absorption and hydride storage beds the active materials are purposefully operated at conditions and with hydrogen concentration exceeding the alpha phase and allowed to form hydrides. During this phase the relationship between equilibrium pressure and hydrogen metal concentration flattens, forming a plateau until all available metal is reacted with. This results in suitable metals having significant storage capacity over a range of nearly constant pressure. This effect is also strongly temperature dependent and thus allows to load or discharge the material by manipulating its temperature. If the hydrogen content in the metal exceeds the plateau region the corresponding equilibrium pressure increases again exponentially.

Uranium hydride beds for storage applications are typically operated in the plateau regime, allowing for expression of the equilibrium pressure dependent on temperature typically expressed as integral Van't Hoff equations of the form

$$\ln\left(\frac{p^*}{Pa}\right) = -\frac{\mathrm{a}}{RT} + \frac{\mathrm{b}}{R}, \tag{4.18}$$

Where *T* is temperature, *R* the ideal gas constant and a, b parameters with values provided in Table B.8 in the Appendix.

The temperature swing absorption process in the isotope rebalancing and protium removal system employs two different metals, palladium featuring a normal isotope effect, as well as a titanium-manganese alloy featuring an inverse isotope effect. Their Van't Hoff parameter values are also provided in Table B.8 in the Appendix.

4.3 Component Mass Transfer Models

The use of detailed mass transfer models for all components facilitating the separation of a tritium carrying stream is a core technique in obtaining an accurate and physics based representation of the fuel cycle. These models are used to mirror the central unit operation of the employed technologies. This section gives the details of each component model, introducing the governing equations, boundary conditions, and assumptions.

4.3.1 Pd-Ag Permeators

Permeation of hydrogen through thin metal foils of palladium has first been employed by Hunter for the generation of pure hydrogen [71]. Since then, this technology has also been quickly adapted to tritium processing applications offering a convenient way to separate hydrogen from inert species and impurities using only tritium compatible materials [72][73]. Permeators exploit a diffusion flux j of a hydrogen isotope i through a solid material along a concentration gradient from a high pressure retentate side to a low pressure permeate side according to Fick's law

$$j_{\mathrm{i}} = D_{\mathrm{i}} \frac{dc_{\mathrm{i}}}{ds}, \tag{4.19}$$

where D is the diffusion coefficient. Integrating over a foil of uniform thickness s and applying Sieverts´ law for the surface concentrations the permeation flux for atomic hydrogen isotopes is obtained as:

$$j_{\mathrm{i}} = \frac{Pe_{\mathrm{i}}}{s} \left(z_{\mathrm{i,ret}} \sqrt{p_{\mathrm{Q2,ret}}} - z_{\mathrm{i,perm}} \sqrt{p_{\mathrm{Q2,perm}}} \right), \tag{4.20}$$

where $Pe_{\mathrm{i}} = K_{\mathrm{s,i}} \cdot D_{\mathrm{i}}$ is the permeability of isotope i, p_{Q2} is the total partial pressure of hydrogen in each gas phase and z_i the atomic fraction of isotope i in each gas phase [74]. The rate is fundamentally a property of the dissolved hydrogen atoms and as such can only be ascribed to the three atomic species. If assuming an ideal mixture, the concentration of the isotopes on a metal surface is directly proportional to the abundance of each species in the molecular gas phase regardless of its molecular form.

This permeation flux is then implemented in a 1-D rate based model for the retentate side of a tubular permeator, combining an arbitrary number of parallel tubes into a single hypothetical one with an equivalent diameter and volume to achieve the same surface area. For each volume element dynamic total and species balances (eq. 4.1 and eq. 4.2) are specified, accounting the incoming and outgoing gaseous flows, as well as the permeation flow. The retentate side is modelled as a single ideally mixed gas hold-up from which a product stream can be drawn. A given bleed flowrate is specified as a boundary condition on the retentate outlet and the composition of the feed stream is a boundary condition on the feed side. The dynamic behavior of the unit is thus governed by the available gas volumes, used to calculate the pressure based on the current hold-up, as well as the achieved permeation flux, which in turn depends on the pressure on the permeate and retentate side.

The model is assumed isothermal with a constant foil temperature and the permeability uses the Sieverts´ constants as given in equation 4.16 and diffusivity data of Serra et al. [75] and extrapolated for tritium [76]. The combined permeability is reported in Table B.9 in the Appendix.

As equation 4.20 only applies to atomic hydrogen, component balances for the retentate hold-up are also specified using only atomic hydrogen. The streams of the fuel cycle simulator, however, contain all six molecular forms, requiring the decomposition of hydrogen contained in the feed stream into its atomic constituents. On both outlets hydrogen atoms are therefore recombined according to the isotopic equilibrium at the operating temperature of the foil. Figure 4.7 shows a sketch of the model domain with all relevant parameters and interfacing streams.

Overall, the model uses the specification in initial and boundary conditions and can be configured by the parameters as given in Table 4.3.

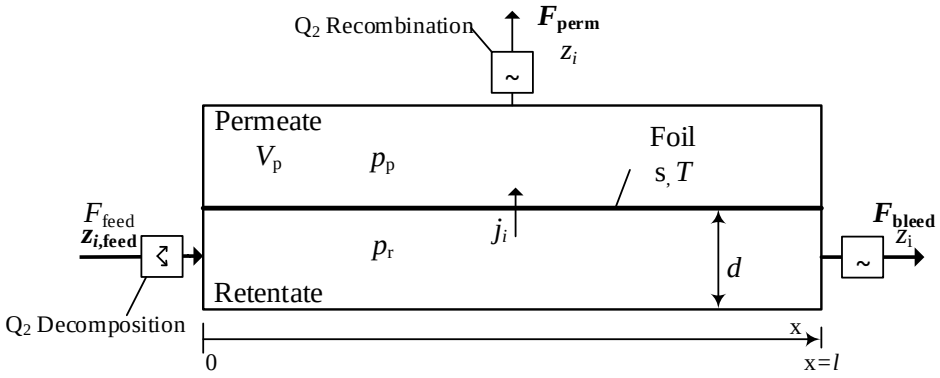

Figure 4.7: Sketch of the permeator model based on a rate based 1-D mass transfer model. A feed stream is introduced at the beginning of the domain and all contained hydrogen molecules are converted to pseudo atomic species. Local permeation rates are then calculated for all hydrogen atomic species between the high pressure feed side (retentate) and low pressure permeate side. Flowrates for the permeate and bleed streams have to be specified as boundary conditions with hydrogen molecules being re-established at both outlets in chemical equilibrium at the temperature of the foil. Bold variables have to be specified as boundary conditions to satisfy the equation system.

Table 4.3: Free parameters as well as boundary and initial conditions for the configuration of the permeator model.

Boundary Conditions	**Unit**	**Description**
F_{bleed}	mol.s^{-1}	Bleed stream flowrate
F_{perm}	mol.s^{-1}	Flowrate evacuated from the permeate chamber
$z_{\mathrm{i,feed}}$	-	Feed stream composition
Initial Conditions		
p_{r}	Pa	Initial pressure on the retentate side
p_{p}	Pa	Initial pressure on the permeate side
$z_{\mathrm{i,perm}}$	-	Initial molar composition on the permeate side
$z_{\mathrm{i,ret}}$	-	Initial molar composition on the retentate side
Parameter		
l	m	Length of the permeator tube
d	m	Combined diameter of all permeator tubes
s	m	Foil thickness
T	K	Foil Temperature

4.3.2 Thermally Cycled Absorption Columns

The model of thermally cycled absorption columns is based on plug flow reactor absorption column models such as developed by Ducret [77], and Zhou [78] which have been adapted to the present application and implemented as a rate based 1-D mass transfer model. The model features hold-ups in a gas and solid phase for which conservation equations are specified (eq. 4.1. and eq. 4.2). The gas phase balance accounts incoming and outgoing gaseous flows, as well as ab- and desorption flows, whereas in the solid phase only ab- and desorption are considered. Figure 4.8 shows a sketch of the model domain.

Each column of length *l* and diameter *d* allows for the extraction of gas at both ends of the domain, as well as the introduction of a feed stream at a specified length and on the right hand side of the column. As gas travels bi-directional within the column, pressure driven flow is implemented using the Carman-Kozeny equation as

$$k_c F = -\frac{dp}{dl}, \tag{4.21}$$

with $k_c = 180RT(1-\varepsilon)^2(pd_p^2\,\varepsilon^3\pi d^2 4^{-1})^{-1}$, assuming spherical pellets of uniform diameter d_p and constant bed porosity ε [79]. The absorption and desorption rate in each node is calculated according to the first order kinetic expression

$$\Phi_i = k \cdot dV \cdot (p_i - p_i^*), \tag{4.22}$$

where k is the rate coefficient and p_i^* the corresponding equilibrium pressure of each hydrogen isotopologue. As with the permeator model, hydrogen in the solid phase exists in atomic form whereas it is present in molecular form in the gas phase. In order to still be able to compute a molecular absorption rate from the gas phase, the molecular composition at the surface of the solid phase is calculated using the hydrogen chemical equilibrium at the solid temperature and composition. The equilibrium pressures for heterogenous isotopologues are then linearly interpolated between its pure constituents, assuming ideal mixture behavior.

As the operating principle of the temperature swing absorption process relies on alternate heating and cooling of each column their model cannot be isothermal. The column is therefore treated adiabatic modelling the heating/cooling operation by allowing the specification of a fixed temperature boundary condition on the outer wall. Heat transfer towards the column internal is then calculated radially from the outer wall temperature T_w towards the column center according to

$$q = \alpha(T_w - T_{col}). \tag{4.23}$$

Here, q is the area specific heat flux, T_{col} is the homogeneous temperature inside the column and α the combined effective heat transfer coefficient between the outer wall and column internal. The model does not consider convective heat transfer by the flowing gas and heat of absorption due to the externally applied heating and cooling load which has to be dominant by design to achieve rapid cycling. The parameters as well as boundary and initial condition used to configure the model are given in Table 4.4.

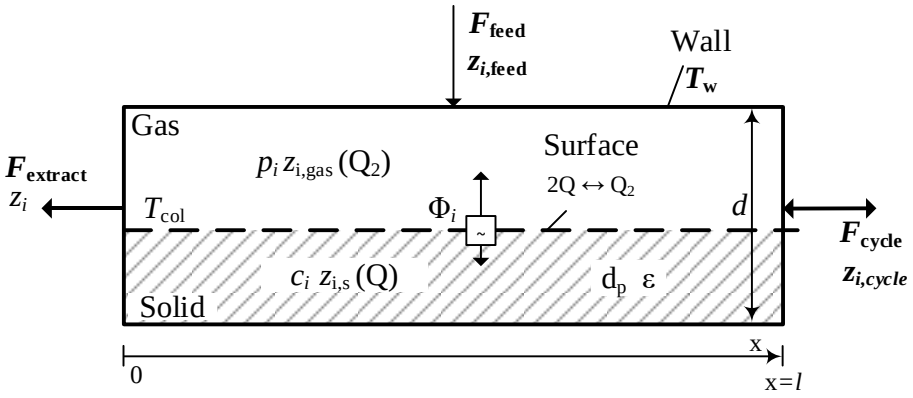

Figure 4.8: Model domain of the thermally cycled absorption column. In each discretization element the model computes the absorption rate, heat transfer rate, as well as pressure driven flow through the packing. Bold variables have to be specified as boundary conditions to satisfy the equation system.

Table 4.4: Free parameters as well as boundary and initial conditions for the configuration of the thermally cycled absorption column model.

Boundary Conditions	**Unit**	**Description**
F_{extract}	mol.s^{-1}	Flowrate extracted at the column left
F_{cycle}	mol.s^{-1}	Flowrate extracted or fed at the column right
F_{feed}	mol.s^{-1}	Feed flowrate introduced in the column center
$z_{\text{i,feed}}$	-	Feed stream composition
$z_{\text{i,cycle}}$	-	Composition of cycle stream if fed into column
T_{w}	K	Column outer wall temperature
Initial Conditions		
p_{gas}	Pa	Initial pressure in the gas phase
c	-	Initial hydrogen concentration in the solid
T_{col}	-	Initial temperature in the column
$z_{\text{i,s}}$	-	Initial atomic composition in the solid (Q)
$z_{\text{i,gas}}$	-	Initial molecular composition in the gas (Q_2)
Parameter		
l	m	Length of the column
d	m	Diameter of the column
s	m	Column wall thickness
N_{s}	mol	Amount of sorbent material
d_{p}	m	Diameter of solid particles
ϵ	-	Porosity of solid packing
α	W.m^{2}s^{-1}	Heat transfer coefficient

4.3.4 Wet Scrubber Columns

Wet scrubber columns exploit a thermodynamic preference of tritium in the liquid phase of a two phase system of tritiated liquid water and vapor and as such offer a convenient way of detritiating large gas streams with common process equipment. The equilibrium between the vapor and liquid phase for this system can be obtained either via isotope exchange reactions (chemical equilibrium) or vapor liquid interactions (physical equilibrium). Both processes occur in parallel, however, the ultimate thermodynamic equilibrium state is independent of the pathway by which it is attained. Consequently, wet scrubber columns are best modelled as equilibrium systems. Here, the vapor liquid equilibrium as described in section 4.2.2 is used in a one-dimensional domain along the column height (h).

The most rigorous model available in literature is that of Busigin [80], which has been adapted to dynamic operation and simplified for isothermal and isobaric operation of the column. This requires the introduction of a saturated feed stream at the operating temperature of the column. Experimental performance characterizations used to determine the number of stages for a given column height by way of the Height Equivalent of a Theoretical Plate (HETP) are available in literature from the work of Perevezentsev et al.[81].

Thereby, the column as illustrated in Figure 4.9 is discretized along its length into equilibrium stages each featuring a constant liquid hold-up of water. For each hold-up element a stationary total material balance, as well as dynamic species balance is specified, considering the incoming and outgoing water flowrates, as well as the transfer to and from the gas phase which in turn in calculated from a stationary balance of the gas phase. The gas phase is assumed hold-up free and the gas stream is considered to leave each stage having fully attained the equilibrium vapor composition corresponding to the current liquid composition. Saturated gas is introduced at the bottom of the column and liquid water at the top. The flowrate of liquid water is controlled by setting a ratio of vapor flow F^{v} to liquid flow F^{l} in the column as $\lambda = F^{\mathrm{v}}/F^{\mathrm{l}}$. Table 4.5 lists all boundary and initial conditions, as well as parameter needed to configure the model.

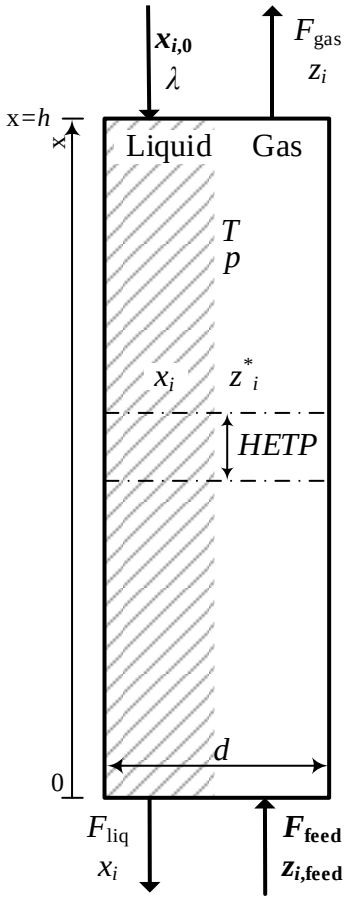

Figure 4.9: Model domain of a wet scrubber column. The column is discretized into a number of equilibrium stages according to their HETP and the column length. A saturated gas stream is introduced at the bottom, a liquid stream at the top. Bold variables have to be specified as boundary conditions to satisfy the equation system.

Table 4.5: Free parameters as well as boundary and initial conditions for the configuration of the wet scrubber column model.

Boundary Conditions	**Unit**	**Description**
F_{feed}	mol.s^{-1}	Feed Flowrate of gas
$z_{i,\text{feed}}$	-	Molar composition of feed stream
$x_{\text{i,0}}$	-	Molar composition of water feed stream
Initial Conditions		
N^{l}	mol	Total hold-up of liquid water on each stage
x_{i}	-	Molar composition of liquid water on each stage
Parameter		
n	-	Number of equilibrium stages
h	m	Column height
HETP	m	Height equivalent of a theoretical plate
λ	-	Vapor to liquid ratio
T	K	Operating temperature
p	Pa	Operating pressure

4.3.5 Liquid Phase Catalytic Exchange Columns

A wide range of mathematical mass transfer models for LPCE columns is available in literature, with their initial applications ranging back to water upgrading needed for heavy water reactors [82]. For the modelling of the CECE process applied in water detritiation the works of Ovcharov [83], Busigin [84][85], and Bornea [86][87] are the most developed. The models can generally be grouped as either two phase models, treating only the liquid phase and a combined gas phase, or three phase models, rigorously calculating all three phases of liquid water, water vapor and hydrogen gas. Both types can be formulated as rate based or equilibrium stage model.

Here, a section of an LPCE column, as illustrated in Figure 4.10, packed with mixed catalyst and without any side feed streams or draw offs is modelled using a three-phase rate based approach. The column is discretized along its height h and a liquid water stream is introduced at the top of the domain, hydrogen and water vapor enter at the bottom. The model features water, hydrogen, and water vapor as distinct phases, each with their individual hold-up and composition in each discretization element. The total hold-up of each phase and segment is kept constant. Consequently, the total flowrates of $F^{\mathrm{l}}_{\mathrm{Q_2O}}, F^{\mathrm{v}}_{\mathrm{Q_2O}}, F^{\mathrm{g}}_{\mathrm{Q_2}}$ in the column are constant across the column length. This assumes isothermal operation and negligible pressure drop variations with time. Steady state total material balances as well as dynamic species balances are then specified, taking into account the incoming and outgoing flowrates, as well as the flowrates resulting from the chemical or physical exchange. The mass transfer rates across the vapor – liquid interface and gas – vapor interface are given by first order kinetics of the form

$$\begin{aligned} \Phi_{\mathrm{i,L-V}} &= k_{\mathrm{d}} \cdot dx \cdot A(y_{\mathrm{i}} - y_{\mathrm{i}}^{*}), && \text{(a)} \\ \Phi_{\mathrm{i,V-G}} &= k_{\mathrm{s}} \cdot dx \cdot A(z_{\mathrm{i}} - z_{\mathrm{i}}^{*}). && \text{(b)} \end{aligned} \qquad (4.24)$$

Molar fractions denoted by * refer to the equilibrium composition of species i in its respective phase, k_{d} and k_{s} are the mass transfer coefficient for the distillation (vapor liquid interaction) and isotope exchange (vapor gas interaction), respectively. The attainable values of these coefficients are a function of the employed packing material and catalyst.

For a given system, the rigorous computation of the 3-phase equilibrium composition as described in section 4.2.2 is challenging and not numerically efficient as only iterative solutions of the resulting non-linear equation system are possible which also offers non-physical solutions (of e.g. negative molar fractions) due to quadratic relationships. A more simplified treatment is obtained when allowing for a number of assumptions:

No interaction between the liquid water phase and hydrogen gas.

Due to the hydrophilic nature of the employed catalyst (not allowing contact of liquid water) it is assumed that the reaction rate of isotope exchange reactions between liquid water and hydrogen gas is small when compared to that of hydrogen gas and water vapor and consequently neglected. This assumption can be considered conservative as this offers another transport route of tritium towards the liquid phase increasing the overall transport rate.

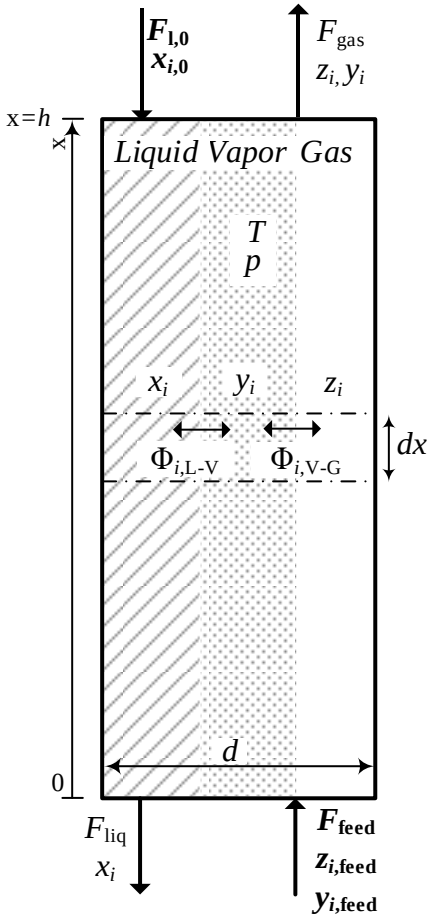

Figure 4.10: Model domain of a LPCE column section. A saturated gas stream is introduced at the bottom, a liquid stream at the top. Mass transfer rates between vapor - liquid and gas – liquid interface are computed in each discretization element. Bold variables have to be specified as boundary conditions to satisfy the equation system.

Protium is the dominant hydrogen species in all phases.

From the self-equilibration process taking place in each phase it then follows that molecular species of the form HQO and HQ are dominant and contribution of e.g. T_2O, or D_2 are negligible. This allows computation of the gas phase isotopic equilibrium considering only the reactions

$$\begin{aligned} &\mathrm{H_2O^v + HD \rightleftharpoons HDO^v + H_2}, && \text{(a)} \\ &\mathrm{H_2O^v + HT \rightleftharpoons HTO^v + H_2}. && \text{(b)} \end{aligned} \qquad (4.25)$$

With y_{H2O} and $z_{H2} \sim 1$ the resulting equilibrium molar fraction of HT and HD in the gas phase are then:

$$z_\mathrm{i}^* = \frac{y_\mathrm{i}}{K_\mathrm{i}}, \qquad (4.26)$$

wherein $z_\mathrm{i}^*$is the equilibrium molar fraction of species i within the hydrogen phase, y_i the current molar fraction of species i in the vapor phase and K_i the equilibrium constant of the associated exchange reaction as reported in section 4.2.2.

HTO and HDO each form a binary mixture with H_2O.

This follows from the excess of H_2 and H_2O and allows the direct calculation of the vapor liquid equilibrium as:

$$y_{\mathrm{i}}^{*} = \frac{\alpha_{\mathrm{H_2O,i}} x_{\mathrm{i}}}{1 + \left(\alpha_{\mathrm{H_2O,i}} - 1\right) x_{\mathrm{i}}}. \tag{4.27}$$

Here, $y_{\mathrm{i}}^{*}$is the equilibrium molar fraction of HDO or HTO in the vapor phase, corresponding to the current liquid molar fraction x_{i}. The separation factor is then given as $\alpha_{\mathrm{H_2O,i}} = p_{\mathrm{i}}^{*}/p_{\mathrm{H_2O}}^{*}$, with p_{i}^{*} the temperature dependent saturation vapor pressure of HTO or HDO. With above equations the mass transfer model is fully specified and the required initial- and boundary conditions, as well as parameters to configure the model are summarized in Table 4.6.

Table 4.6: Free parameter as well as boundary and initial conditions for the configuration of the LPCE column segment model.

Boundary Conditions	**Unit**	**Description**
$F_{\mathrm{l,0}}$	mol.s^{-1}	Flowrate of liquid entering at the top of the column
F_{feed}	mol.s^{-1}	Flowrate of humid feed gas entering at the bottom
$x_{\mathrm{i,0}}$	-	Composition of liquid water entering at the top
$z_{\mathrm{i,feed}}$	-	Composition of hydrogen in the feed gas stream
$y_{\mathrm{i,feed}}$	-	Composition of water vapor in the feed gas stream
Initial Conditions		
N_{Q2}	mol	Total hold-up of hydrogen gas in the column
N_{Q2O}	mol	Total hold-up of water vapor in the column
N_{Q2O}	mol	Total hold-up of liquid water in the column
z_{i}	-	Compositon of hydrogen gas
y_{i}	-	Compositon of water vapor
x_{i}	-	Compositon of liquid water
Parameter		
k_{d}	mol.m^{-3}.s^{-1}	Mass transfer coefficient vapor - liquid
k_{s}	mol.m^{-3}.s^{-1}	Mass transfer coefficient gas - vapor
h	m	Height of the column segment
dh	m	Height of a discretization element
A	m²	Cross section area of the segment
T	K	Operating temperature
p	Pa	Operating pressure

4.3.6 Cryogenic Distillation Columns

Cryogenic distillation can be considered the default technology for isotope separation in any tritium system of sufficient size to warrant its infrastructure demand. It, however, suffers from drawbacks such as potentially high tritium inventories and challenging operation and is therefore a strong focus of modelling and simulation activities to design and optimize such systems. At the same time their development also benefits from a vast wealth of distillation theory developed for more common applications. While for binary systems analytical tools like the Fenske-Underwood equation and McCabe-Thiele method are available [88][89], most practical applications of cryogenic distillation for hydrogen isotopes are a multi-component system of up to six species requiring more sophisticated methods. As for any mass transfer process, distillation can be described using a rate based or equilibrium stage approach, with the latter being the most prevalent in literature as theoretical stages are commonly used in the design procedure of columns. Most notable the FLOSHEET code has been used extensively in the past to model and optimize cryogenic isotope separation systems of the ITER fuel cycle and in turn validated extensively [90]. This code has later been expanded into DYNSIM for the dynamic simulations using stage by stage calculation of mass and energy balances [91].

Here, the same approach is employed, yielding a dynamic non-isothermal equilibrium stage model, as sketched in Figure 4.11. For each stage dynamic species balances as well as stationary total mass and energy balances are specified. The dynamic composition change on each stage is then modelled using a series of dynamic species balances around the liquid hold-up. This correspond to the assumptions that the column is adiabatic with constant liquid hold up on each stage and comparably small molar vapor hold-up such that the liquid phase dynamics are always limiting and governing the vapor composition. The vapor composition leaving each stage is then calculated by the Sherwood –Souers model (see section 4.2.2). The column is assumed to be operated at constant pressure and the stage temperature can be derived from the vapor pressure on each stage using the vapor pressure correlations given in section 4.2.1. The feed stream is assumed to be introduced as saturated liquid at the corresponding stage temperature. The model also considers the decay heat of tritium, releasing 1.95 W of thermal energy per mol of T_2-equivalent hold-up [92].

The flowrates around the reboiler and condenser are specified by global mass balances and the use of a Distillate to Feed Ratio (DTF) and Reflux Ratio (RR) using a full reboiler and partial condenser as to always obtain gaseous products. The following relationships and definitions fully determine the total mass balances of the column:

$$F_{\mathrm{feed}} = F_{\mathrm{bot}} + F_{\mathrm{top}}, \tag{4.28}$$

$$DTF = \frac{F_{\mathrm{top}}}{F_{\mathrm{feed}}}, \tag{4.29}$$

$$RR = \frac{F_{\mathrm{l,0}}}{F_{\mathrm{feed}}}. \tag{4.30}$$

The full set of boundary and initial conditions, as well as parameter used to configure the model are given in Table 4.7.

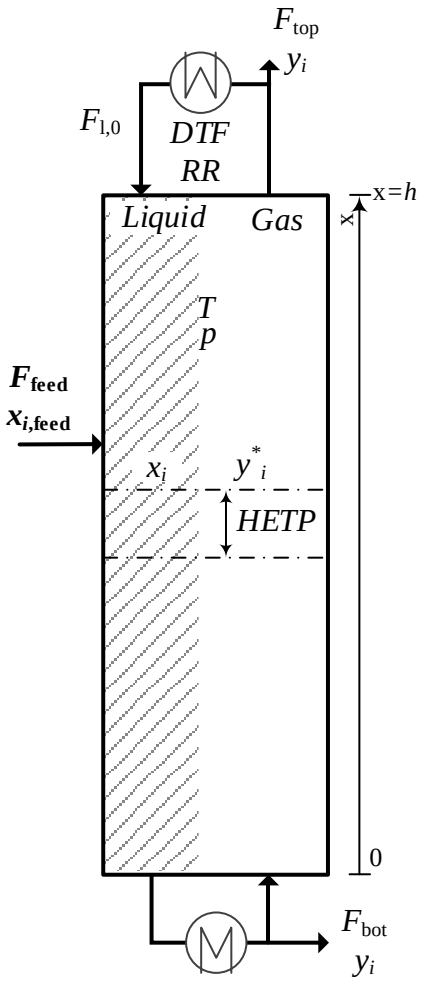

Figure 4.11: Model domain of a cryogenic distillation column. A feed stream of saturated liquid is introduced along the column height. From the top and bottom gaseous product streams are drawn off. Bold variables have to be specified as boundary conditions to satisfy the equation system.

Table 4.7: Free parameter as well as boundary and initial conditions for the configuration of the cryogenic distillation column model.

Boundary Conditions	**Unit**	**Description**
F_{feed}	mol.s^{-1}	Feed stream flowrate
$x_{\mathrm{i,feed}}$	-	Molar composition of feed stream
Initial Conditions		
N^{l}	mol	Total hold-up of liquid hydrogen on each stage
x_{i}	-	Molar composition of liquid hydrogen on each stage
Parameter		
n	-	Number of equilibrium stages
DTF	-	Distillate to Feed Ratio
RR	-	Reflux Ratio
p	Pa	Operating pressure

4.3.7 Single Volume Unit Operations

Besides the mass transfer models requiring the calculation of species dependent concentration profiles, the fuel cycle and also its simulation rely on the use of smaller unit operations without concentration profiles that can be modelled as a single volume element. Their models and governing principles are briefly introduced in this section.

Water Electrolyser

The operation of the CECE process requires the use of an electrolyser unit in order to generate a hydrogen gas stream. This process has a significant isotope effect as measured by Roy [93], leading to the enrichment of heavy isotopes in the liquid phase. The model for the electrolyser unit consists of a single hold-up of liquid water with a feed stream of liquid water from which two product streams are obtained, a hydrogen gas stream and an oxygen gas stream, as depicted in Figure 4.12. Both streams are assumed to leave the electrolysis cell saturated with water vapor at the operating temperature using the water vapor liquid equilibrium. The composition of the gas stream is further determined using the temperature dependent separation factors of the form:

$$K_{\mathrm{H-D}} = \frac{\left[\frac{H}{D}\right]^{\mathrm{g}}}{\left[\frac{H}{D}\right]^{\mathrm{l}}} = \exp\left(-\frac{7056}{2.3RT}\right), \tag{4.31}$$

$$K_{\mathrm{H-T}} = \frac{\left[\frac{H}{T}\right]^{\mathrm{g}}}{\left[\frac{H}{T}\right]^{\mathrm{l}}} = \exp\left(-\frac{9492}{2.3RT}\right), \tag{4.32}$$

where the bracketed terms refer to the ratio of the indicated isotopes in the specified phase as given in [94]. The model further assumes protium excess and thus only allows for the formation of molecules with at least one constituent being protium. The amount of water processed is then controlled as to maintain a constant total liquid hold-up by a steady state total material balance. Composition changes with time in the electrolyser liquid hold-up are modelled using dynamic species balances. Isothermal operation is assumed. The full set of boundary and initial conditions, as well as parameter used to configure the model are given in Table 4.8.

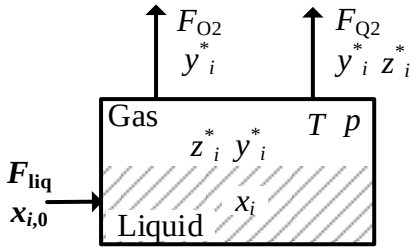

Figure 4.12: Model domain of the electrolyser. Bold variables indicate boundary conditions needed to satisfy the equation system.

Table 4.8: Free parameter as well as boundary and initial conditions for the configuration of the electrolyzer model.

Boundary Conditions	**Unit**	**Description**
F_{liq}	mol.s^{-1}	Feed stream flowrate of liquid water
$x_{\mathrm{i},0}$	-	Molar composition of feed stream
Initial Conditions		
N^{l}	mol	Total hold-up of liquid water
x_{i}	-	Initial molar composition of liquid water
Parameter		
T	K	Operating temperature
p	Pa	Operating pressure

Condenser / Saturator

Systems in the fuel cycle processing humid gas streams often require the control of the humidity level, either reducing it by lowering its temperature below the dew point and collecting the resulting liquid phase, or saturating it by introducing additional water. Both applications make use of the same underlying physical equilibrium and thus can both be provided by the same model corresponding to a single equilibrium stage of the wet-scrubber column model (c.f. section 4.3.4), which is illustrated in Figure 4.13. The model is based on a constant liquid hold-up with which the incoming gas stream is equilibrated using the water vapor liquid equilibrium at the specified operating temperature of the component. By also computing the overall water balance, either a stream of excess water is discharged or additional water is taken up from a connected source. The full set of boundary and initial conditions, as well as parameter used to configure the model are given in Table 4.9.

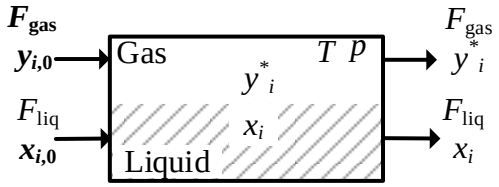

Figure 4.13: Model domain of the condenser / saturator. Bold variables have to be specified as boundary conditions to satisfy the equation system.

Table 4.9: Free parameter as well as boundary and initial conditions for the configuration of the condenser / saturator model.

Boundary Conditions	**Unit**	
F_{gas}	mol.s^{-1}	Feed stream flowrate of gas
$y_{\mathrm{i},0}$	-	Molar composition of feed stream vapor
x_0	-	Molar composition of supplementary water
Initial Conditions		
N^{l}	mol	Total hold-up of liquid water
$x_{\mathbf{i}}$	-	Initial molar composition of liquid water
Parameter		
T	K	Operating temperature
p	Pa	Operating pressure

Hydrogen Equilibrators

Interactions of hydrogen with catalytic surfaces or recombination of atomic hydrogen forms hydrogen isotopologues in a composition distribution according to their temperature dependent equilibrium distribution (see Chapter 4.2.2). This effect is purposefully exploited in the Isotope Separation System, using catalytic equilibrium reactors to promote the formation of homogenous isotopologues (H_2, D_2, T_2) from streams of predominantly heterogeneous isotopologues (HD, HT, DT) to facilitate the isotopic separation of the constituents. This equilibrator is modelled as a single, hold-up free equilibrium stage. The model is fully specified by three atomic balances for H, D, T, and three equilibrium relations (see equation 4.7 and equation 4.8), as well as a total material balance. The model is assumed isothermal with a temperature parameter that allows configuration to the operating temperature of the unit. Table 4.10 lists all boundary conditions as well as parameter used to configure the model.

Table 4.10: Free parameter as well as boundary and initial conditions for the configuration of the hydrogen equilibrator model.

Boundary Conditions	**Unit**	
F_{gas}	mol.s^{-1}	Feed stream flowrate of gas
$z_{\text{i,0}}$	-	Molar composition of feed stream
Parameter		
T	K	Operating temperature

Gas Volumes

Hold-ups of gas where they are not negligible are considered using the model of an isothermal free volume computing total material and species balances. No source or sink terms are considered. Any number of incoming and outgoing flowrates are specified as boundary conditions and the pressure in the vessel is computed using the ideal gas law. As the upper nominal operation pressure in the fuel cycle is 2 bar (in the exhaust processing system) and all relevant locations are operated at ambient temperatures or above its application is deemed valid. Table 4.11 lists all boundary and initial conditions as well as parameter used to configure the model.

Table 4.11: Free parameter as well as boundary and initial conditions for the configuration of the gas volume model.

Boundary Conditions	**Unit**	**Description**
F_{gas}	mol.s^{-1}	Feed stream flowrates of gas
$z_{\text{i,in}}$	-	Molar composition of feed streams
F_{out}	mol.s^{-1}	Outgoing flowrates
Initial Conditions		
p_0	Pa	Initial pressure
z_{i}	-	Initial composition
Parameter		
T	K	Operating temperature
V	m^3	Vessel volume

Parametric Units

Next to dynamic mass transfer models, parametric units are also employed in places where the design of the system in the fuel cycle is not progressed sufficiently, the technology is not yet selected, or the overall impact on the fuel cycle performance and dynamic is negligible. These units are generally considered hold-up free and allow the direct specification of their performance. Wherever they are used in a model assembly of a fuel cycle system their use will be elaborated in the corresponding sections of Chapter 5.

5 Dynamic Process Simulation of Fuel Cycle Systems

5.1 Implementation into a Simulation Environment and Numerical Methods

By combining the developed mass transfer and unit operation models into process chains, systems of the fuel cycle can be simulated. This requires their impleentation into a simulation environment and numerical computation. The simulation environment has to efficiently solve the equation system for each individual model as well as for groups of models connected to each other by streams. For this purpose the overall simulation is set up in the Aspen® Custom Modeler V12 which provides the required numerical tools as well as a flow-sheet based interface. For the present work the Aspen Custom Modeler has been selected as the most suitable framework and previously successfully employed in the modelling of the EU-DEMO fuel cycle by Hörstensmeyer [43].

The Aspen Custom Modeler distinguishes between time settings for numerical and for evaluation purposes. Numerical time setting impact the employed solvers, while the evaluation time step dictates in which time intervals variable values are made available to the user for export. The driving dynamic characteristics of the fuel cycle are the burn-dwell cycling of the tokamak, as well as the semi-continuous operation of the temperature swing absorption system in the isotope rebalancing and protium removal system. Both feature dynamic events that occur over periods in the 10 – 100 second range. A minimum evaluation time step of one second is therefore specified to resolve these events with sufficient fidelity.

The numerical implementation of the model equation systems requires three distinct types of equations that are computed using inbuilt solvers follows:

- Algebraic, linear equations are directly computed to machine precision using the MA48 algorithm [94].
- Nonlinear equation systems are solved iteratively using the mixed Newton method
- Time dependent differential equations are solved as difference equations using implicit Euler integration

Relative and absolute tolerances are set to $\epsilon = 1 \cdot 10^{-5}$, allowing results to be reported with three significant digits while guaranteeing no impact of tolerances on the reported results.

The Aspen Custom Modeler offers dynamic resolution scaling for the employed integration time step, automatically adjusting the time step length between a minimum value and the evaluation time step, ensuring a stable solution with accuracy of the results within the specified tolerances. A minimum time step of $\Delta t = 1 \cdot 10^{-3} s$ is enforced and an error is raised if an unstable simulation is obtained by poorly selected space discretization or tolerances. The suitability and sensitivity of the employed solver settings is verified for the example of the water detritiation system, which exhibits the largest throughputs and composition gradients of all rate-based mass transfer models, in section 5.2.7.

The integration governs the time progression of the simulation, starting at $t = 0$ with all values set as specified by their initial conditions. The simulation is then continuously advanced until a user specified upper limit is reached. All parameter values and boundary condition values can be manipulated during the runtime, either from within the simulation by other models and control loops, or externally from events triggering automatically on reaching specified conditions.

5.2 System Models

Using the flow sheet functionality of the Aspen Custom Modeler mass transfer models and supplementary units are arranged to mirror the architecture of each individual fuel cycle system which in turn are arranged to mirror the overall fuel cycle architecture. The following section introduces the constructed system models, their architecture and components. Each system is configured to represent a viable fuel cycle operation point. The system stand-alone dynamic behavior is then investigated using a series of single variable steps in order to verify their correct implementation and physical behavior. Each test case is based on a reference operation point as defined in section 3.2.

5.2.1 Gas Distribution and Storage

The model of the gas distribution and storage system, as depicted in Figure 5.1, is constructed from a gas volume, infinite supplies of deuterium, xenon, and argon, a dynamic reservoir of tritium rich fuel (DT+), as well as a series of control units and mixers. The mixers control the flowrates of fuel constituents from the available storage units. The first unit is connected directly to the buffer vessel and features an on-off controller governing its pressure, engaging once the pressure reaches a lower threshold and replenishing fuel with a constant flowrate until an upper set point is reached. The flowrate is requested from both deuterium and tritium rich storages such that the total in-flow has a 50/50 D/T ratio. This controller also acts as overpressure protection discharging with a constant flowrate into empty gas storage reservoirs if an upper pressure threshold is reached.

The second set of control units are used to model the mixing vessels 1 and 2, continuously measuring the offset in the composition of the feed stream received from the buffer vessel and requesting the required flow rate from the individual storages to establish the set fuel composition within a relative margin of 1%. In order to keep a constant pressure in each unit the flowrate requested from the buffer vessel is adapted accordingly. The full system configuration as given in Table A.1 in the Appendix, representing the design of the corresponding fuel cycle system.

In order to investigate the dynamic behavior of the system a test case on the standalone system is set up with the following conditions:

- The buffer vessel is initialized with 99% DT and 1% H_2 at a pressure of p_0 = 900 mbar.
- The system supplies a constant output of 380 $Pa.m^3s^{-1}$ of fuel to the pellet injection and 50 $Pa.m^3s^{-1}$ to the gas puffing fueling systems corresponding to the flat-top fuel demand.
- The buffer vessel receives a constant input of 350 $Pa.m^3s^{-1}$ from DIRL and 90 $Pa.m^3s^{-1}$ from INTL.
- Both feed streams have a composition of 99% DT and 1% H_2.
- The available composition in the tritium rich storage is 50% T_2 and 50% DT.

The following sequence of events is assumed:

- At $t = 1000\ s$ the composition of the feed stream received from INTL is changed to 89% DT, 10% D_2 and 1% H_2.
- At t = 3500 s the feed stream flowrate from DIRL is reduced to 300 Pa.m^{3}s^{-1}

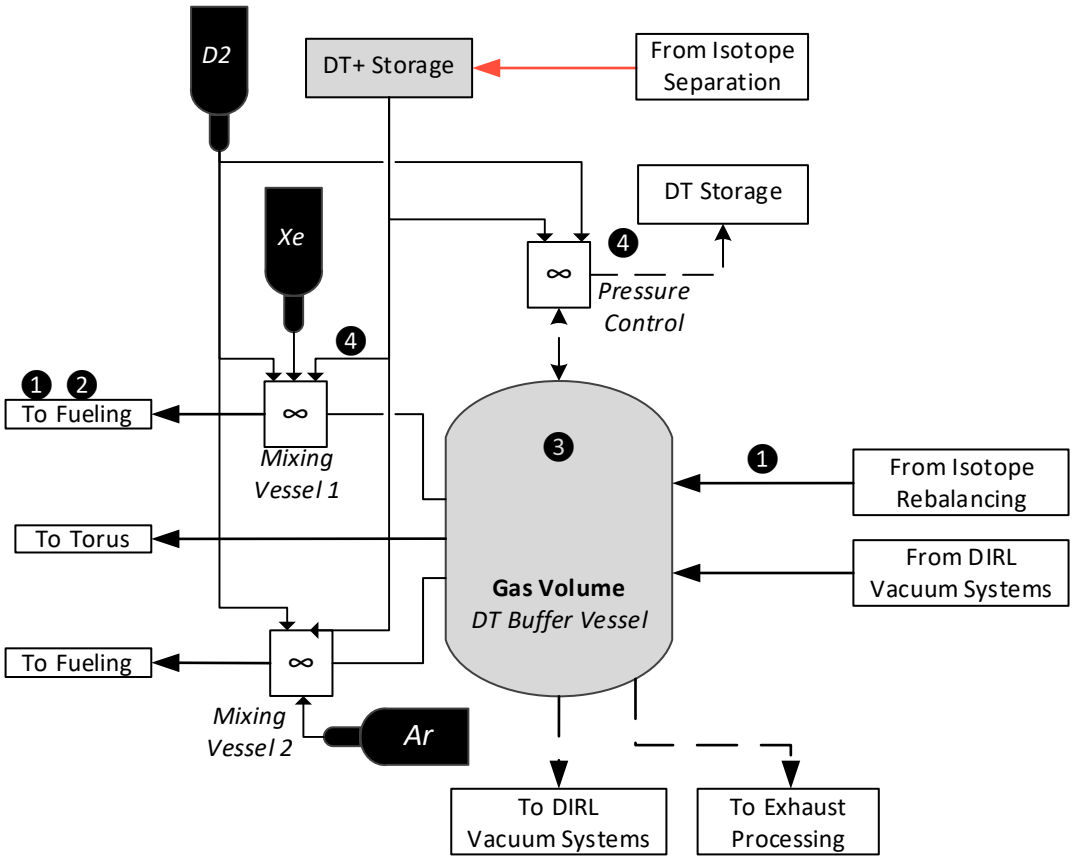

Figure 5.1: Model layout of the gas distribution and storage system. Grey components indicate areas of gaseous hold-up, black components provide an infinite supply and white components are hold-up free. Black numbers correspond to Figure 5.2.

The initial throughput and composition correspond to the flat-top reference case. The first step-change is intended to prompt only a reaction of the fuel composition control system to maintain the set D/T ratio. The second change is intended to find the system response for both control systems active at the same time.

Figure 5.2 shows the time trace of relevant variables. As expected the content of pure DT in the product streams decreases while D_2 and T_2 increase simultaneously and lacking tritium is being requested from the DT+ storage. This in turn leads to a lower flowrate being drawn from the buffer vessel resulting in a pressure build-up, ultimately engaging the over pressure protection system and discharging gas every time the upper pressure threshold of p_{high} = 1 bar is reached.

The second step-change leads to an overall deficiency in gas supply, requiring the engagement of fuel make-up to the buffer vessel, replenishing gas at intervals once the lower pressure threshold of p_{low} = 0.7 bar is reached. The make-up of fuel with a different D/T ratio than the new steady state in the buffer vessel (which is now offset from 50/50) also reflects in the composition control system

briefly reducing the DT+ flow rate. In both cases the control systems are able to maintain the buffer vessel within the specified operation pressure range while simultaneously maintaining the set-point D/T ratio of the fuel stream sent to pellet injection within 0.1% by adjusting the tritium rich flowrate. As the buffer vessel is the only component model featuring a hold-up, the dynamic responses and characteristics of the systems are governed by the vessel volume, currently selected to be V = 1 m³. Larger volumes will result in a slower system response for pressure and composition changes, and lower volumes would prompt a quicker system response. Too low volumes however, will ultimately lead to an undesirable frequency of valve actions for over- or under pressure protection, thus circumventing the buffer functionality.

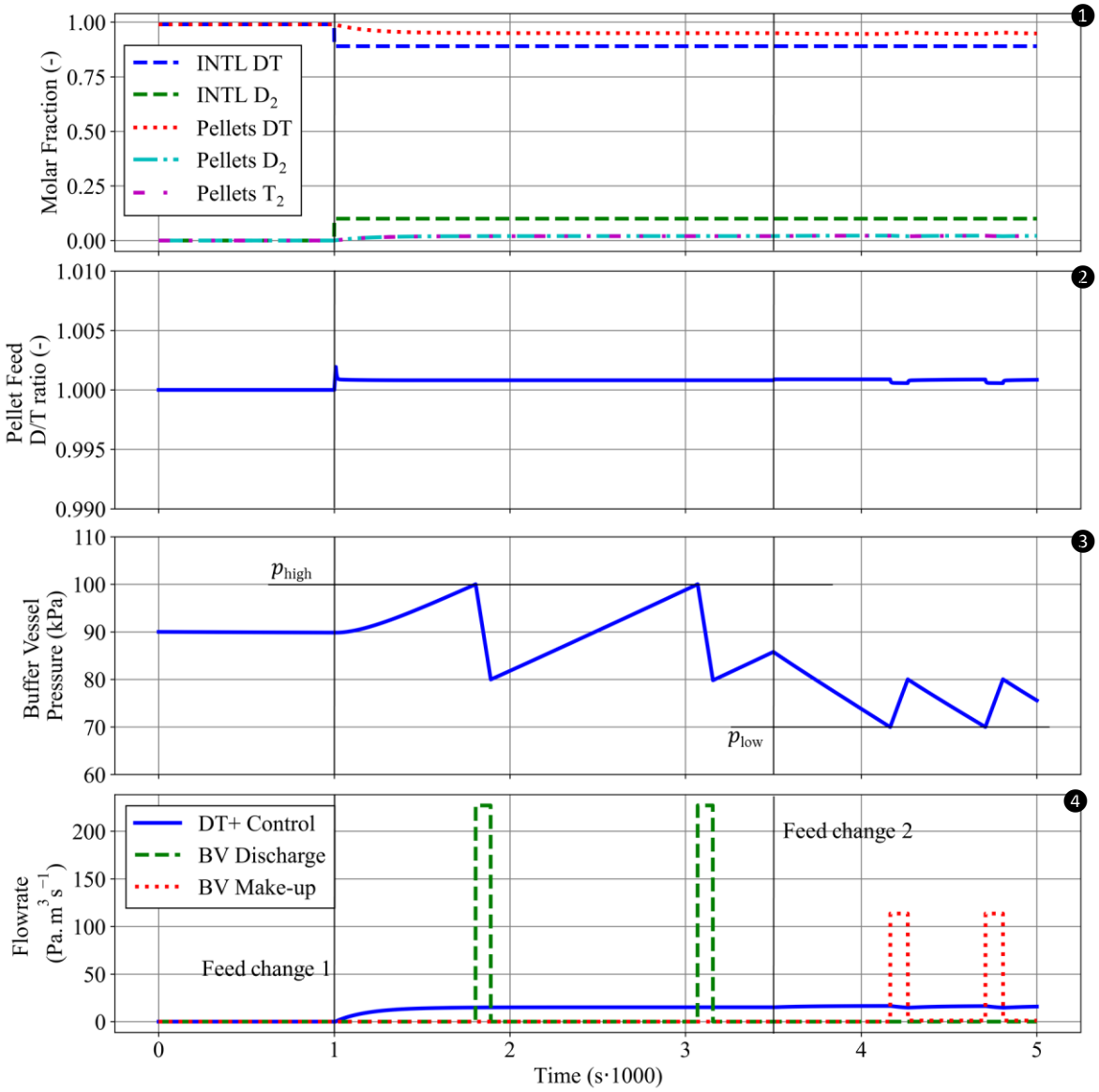

Figure 5.2: Calculated temporal evolution of the step change response of the gas distribution system. ❶: Composition in the buffer vessel. ❷: D/T ratio in the product stream towards pellet fueling. ❸: Pressure in the buffer vessel. ❹: Flowrates governed by the control system.

5.2.2 Torus Fueling and Torus

The torus fueling systems do not provide a separation functionality and only process the fuel feed stream to the conditions required for injection and directing it to the desired location. Their dynamic behavior, especially that of the pellet fueling system, can however still impact the overall operation of the fuel cycle and therefore a series of hold-ups and parametric elements is used to model the pellet fueling system.

The reactor may have multiple identical pellet fueling systems distributed around it, which are represented by one superficial system providing the total throughput. A gas volume of V = 0.1 m³ is used to model the gas phase and inlet feed manifold of the liquefier which is controlled to constant pressure by requesting a corresponding feed flowrate from the gas distribution system. The liquefier is modelled as an ideally mixed constant hold-up, corresponding to a liquid inventory of V = 2 liter. No mixing is considered in the extruder through which the now solid fuel passes which thus exhibits a dead time corresponding to the extrusion rate and physical dimensions of the extruder, estimated to a solid inventory of approximately V = 2 liter. The pellet selector mechanism of chopper, selector and evaporator, as well as the guide tube are modelled as a single parametric flow splitter with a combined separation fraction that is controlled by the fuel demand pattern of the torus, returning any unwanted pellets and pellet losses to the inlet manifold.

Fuel from gas puffing and gas injection is directly injected into the torus by forwarding their flowrate and composition as requested from the gas distribution system. The torus is modelled as a single balance area, imposing a fusion power and fueling pattern (see section 3.1.1). Inside the hold-up the fuel conversion based on the current fusion power as well as parametric outgassing and fuel implantation into the first wall are considered as sink and source terms. At the outlet of the torus model a neutral gas pressure is calculated based on the average particle density in the volume as well as the temperature of the divertor. Due to the interactions with the plasma and hot surfaces, molecular hydrogen leaving the volume is equilibrated to its equilibrium distribution at that temperature. Table A.1 in the Appendix lists all configurations and parameters employed in the component models of the torus and its fueling systems.

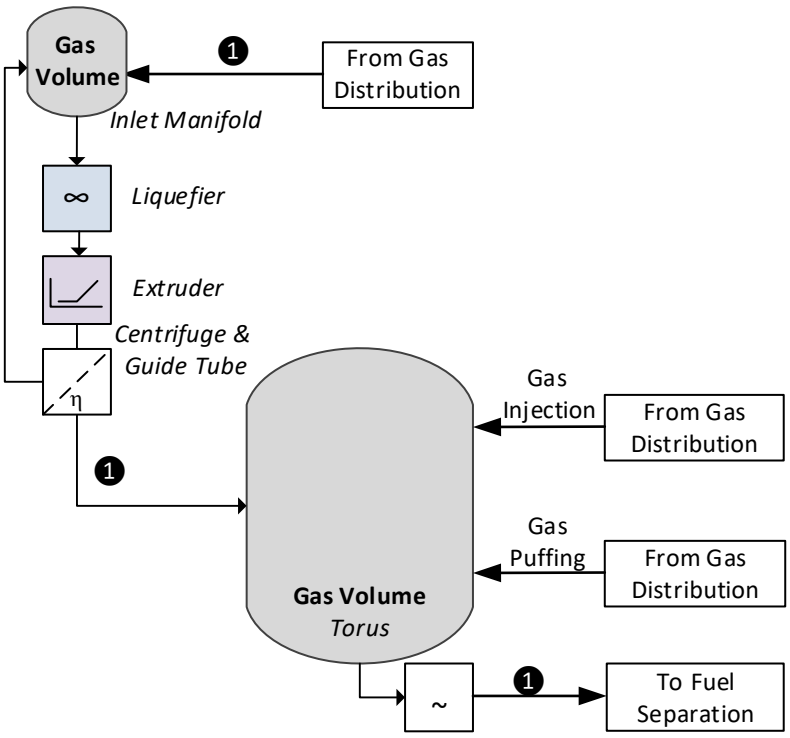

Figure 5.3: Model layout of the fueling system and torus. Grey components indicate areas of gaseous hold-up, blue liquid, purple solid, white components are hold-up free.

The dynamic behavior of the assembly is tested using the following case:

- All fueling system provide their nominal flat-top throughput with pure DT.
- All volumes are initialized with pure DT.
- The pressure in the sub-divertor is fixed to $p = 3\ Pa$.
- At $t = 1000\ s$ the composition of the pellet injection feed stream is changed to 90% DT and 10% D_2.
- The change in fueling DT ratio is assumed to have negligible effect on the exhaust helium content.

Figure 5.4 shows the time trace of the composition of the fueling pellets and at the outlet of the torus. Since hold-ups are considered in the gas vessel, as well as solid and liquid in the extruder the system dynamic response and characteristic is governed by the selected values. The system response to the step-change in the feed stream is observed with a negative exponential decline, in the pellet DT fraction after a dead time corresponding to the ice volume and thus residence time in the extruder. Larger or smaller liquid and gaseous volumes will affect the time constant of the composition change, whereas the solid inventory directly impacts the observed delay time. The composition at the torus outlet reflects the re-equilibration process taking place, yielding a mixture of DT, T_2 and D_2 close to the statistical equilibrium (see 4.2.2). Once the composition change reaches the torus the equilibrium shifts towards higher fractions of D_2 and proportionally reduced T_2 in the exhaust, with the DT fraction remaining unaffected.

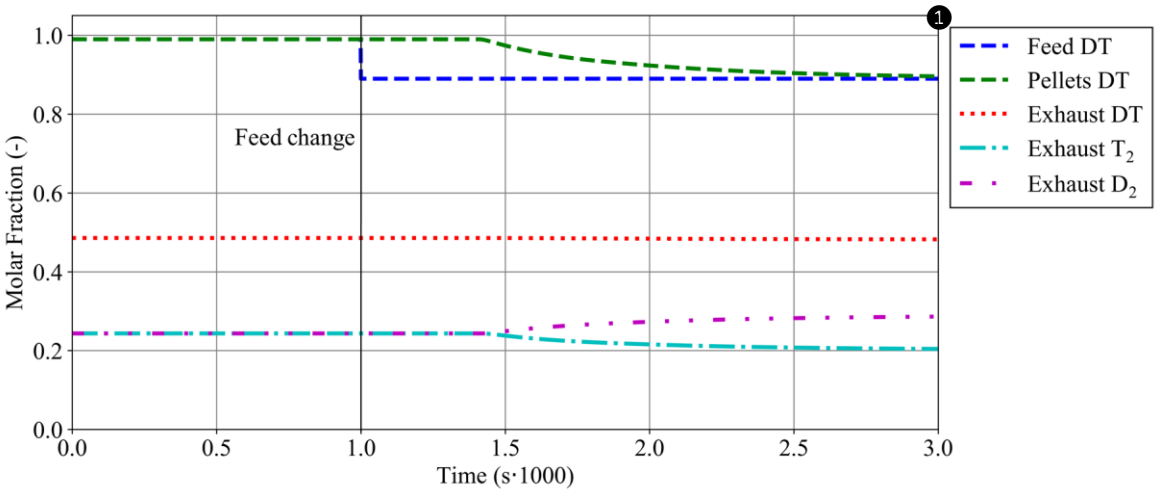

Figure 5.4: Calculated temporal step change response of the pellet composition and torus exhaust to a composition change in the pellet fueling feed.

5.2.3 Fuel Separation and Torus Vacuum

The vacuum system is modelled as a network of free gas volumes and vacuum pumps, as illustrated in Figure 5.5. All pumping trains are combined into one superficial train which is connected to the torus model. Each pumping stage is configured with a total effective pumping speed $S_{\mathrm{tot}} = n \cdot S$ where n is the number of parallel pumps employed. The system model further combines sequential stages of liquid ring pumps that are located close to each other into a single unit, having the same pumping speed as the first pumping stage of that sequence but achieving higher compression ratios. The metal foil pump is considered as a parametric separation unit configured with a recovery fraction η_{i} for each molecular hydrogen species. A lower pressure threshold can be specified at which this recovery fraction becomes zero, modelling the disengagement of the collisional plasma source at too low pressures. The ring line on the permeate side of the metal foil pump is controlled for a minimum pressure level, requesting make-up gas from the gas distribution system as needed. All volumes are assumed isothermal at $T = 300\ K$. The configuration of the contained models given in Table A.1 in the Appendix.

To test the dynamic behavior of the assembly it is interfaced to a gas volume of V = 6000 m³ initialized with p = 3 Pa and a composition of 99% DT and 1% ^{4}He with no incoming flows, resembling the plasma chamber state at the beginning of the dwell phase.

Figure 5.6 shows the time evolution of the pressure in the volume elements of the system assembly. The pressure in the primary veseel decreases logarithmically, with a kink at t = 45 seconds, coinciding with the shut-off point of the metal foil pump at $p_{\mathrm{low,MFP}}$ = 1 Pa and corresponding reduction of the overall pumping speed of the system. The presures in the other volumes in the retentate stream (INTL) are largely unaffected by this behaviour as the gas load is limited by the effective pumping speed of the linear diffusion pump and show the typical evacuation behaviour. The permeate side of the metal foil pump (DIRL) is also evacuated, initially against the gas load from the active metal foil pump. Once the pressure in the DIRL ring line reaches $p_{\mathrm{low,DIRL}}$ = 100 Pa the dwell bypass stream is engaged, controlling the volume to a constant pressure. The pressure in the subsequent volume of the transfer line then also establishes as constant. As the employed gas vessels feature a time variant hold-up, the dynamic characteristic of the system is governed by the

individual volumes. With the largest volume of the DIR ring-line being only V = 52.5 m³ their overall impact is however minor when compared with the prefacing plasma chamber volume.

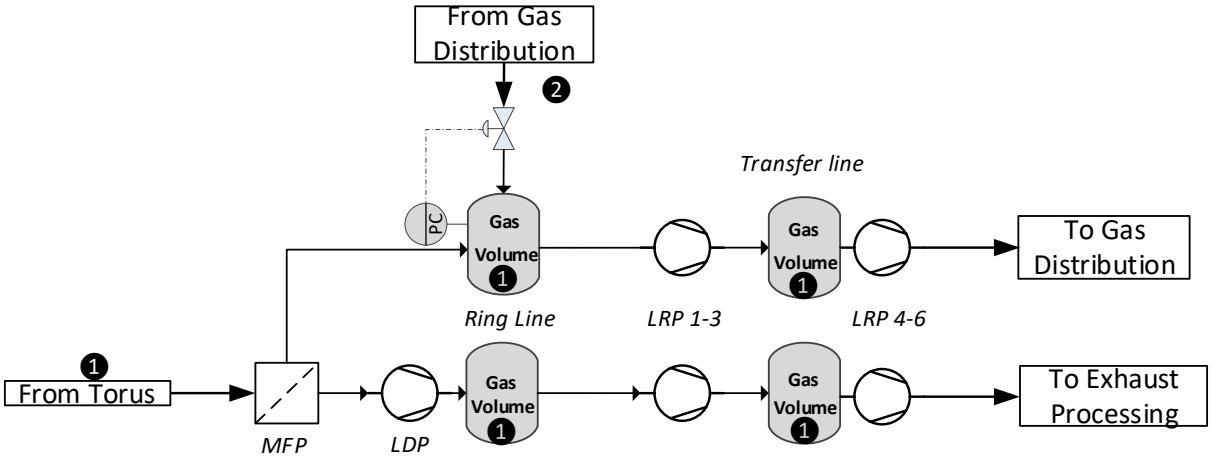

Figure 5.5: Model layout of the fuel separation and torus vacuum system. Grey components indicate areas of gaseous hold-up, white components are hold-up free. Black numbers correspond to Figure 5.6.

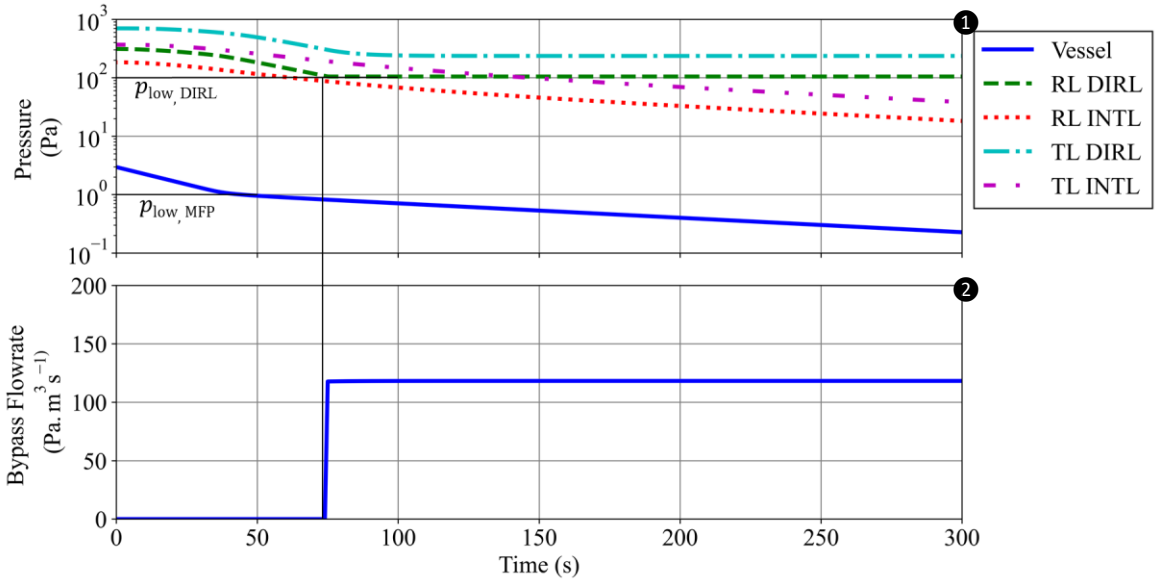

Figure 5.6: ❶: Calculated pressure evolution in the fuel separation and torus vacuum system for evacuation of a V = 6000 m³ vessel. RL: Ring Line. TL: Transfer Line. ❷: Calculated flowrate of the DIRL dwell bypass during that process.

5.2.4 Exhaust Processing

The model of the exhaust processing system (Figure 5.7) is constructed from the permeator model (section 4.3.1), which is supplemented by volume elements and parametric units. Gas from the vacuum pumping system and gas distribution system is received in a volume element (V = 5 liter) representing the inlet manifold of the first permeator stage. The volume is controlled to a

lower pressure limit taking up gas from the gas distribution system if necessary. One superficial permeator model configured to represent an equivalent diameter and volume of an integer number of parallel smaller tubes is used. The retentate of the first permeator stage is controlled to a constant flowrate and routed to a parametric unit prefacing a gas volume (V = 10 liter) , which in combination represent the low and high temperature convertors which can be specified by a decomposition efficiency η_i for each impurity species. The gas volume feeds into the second permeator stage which is set up equivalent to the first stage and employing a pressure controller for the bleed valve at its outlet, maintaining a constant pressure level at the permeator inlet. The permeate of both stages is collected in a gas volume (V = 1 m³) connected to a vacuum pump model specified by a constant pumping speed and the exhaust sent towards the isotope rebalancing system. Due to the requirements of the permeator model (see 4.3.1) molecular hydrogen contained in the feed stream of the first permeator stage is decomposed into its atomic constituents and recombined and re-equilibrated to the operating temperature of the permeator foil at the outlet of the second permeator stage and outlet of the permeate vacuum pump.

The gas detritiation system and PEG removal system are modelled parametrically, since, as per the reference design point (see 3.2) only 0.005% of the circulated tritium in the inner fuel cycle is expected to be routed through these systems. A recovery efficiency for hydrogen and each plasma enhancement gas species is specified. Recovered hydrogens are mixed with the retentate hydrogens and each PEG species is routed individually to the composition control system. The final exhaust of the system is then sent towards the exhaust detritaition system. The configuration of the employed models forming the system is given in Table A.1 in the Appendix.

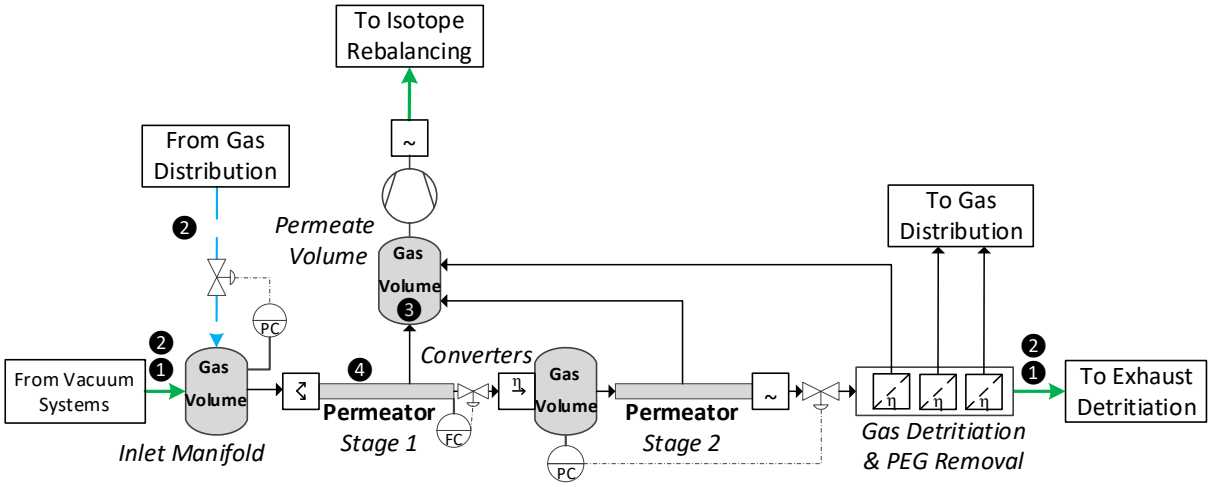

Figure 5.7: Model layout of exhaust processing system. Grey components indicate areas of gaseous hold-up, white components are hold-up free. Black numbers correspond to Figure 5.8.

The dynamic behavior and performance of the system is analyzed assuming the following sequence:

- A constant feed stream flowrate of 89 Pa.m³.s^{-1} of a 50/50 D/T mixture containing 1% protium, 3% helium, 0.2% xenon, and 0.5% argon is introduced to the inlet manifold.
- At t = 0 s the helium content in the feed stream is reduced by 25%.

The system is first operated until a steady state is achieved with the first composition resembling the expected feed stream during flat-top operation as results from the reference design point. Figure 5.8 shows the time evolution of the system response in relevant variables.

The reduction in inert concentration in the system leads to an increase in the total permeated flowrate. In order to maintain the minimum feed side pressure the dwell bypass engages, further amplifying this effect. The pressure in the permeate volume increases accordingly until a new steady state is established. This also leads to an increase in the hydrogen content and simultaneous decrease in the discharged flowrate at the outlet of the system. The overall dynamic characteristic of this system response depends on the available gas volume, which governing the composition and pressure change, with larger volumes increasing the characteristic time needed to establish a new steady state.

The outlet composition furthermore develops an isotope effect with increased tritium and reduced deuterium content. This stems from the internal composition profiles of the permeators. Initially the composition of all hydrogens decreases to the same relative level, given by the equilibrium between the permeate and retentate partial pressures. Even though a partition between the different species over the length of the tube due to different permeation rates is observed, ultimately the same terminal composition is reached and no macroscopic isotope effect occurs. With the increased hydrogen throughput the permeator tube then no longer provides sufficient length to reach a pressure equilibrium for all isotopes. This behavior is also referred to as break-through, showing the same fractionation as reported in [74], leading to an isotopic separation between the permeate and retentate stream.

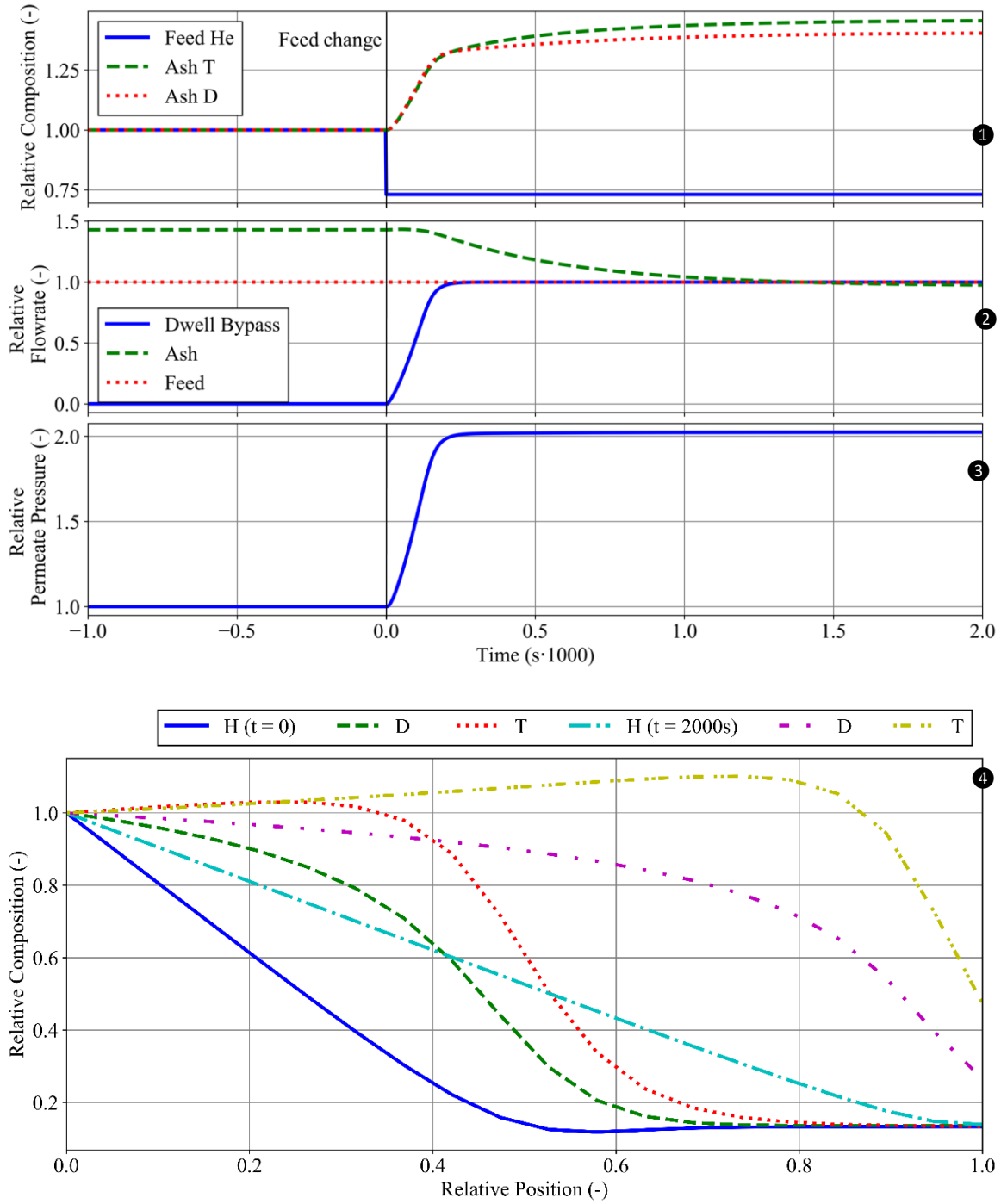

Figure 5.8: Calculated system response of the exhaust processing system to a reduction in the feed helium content. ❶: composition of the exhaust stream overt time. ❷: Flowrates. ❸: Permeate side pressure. ❹: Composition profile in the second permeator stage at the initial (t = 0 s) and final (t = 2000 s) state.

5.2.5 Isotope Rebalancing and Protium Removal

The model of the isotope rebalancing and protium removal system, shown in Figure 5.9, is constructed from two temperature swing absorption column models, a gas volume as feed tank, and a series of parametric valves (open or closed), which in combination with the flexible outer wall temperature boundary condition of the columns are used to govern the cyclic behavior of the system. Table 5.1 gives the series of valve positions and heating/cooling indications for both columns over a series of two cycles, one in which gas is extracted and fed (open cycle) and one where gas is only exchanged between the columns (closed cycle). This set of cycles is then repeated indefinitely. Contrary to other models and systems in the fuel cycle, the dynamic behavior of this system is actively controlled by externally manipulating these boundary conditions. Governing factor for how fast this series of events can be executed is the time required for heating and cooling of the columns. Next to the achieved heat transfer rate, this is influenced by the thermal mass of the system, which is primarily that of the column structural material.

The first column is configured to contain a palladium packing, the second for the titanium – manganese alloy. A constant flowrate of the incoming gas is fed towards the feed tanks, the remainder is routed directly to the gas distribution system. The throughput of the system is scaled by simulating one pair of columns and adapting a given number of pairs operating in parallel. The configuration of the models is given in Table A.1 in the Appendix.

Figure 5.10 shows the resulting system behavior for a series of two cycles. The temperature profile of both columns directly follow the external temperature shift, changing proportional to the offset and achieving thermal equilibrium in approximately half the allotted time. The pressure in the columns also reflects the temperature change according to the absorption isotherms, desorbing gas and building up pressure at high temperatures, absorbing gas at low temperatures. Feed and extraction flowrates (V1 – V3) have sufficient pressure difference available to establish according to their set rate, whereas the flowrate for the exchange between the two columns (V4) is limited by the pressure – flow relationship inside the column packing resulting in a decreasing flowrate as the pressure difference between the columns diminishes.

The dynamic separation behavior of the system is characterized by initializing all hold-ups protium free with an equimolar deuterium tritium mixture and then introducing a constant feed stream to the buffer vessel containing 1% protium in otherwise DT, corresponding to the expected feed composition. Figure 5.11 hows the evolution of the H_2 equivalent flowrates extracted from both columns. Protium starts to slowly build up in both columns, propagating through the column hold-up, which is limited by the available gas volume and maximum allowable pressure in the desorbed state, limited to not exceed p = 4.2 bar. Noticeable quantities of protium start appearing in the extracted streams after approximately two hours and approximately twelve hours are required to reach a steady state in both streams. Larger inventories will consequently delay this characteristic time. The steady state occurs once sufficient protium has build-up in the column to maintain a stable composition profile over the column length, providing the enrichment in the extract of column 2.

Table 5.1: Anticipated valve states (O = open, X = closed) and column outer wall temperature boundary conditions (H = Hot, C = Cold) used to govern the system cyclic behaviour.

Time (s)	**Valve Position**				**Wall Temperature**		
	V1	*V2*	*V3*	*V4*	*C1*	*C2*	
0	X	X	X	X	H	C	Open Cycle
500	X	X	O	X	H	C	
560	X	X	X	O	H	C	
760	X	X	X	X	C	H	
1270	X	O	X	X	C	H	
1320	X	X	X	O	C	H	
1520	O	X	X	X	C	H	
1570	X	X	X	X	H	C	Closed Cycle
1770	X	X	X	O	H	C	
2270	X	X	X	X	C	H	
2470	X	X	X	O	C	H	

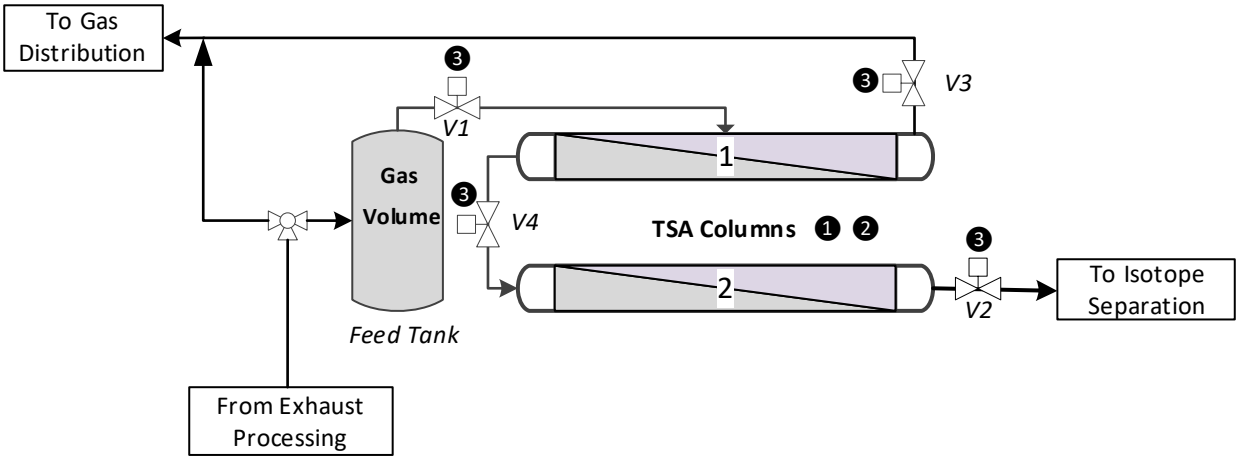

Figure 5.9: Model layout of the isotope rebalancing and protium removal system. Grey components indicate areas of gaseous hold-up, purple solid, white components are hold-up free. Black numbers correspond to Figure 5.10.

Even though only 15% of the total system throughput is extracted from column 2 the total amount of protium withdrawn therefrom is six times higher than from column 1, thus effectively achieving the separation task.

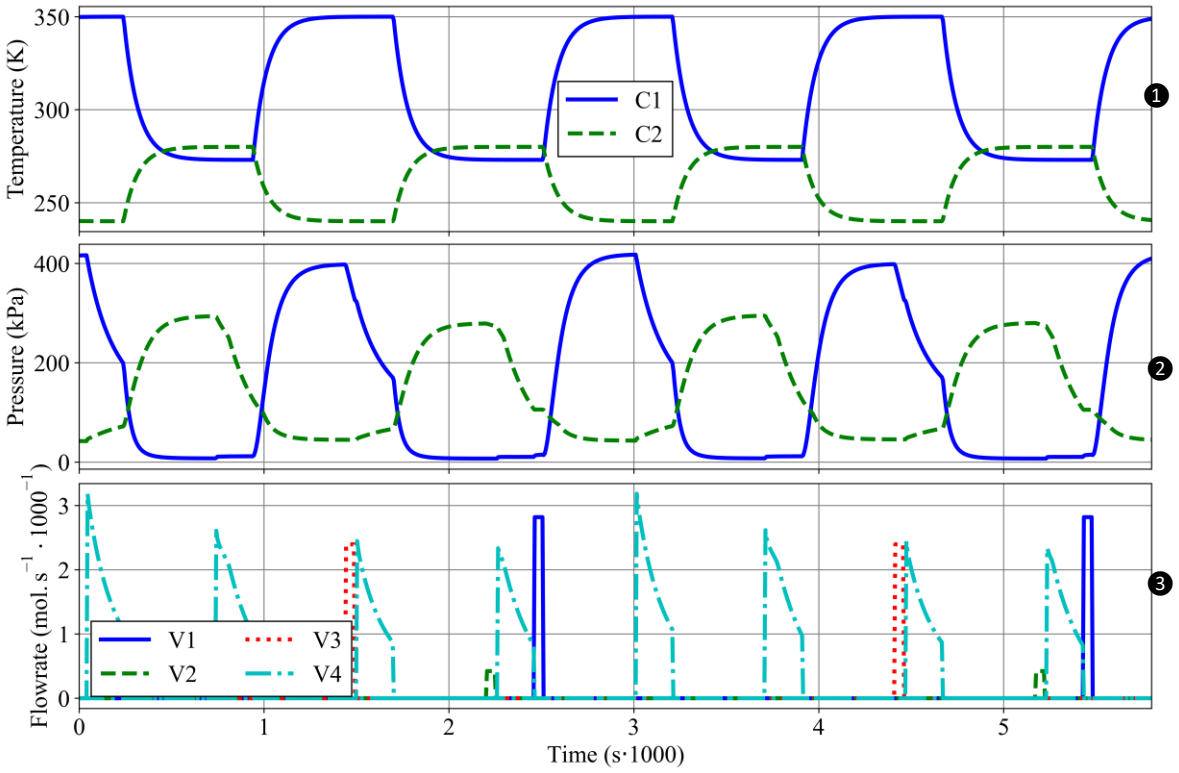

Figure 5.10: Cyclic behavior of the isotope rebalancing and protium removal system. ❶: Internal column temperature. ❷: Column pressure. ❸: Total flowrates through valves 1- 4 (Figure 5.9).

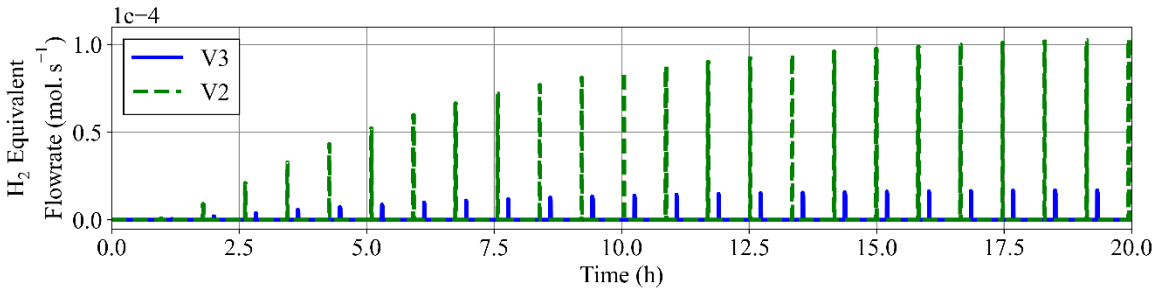

Figure 5.11: Calculated time evolution of the H_2 equivalent flowrate extracted from both columns after protium free initialization.

5.2.6 Exhaust Detritiation

The exhaust detritiation system model, illustrated in Figure 5.12, is constructed of a gas volume with fixed pressure representing the inlet manifold where all feed streams from interfaces and the inner fuel cycle are received. The combined gas stream is passed through a condenser model and parametric units representing the low and high temperature recombiner before being introduced into a saturator prefacing a wet-scrubber column model. The saturator is fed with the water discharged from the bottom of the wet-scrubber column. Liquid water from the saturator and condenser outlets are combined and sent towards the water detritiation system. Gas from the top of the wet-scrubber column is passed through a second condenser and discharged to stack leaving the simulation domain. Liquid water from this condenser is combined with the supplied purified water and introduced at the top of the column. Table A.1 in the Appendix gives the parameter values

employed to configure the used models. One superficial set of models is used to represent multiple parallel trains.

The system behavior is assessed by initializing all hold-ups in a tritium free state and then introducing a feed stream of 12000 $Nm^3.h^{-1}$ at T = 25°C containing 65% relative humidity and a T_2-equivalent tritium fraction of $z_{T2} = 7.30 \cdot 10^{-8}$ at the inlet of the system, corresponding to the steady state reference design point. Figure 5.13 then shows the time evolution of the achievable detritiation factor (DF) of the train, measured as ratio of all tritium, regardless of form, contained in the combined feed stream to all tritium contained in the gas stream discharged from the system. Due to its definition and tritium free initialization the detritiation factor is initially infinity and then rapidly starts to decline as tritium reaches the outlet of the system expressed by a negative exponential decline in time. After one hour a detritiation factor greater than DF = 6500 is reached, which is within is within 15% of the establishing steady state value of DF = 6002 reached after three hours, exceeding the required specification of DF =1000 of the reference design point in this case. With fixed inputs this dynamic behavior is limited by the overall liquid hold-ups in the column and condenser/saturators, corresponding to approx. V_{liq} = 113 liters. Consequently, higher hold-ups will lead to greater characteristic time until steady state is achieved.

Figure 5.13 then also shows the composition profile of HTO in the liquid and gas phase over the length of the column once the system has reached steady state. Both profiles progress in parallel with decreasing concentration towards the top of the column. The concentration in the gas phase is always significantly lower due to the isotope effect, as well as due to the presence of inert species amounting to a total difference of approximately one order of magnitude.

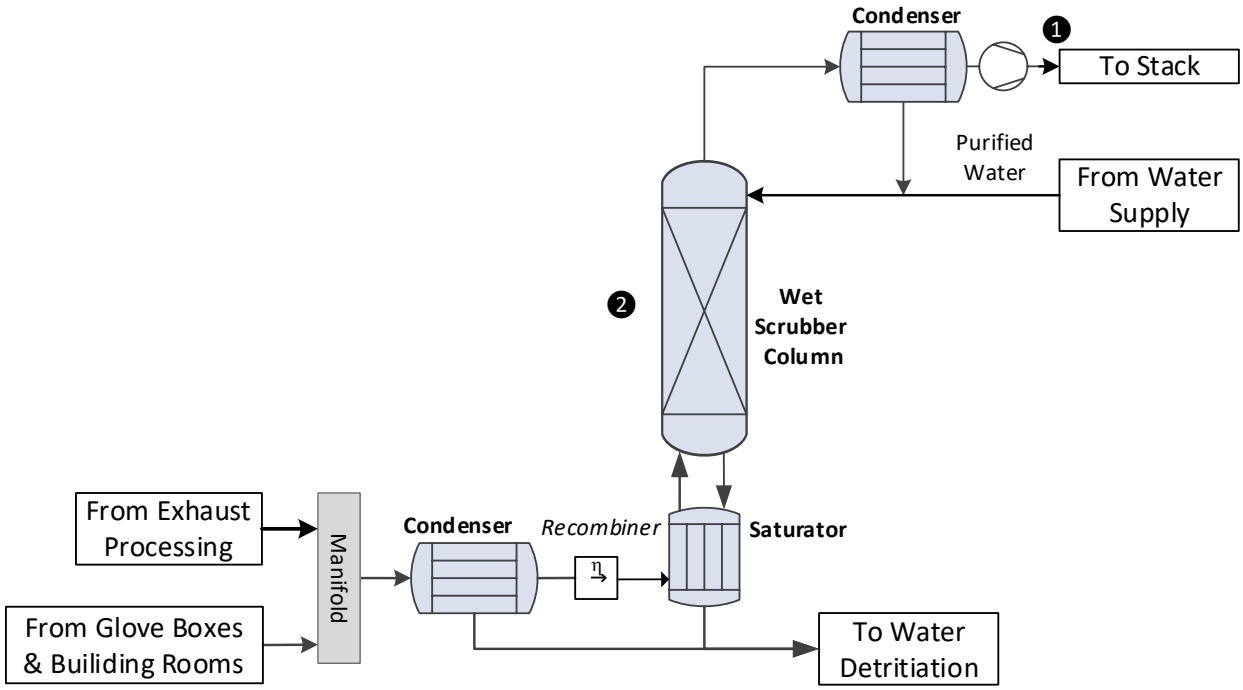

Figure 5.12: Model layout of exhaust detritiation system. Grey components indicate areas of gaseous hold-up, blue liquid, white components are hold-up free. Black numbers correspond to Figure 5.13.

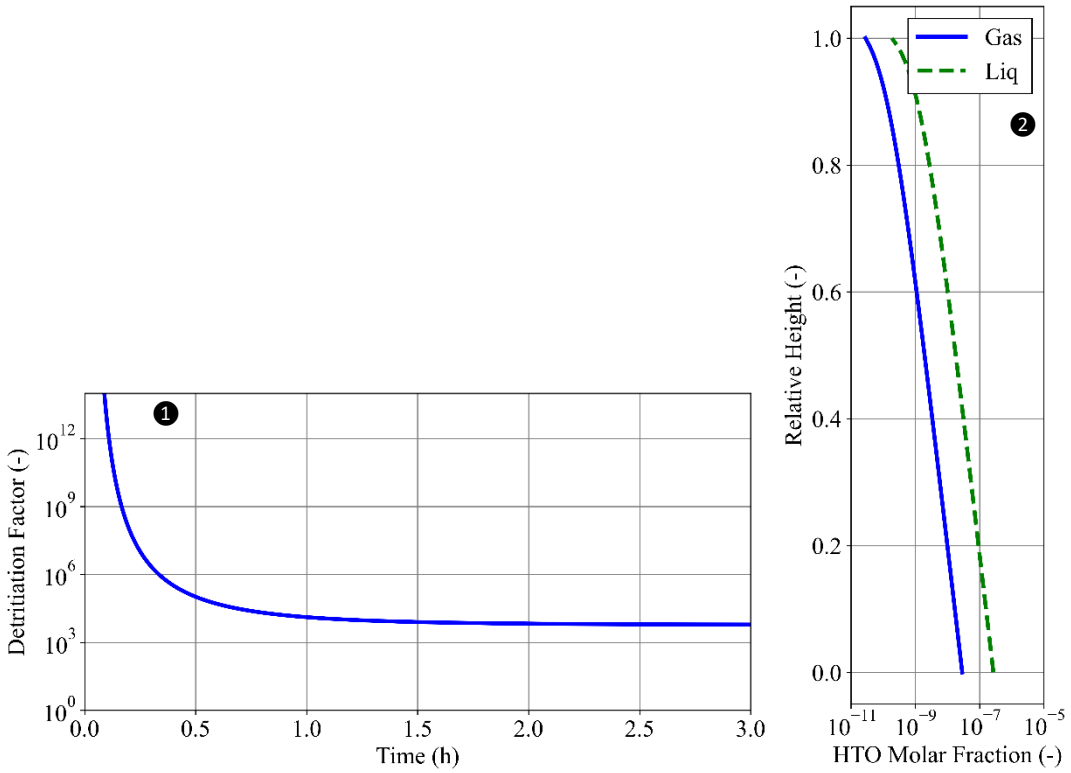

Figure 5.13: ❶: Time evolution of the exhaust detritiation system detritiation factor after tritium free initialization. ❷: Profile of the HTO molar fraction in the liquid and gas phase in the wet scrubber column at steady state.

5.2.7 Water Detritiation

The system model of the water detritiation system as shown in Figure 5.14 is constructed of three LPCE column section models with feed streams located between sections. Each gaseous stream entering a column section is passed through a saturator model configured to the same operating temperature and pressure as the column to guarantee saturated conditions of the inlet gas stream. Liquid from the bottom most saturator is fed into the electrolyzer model which returns the generated hydrogen gas stream to the third LPCE section after passing it through a parametric separation unit modelling the permeator assembly where a set-flowrate of pure hydrogen is taken off. The oxygen stream is similarly passed to a parametric separation unit modelling the oxygen detritiation system, returning a specified fraction of the humidity contained in the stream to the electrolyzer. Gas from the top of the last LPCE segment is passed through a condenser and put into storage, leaving the simulation domain. Liquid water from this condenser is combined with the supplied purified water and introduced at the top of the section. Table A.1 in the Appendix gives the parameter values used to configure the models.

In order to investigate the dynamic behavior and performance of the system it is initialized into a tritium free state and a feed streams corresponding to the reference steady state operation point are introduced. A liquid feed stream of $\dot{m}$ = 200 kg.h^{-1} (= 3.07 mol.s^{-1}) with a tritiated water molar fraction of x_{HTO} =7.6·10^{-6} is introduced between the second and third section, as well as a gaseous hydrogen stream of 1.06 mol.s^{-1} containing a HT molfraction of z_{HT} = 1·10^{-8} between the second and third section.

Figure 5.16 then shows the time evolution of the tritium content in the stream drawn off towards the ISS as well as the HTO and HT content in the detritiated stream of the top of the column. The ISS draw-off initially enriches faster, it is however limited in reaching its new steady state by the slower establishing tritium concentration profile in the column, only reaching steady state once the LPCE segments also do. Overall the system needs approximately 19 hours to reach steady state. This dynamic behavior is primarily dominated by the liquid hold-up on the column packing and in the electrolyser, totaling approx. V_{liq} = 4.6 m³, far exceeding any gaseous hold-ups.

Figure 5.15 shows the concentration profile over the length of the individual LPCE sections once steady state is achieved. The relative content of HTO in their respective liquid and gaseous phase coincide, resulting from a rate limitation of the mass transfer between the liquid and gas phase. The bottom two section also show a “flat lining” of the concentration profile, stemming from an insufficient liquid to vapor ratio, resulting in slightly oversized segments for the achievable total separation.

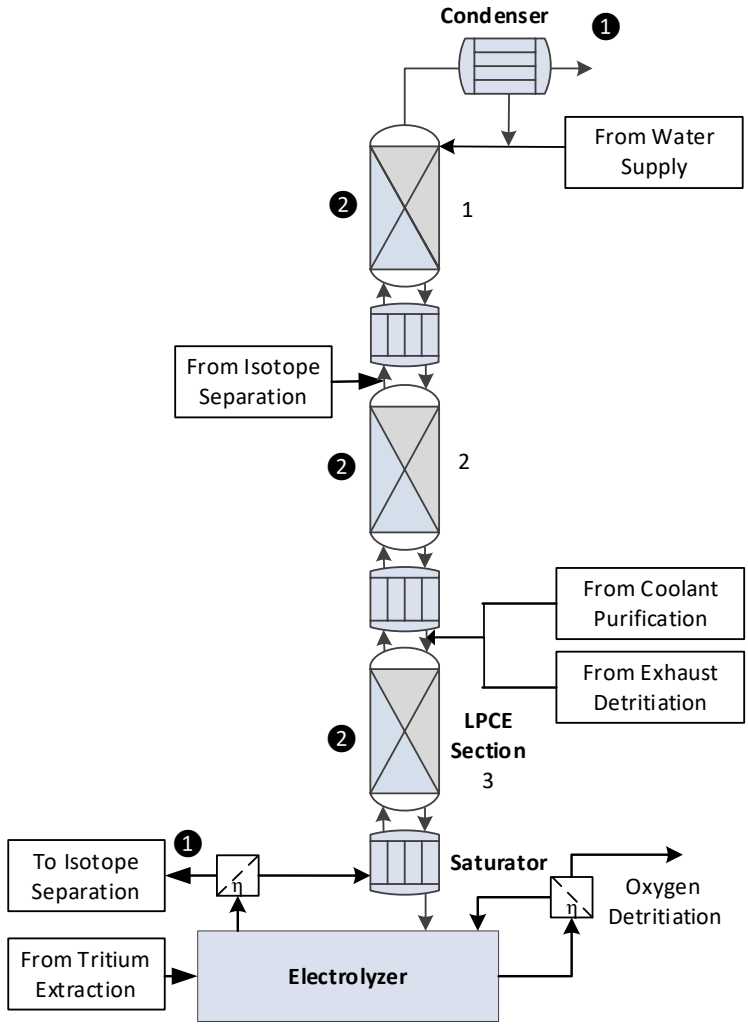

Figure 5.14: Model layout of the water detritiation system. Grey components indicate areas of gaseous hold-up, blue liquid, white components are hold-up free. Black numbers correspond to Figure 5.15 and Figure 5.16.

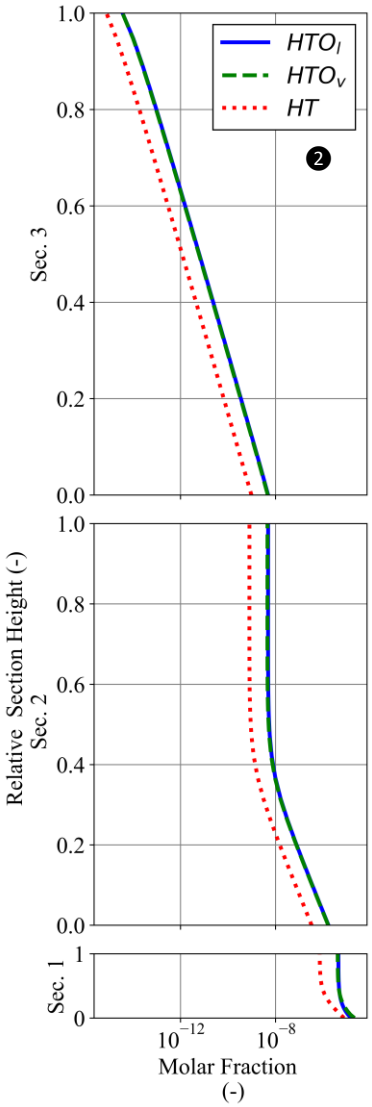

Figure 5.15: Calculated composition profiles for tritiated molecules in gas vapor and liquid phases in the LPCE column at steady state (t = 20 h).

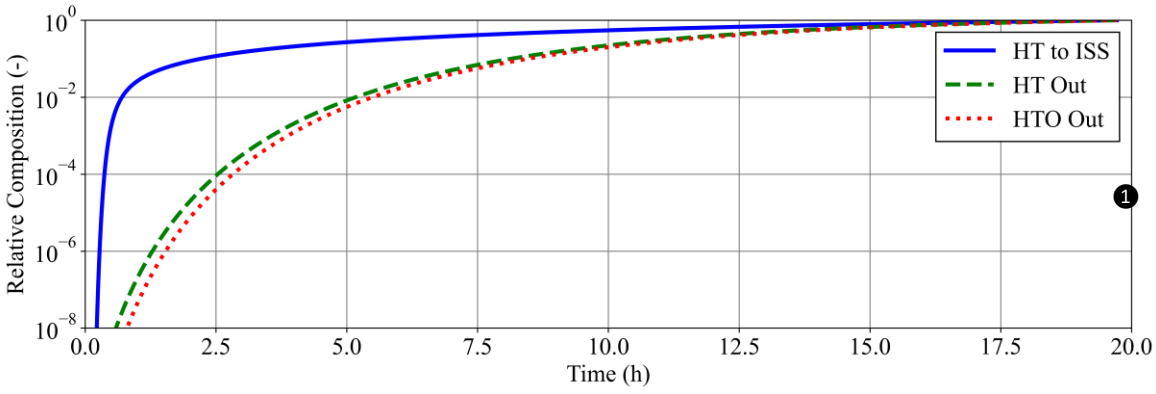

Figure 5.16: Calculated time evolution of the relative tritium content in the product streams of the water detritiation system (❶) after a tritium free initialization.

Verification of solver settings

The processing rate of 3.07 mol.s^{-1} and a concentration gradient over the length of the LPCE column model spanning more than eight orders of magnitude mark the most challenging numerical environment of all rate-based models in the fuel cycle simulation. It is therefore used to verify adequate settings for the employed solvers (see section 5.1). These are the longest discretization length of a LPCE column segment $\Delta x_{\max}$, the enforced minimum time step of the implicit Euler integrator $\Delta t_{\min}$, as well as the selected absolute and relative tolerances ϵ. For this purpose the run presented in Figure 5.16 is repeated, selectively relaxing first each single parameter and then all in conjunction. The employed parameter values for each run are reported in Table 5.2.

Figure 5.17 shows the sensitivity of the temporal evolution of the HT fraction in the stream directed to ISS relative to that of the reference case (solid line in Figure 5.16), calculated as $s = z_{\mathrm{HT,i}} \cdot z_{\mathrm{HT},1}^{-1} - 1$. In all case a deviation at the beginning of the simulation, where gradients are highest due to the step change, is observed. However, the deviation between solutions does not exceeded the specified tolerances in any case and converges to negligible values in all cases, confirming that the simulation result is not sensitive to the selected parameters.

Table 5.2: Cases of different numerical solver settings to test the sensitivity of the obtained simulation solution. Case 1 marks the reference case employed in this work.

Case #	$\boldsymbol{\Delta x_{\max}}$ **(m)**	$\boldsymbol{\Delta t_{\min}}$ **(s)**	$\boldsymbol{\epsilon}$ **(-)**
1 (Reference)	1.5	$1 \cdot 10^{-3}$	$1 \cdot 10^{-5}$
2	1.6	$1 \cdot 10^{-3}$	$1 \cdot 10^{-5}$
3	1.5	$2 \cdot 10^{-3}$	$1 \cdot 10^{-5}$
4	1.5	$1 \cdot 10^{-3}$	$2 \cdot 10^{-5}$
5	1.6	$2 \cdot 10^{-3}$	$2 \cdot 10^{-5}$

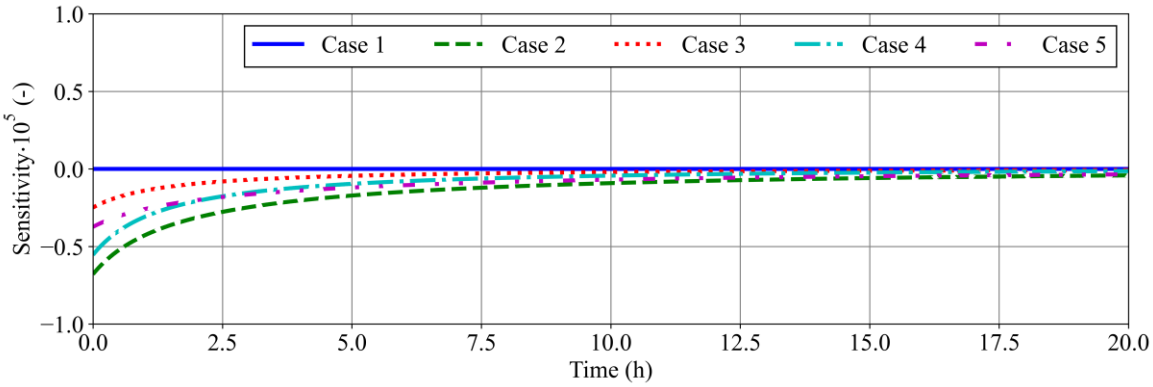

Figure 5.17: Sensitivity of the calculated temporal evolution of the HT fraction to ISS to variations in numerical solver parameters, calculated as $s = z_{\mathrm{HT,i}} \cdot z_{\mathrm{HT},1}^{-1} - 1$. The cases are listed in Table 5.2.

5.2.8 Isotope Separation

The model of the isotope separation system is constructed from cryogenic distillation column models mirroring the systems 3-column architecture, and is sketched in Figure 5.18. Streams interconnecting two columns are re-equibrilated to their isotopic equilibrium at a specified temperature. The first column directly interfaces to the water detritiation system receiving a tritium rich feed stream and returning a depleted protium stream for final detritiation. The feed stream from tritium extraction is received in a buffer tank and passed with a constant flowrate to the second column, mixed with the bottom product of the first column and the return stream from the third column. The feed stream from isotope rebalancing is received in a buffer tank and passed with a controlled flowrate to the third column mixed with the bottom product of the second column. The bottom product of the third column is passed to the gas distribution system as tritium rich stream for composition control and burn-up make-up. Table A.1 in the Appendix gives the configuration of the models used to construct the system.

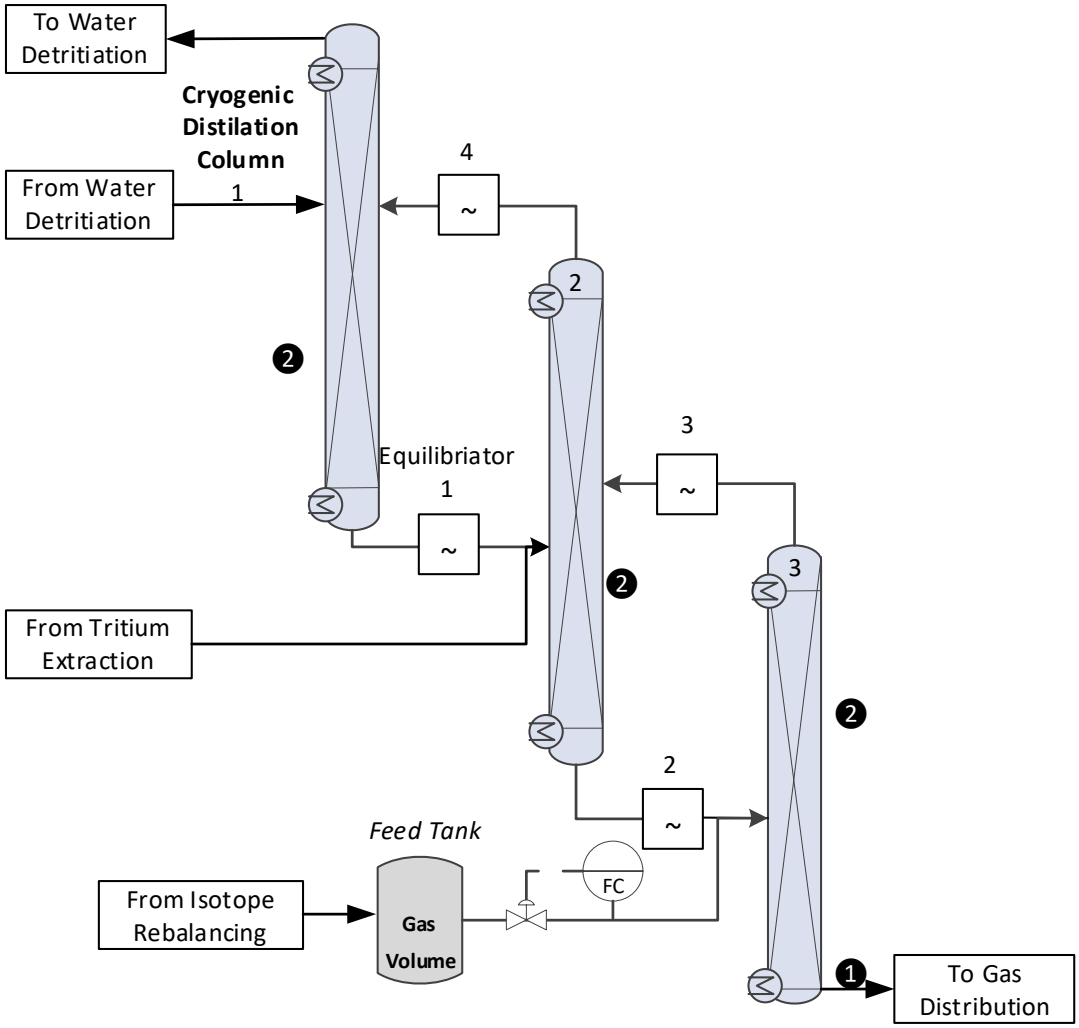

Figure 5.18: Model layout of the isotope separation system. Grey components indicate areas of gaseous hold-up, blue liquid, white components are hold-up free. Black numbers correspond to Figure 5.19 and 5.20.

The stand-alone behaviour of the system is analyzed by initializing it into a tritium free state (pure H_2 in columns 1 and 2, pure D_2 in column 3) and then introducing the following feed streams, representing the reference design point in case of a WCLL breeding blanket being employed:

- A constant feed stream of F_{feed} = 0.60 mol.s^{-1} protium with a tritium content of x_T =1·10^{-5} present in the form of HT is received from the WDS.
- A constant feed stream of F_{feed} = 0.22 mol.s^{-1} hydrogen containing 0.26% tritium present in the form of HT is received from tritium extraction.
- A constant feed stream of F_{feed} = 7.1·10^{-4} mol.s^{-1} with an atomic composition of 32% T, 61% D and 7% H in isotopic equilibrium at T = 300 K is received from isotope rebalancing.

Figure 5.19 then shows the simulated time evolution of the composition in the systems tritium rich product stream for all isotopologues as well as overall atomic isotope fractions. Even though the system requires more than 160 hours to reach a steady state in the isotopological composition of its product stream, the overall deuterium and tritium fraction establishes much faster, attaining a usable product for fueling after 20 hours. At this time the protium content drops below 1% and a total tritium enrichment of 65% is achieved. The final product consists of DT and T_2, containing 0.6% D_2 and 0.03% HT. The dynamic response is characteristic for the superposition of individual dynamic responses of each column. With different throughputs and hold-ups, each column features its own characteristic time. As the last column is the smallest, the concentration of its key species (T_2, DT) establishes fast compared to that of non-key species (H_2, HD, HT, D_2) which are refluxed through the other, larger, columns.

Figure 5.20 shows the concentration of the gas phase in the 3 columns on each equilibrium stage, once steady state is established. The first column acts primarily as a volume reduction step, rejecting 99% of its feed stream while passing all isotopologues heavier than H_2 towards the second column, with the stream still being made up of dominantly protium. The second column then achieves a notable reduction in protium content, enriching the heterogenous isotopologues. The last column finally achieves the separation of all protium containing isotopologues enriching DT and T_2 in the final product.

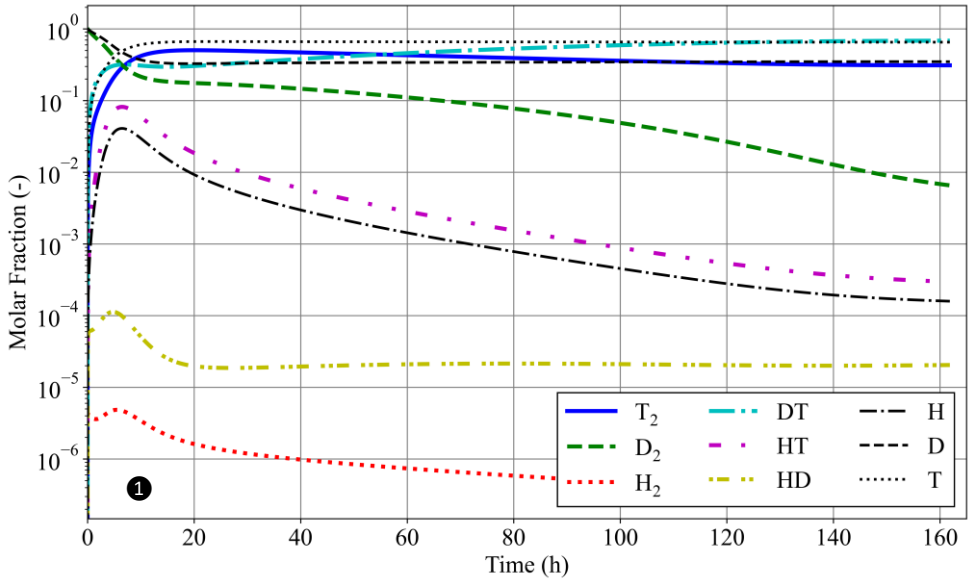

Figure 5.19: Calculated temporal evolution of the tritium rich product composition of the isotope separation system after tritium free initialization.

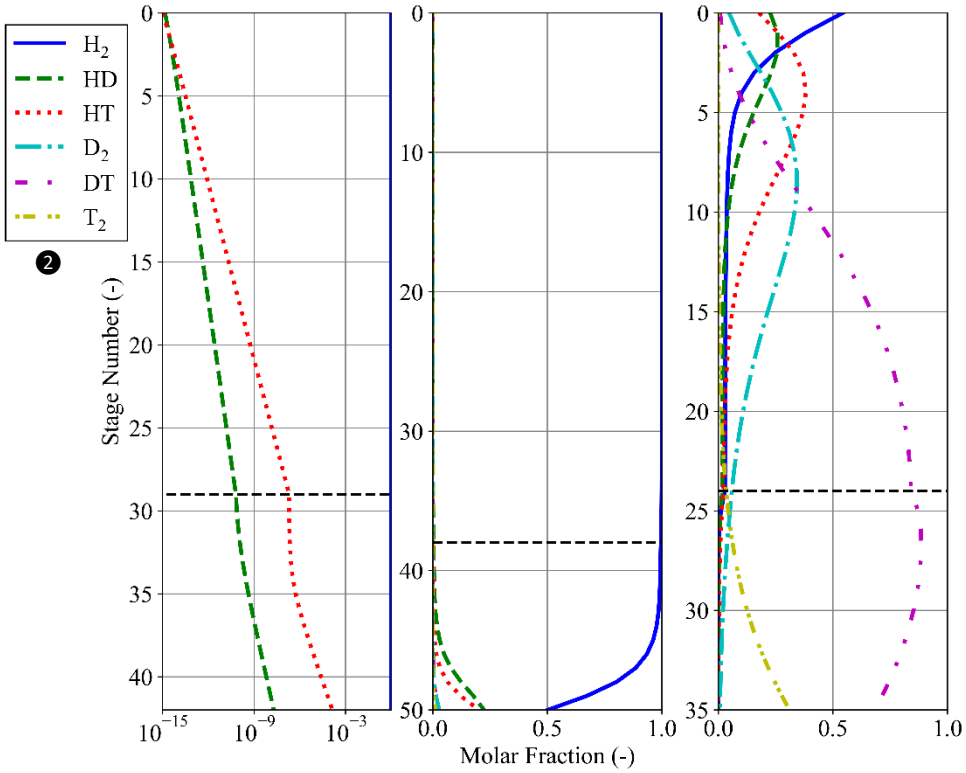

Figure 5.20: Simulated composition in the gas phase of each stage of the three cryogenic distillation columns (❷) in the isotope separation system at steady state (t = 160 h). Dashed horizontal lines indicate the feed location. Stage 0 marks the top of each column.

6 Evaluation of the EU DEMO Fuel Cycle Dynamic Operation

Having developed a desirable steady state design point and tested the dynamic behavior of fuel cycle system models in a pre-defined environment, the final step is the integrated dynamic simulation of the entire closed fuel cycle to analyze its performance and robustness. Figure 6.1 shows the complete simulation domain containing all models, streams and interfaces. All areas of hold-up are indicated and Table A.1 in the appendix then summarizes the configuration of all components and interfaces. The figure also contains unique labels for each stream that will be referred to in the following discussion and figures.

When investigating the behavior of complex processes and systems two type of sensitivity studies are commonplace.

- Firstly, the design space is explored by imposing varying design scenarios and optimization criteria, aiming to find sets of design and operating parameters that allow to either cover a wide range of different scenarios, or yield optimal performance in few select cases.
- The second type of sensitivity study then is that of the operational space, investigating a fixed system design representing an “as built” status, for variations in operating conditions and defining the feasible operating space.

As the fuel cycle simulator is purpose-built to test the integral behavior of the fuel cycle by consolidating all sub-system designs initially developed, the following analysis is limited to the operational space. For this purpose first the normal operation characteristic of the fuel cycle in dynamic operation is explored, investigating the achievable performance. In a second step the tolerance to deviations in its interfaces is discussed, characterizing the fuel cycle operational space.

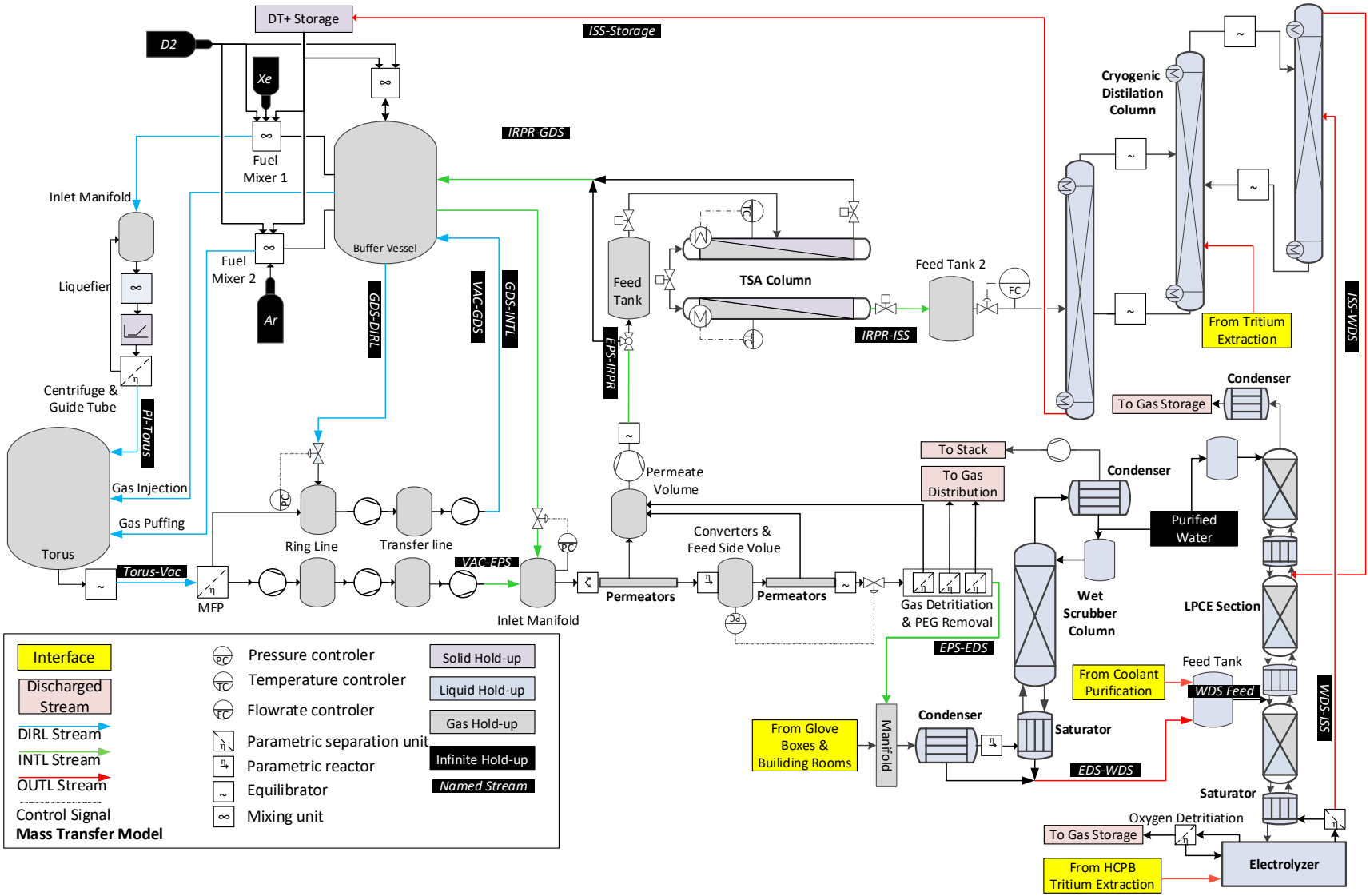

Figure 6.1: Simulation domain of the integrated fuel cycle process simulation.

6.1 Normal Operation Characteristics

The normal operation of the fuel cycle is given by the reference configuration of all of its systems and interfaces, operating with uninterrupted repetition of standard burn-dwell pulses and employing a WCLL breeding blanket. This operation point corresponds to a configuration in fuel cycle boundary conditions of a fueling rate of $R_{\mathrm{F}} = 0.06$, a isotope rebalancing fraction of $R_{\mathrm{H/D/T}} = 0.025$, a tritium extraction load of $R_{\mathrm{E}} = 1.05$, as well as a predicted tritium recovery load of $R_{\mathrm{R}} = 0.011$. The simulation containing all integrated system models and interfaces is run until a steady state or pseudo steady state has established in all systems before being evaluated, starting at the beginning of a flat-top phase marking t = 0 s.

The most important figures of merit for the fuel cycle are the availability of fuel in the desired compositions, as well as tritium inventories and discharges to the environment. Hence the dynamic operation of the fuel cycle is analyzed with respect to these. The dynamic evolution of the following variable values is therefore recorded for each simulation run:

- The total flowrate and tritium equivalent flowrate between each system.

  These results include a direct measurements of the tritium flowrates discharged from the fuel cycle. The full set of dynamic throughputs in all systems furthermore allows for a direct comparison to the formulated reference design point, enabling trace back of causes and effects if deviations are observed.

- The total tritium inventory in each area of hold-up.

  While tritium inventories in fuel cycle systems are in-itself a figure of merit the observation of their dynamic behavior allows to monitor the transfer of tritium through the systems and, in combination with storage and reserve inventories, to also judge the availability thereof for operation of the Tokamak.

- The composition of fuel in the gas distribution DT buffer vessel.

  Next to the availability of tritium, the composition with which it is supplied to the fueling systems has to be within acceptable limits. Any deviations from the nominal D/T ratio must be small enough to be able to be compensated by the composition control system and the long term trend of the protium contamination must be stable and show no accumulation with time.

Figure 6.2 shows the simulated tritium equivalent flow rate of all major streams between fuel cycle systems over the duration of eight pulses. The strongest transients are observed in the direct internal recycling loop, simultaneously showing the highest absolute flowrates of 0.57 $g.s^{-1}$ tritium being cycled through the plasma chamber during the flat-top phase. The flowrates of all streams directly follow the burn-dwell cycle, dropping to negligible values over the duration of the dwell phase. The only exception is the dwell-bypass loop of the torus vacuum system (GDS-DIRL), providing approximately one third of the flat-top throughput in order to maintain a sufficiently high pressure on the metal foil pump permeate side.

The inner tritium plant loop throughputs also reflect the burn-dwell cycle and additionally the cyclic operation of the isotope rebalancing system which discontinuously discharges products towards the gas distribution buffer vessel. Due to the use of direct internal recycling, tritium throughputs are

naturally lower, with 0.11 $g.s^{-1}$of tritium being received from the DIRL during flat-top (VAC-EPS). During the dwell phase the torus bypass between the central buffer vessel and the exhaust processing inlet is engaged in order to maintain a constant feed pressure (GDS-INTL). The absence of fusion ash (helium) in that stream leads to elevated throughput of the employed permeators (see section 5.2.4), resulting in an increased tritium flowrate of up to 0.27 $g.s^{-1}$ having to be supplied at peak during the dwell phase and dropping off as flat-top throughputs re-establish during the burn phase. This increase then also propagates towards the IRPR system (EPS-IRPR). The outgoing flow of the isotope rebalancing system towards the DIRL (IRPR-GDS) is the superposition of the continuous flow not taken up to fill its feed buffer vessel, as well as the enriched fraction of the system being discharged up to three times per pulse.

Tritium flowrates in the outer tritium plant loop are significantly less affected by the cyclic operation of the Tokamak and IRPR system. Oscillations incurred from the intermittent discharge from the IRPR system can be completely negated by the means of a buffer tank from which a constant flowrate is extracted and consequently a constant input for the isotope separation system in flowrate and composition can be obtained (IRPR-ISS).

Figure 6.2 also shows the variation of each tritium flowrate of each major connection in the OUTL. For convenience each streams average position is offset by 10% in negative y-direction to avoid overlapping. The large hold-ups in systems of the outer fuel cycle act as an efficient damping element for any transients received from the inner fuel cycle (EPS-EDS). A reduction of fluctuations with distance from the interface to the inner fuel cycle (along the route of EDS – WDS – ISS) towards the product received from isotope separation (ISS-Storage) is observed until ultimately no significant oscillation remains in the product streams from ISS. This stream is also the largest absolute tritium flowrate in the OUTL at $5.01 \cdot 10^{-3}$ $g.s^{-1}$s, containing all tritium that is routed to the outer fuel cycle from its interfaces and the inner fuel cycle, marking the first product stream.

The second fuel cycle product is the tritium free stream discharged to stack (Stack), totaling a time averaged tritium flowrate of $5.46 \cdot 10^{-9}$ $g.s^{-1}$ tritium is discharged from stack and still showing periodic oscillations with a standard deviation of +- $2.88 \cdot 10^{-11}$ $g.s^{-1}$, resulting in an annual tritium discharge of 0.17 gram tritium per year in the form of HTO. This is significantly lower than the predicted 0.92 gram per year for the reference design point, even though more tritium is received from the inner fuel cycle (EPS-EDS) ($6.41 \cdot 10^{-5}$ $g.s^{-1}$ vs. predicted $2.81 \cdot 10^{-5}$ $g.s^{-1}$), however, the better than specified exhaust detritiation system performance (see section 5.2.6) is able to still provide the necessary detritiation. This also marks a further reduction from the 1.6 $g.year^{-1}$discharge estimated for an earlier design iteration as reported by Hörstensmeyer in [43] and can be attributed to the further optimization of the inner fuel cycle architecture and performance aiming to minimize tritium efflux to the OUTL.

The tritium flowrate in the fueling product from the isotope separation system (ISS-Storage) is slightly higher than predicted from the reference design point ($5.01 \cdot 10^{-3}$ $g.s^{-1}$ vs. $4.77 \cdot 10^{-3}$ $g.s^{-1}$), with the difference arising from more tritium being discharged from the inner tritium plant loop to EDS (EPS-EDS), as well as from the isotope rebalancing system ($1.58 \cdot 10^{-3}$ $g.s^{-1}$ vs $1.41 \cdot 10^{-3}$ $g.s^{-1}$) (IRPR-ISS). At the same time the isotopic composition of the product stream ($y_H = 3.65 \cdot 10^{-5}$, $y_D = 0.325$, $y_T = 0.675$) does not meet the specification of the reference design point, requiring at least 70% enrichment in tritium. This is due to the fact that the isotope separation system has no active means to control for deuterium content, as only a heavy and light stream is produced. An additional

product stream and distillation column is required to enable arbitrary adjustments to the deuterium content in both products.

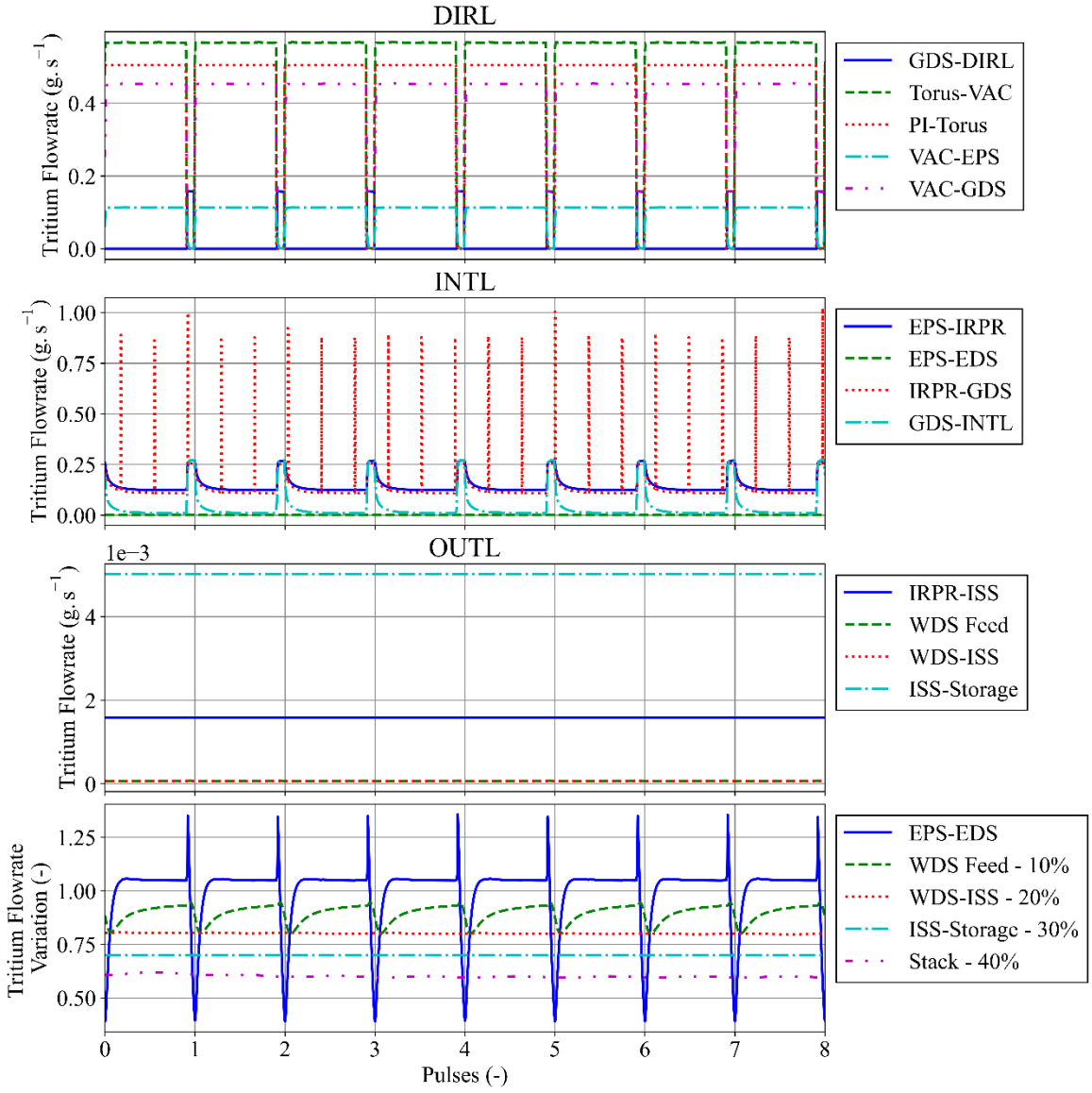

Figure 6.2: Simulated dynamic tritium flowrates in the three loops of the EU-DEMO fuel cycle as a function of reactor pulses. From top to bottom: direct internal recycling loop, inner tritium plant loop, outer tritium plant loop, time variations in selected streams.

These deviations from the reference design point, however, do not threaten the operational aspects of the inner fuel cycle. Figure 6.3 shows the evolution of the D/T ratio of gas in the central buffer vessel as well as the protium content of the contained gas. Deviations from unity, towards higher tritium content, are observed whenever product from the temperature swing absorption columns in isotope rebalancing is discharged. On the other hand, deviations towards higher deuterium content occur during burn-dwell cycling due to the isotope effect observed in the exhaust processing system (see section 5.2.4). The overall time averaged D/T ratio in the vessel is slightly tritium rich at 0.998. The highest localized deviation towards deuterium excess amounts to 0.9%, occurring when burn-dwell cycling does not coincide with an IRPR discharge. As a result only minimal adjustments with tritium rich fuel are needed for which the achieved tritium enrichment in the fuel product stream is more than sufficient. This means that the criterion for tritium enrichment

can even be relaxed in order to not force unnecessary tritium inventories in the isotope separation system.

The protium fraction in the buffer vessel exhibits a similar temporal behaviour as the D/T ratio, naturally drifting upwards and being reduced by discharges from the isotope rebalancing system and fuel take-up, while increasing more strongly during burn-dwell cycling. In total a stable time averaged protium content of 0.063% with fluctuations between 0.066% and 0.056% is obtained.

The combination of all cyclic processes also uniquely reflects on the pressure in the buffer vessel. At all times a lower limit of 700 mbar is ensured by the control system by feeding gas from storage until a pressure of 800 mbar is reached. When receiving a discharge from the IRPR system the pressure increases to approx. 1100 mbar, depending on the initial pressure. Pressure increases are also observed during burn-dwell cycling, leading to pressure spikes of up to 1300 mbar when both events coincide.

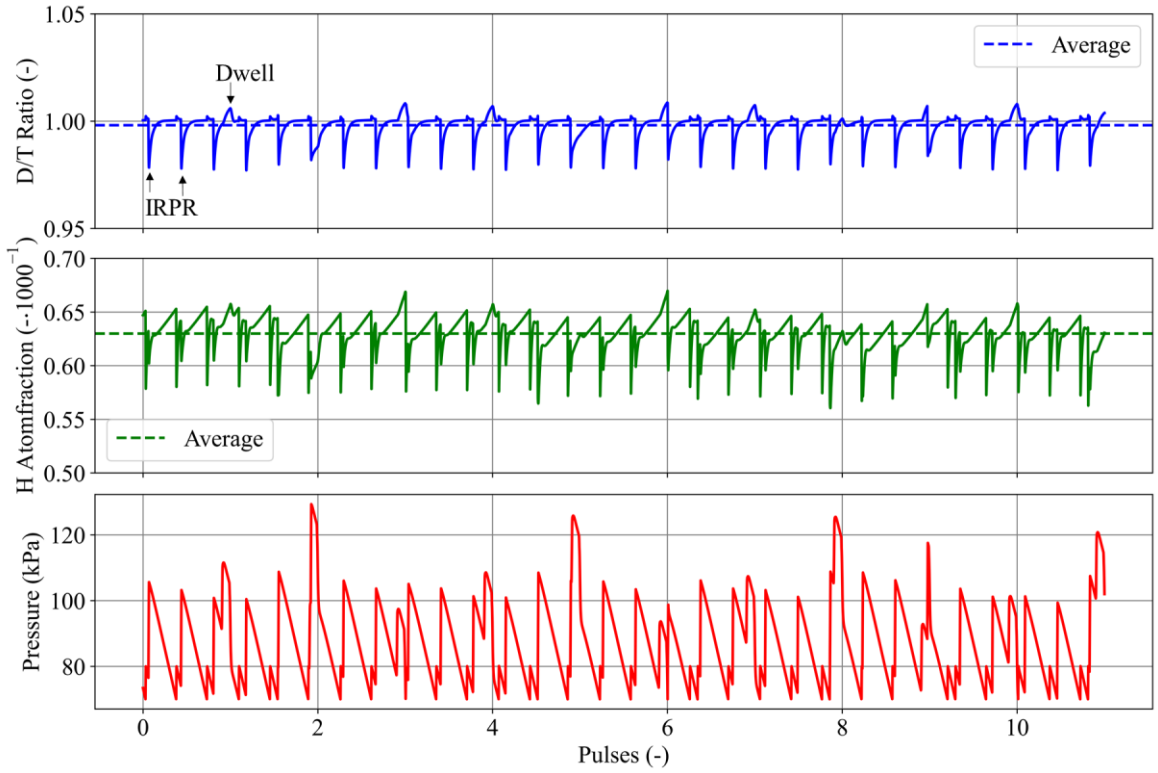

Figure 6.3: Simulated time evolution of variables in the central DT buffer vessel of the gas distribution system. Top: D/T ratio, mid: Protium contamination, bot: Pressure. Dashed lines indicate the time average over the depicted time interval.

As strong oscillations in the tritium flowrates occur in the inner fuel cycle, and to a reduced degree also in the outer fuel cycle, tritium inventories in the individual hold-ups are also affected. Figure 6.4 shows the simulated evolution of the tritium inventory in each system over the duration of eight burn – dwell cycles.

Once having attained a steady state the matter injection system tritium inventory remains constant, as here hold-ups are controlled to constant levels and a controlled composition of the fuel is received. The torus tritium inventory directly follows the burn-dwell cycle without any significant delay, dropping to negligible amounts during the dwell phase from approximately 8 g during the burn phase. The torus vacuum system shows the same behavior in volumes of the INTL pumping

train which experience the same evacuation. As the permeate side of the metal foil pump is controlled to a minimum pressure, tritium inventories in the DIRL system are not as heavily affected. A total of 30 g tritium inventory as gas is present in the systems volumes during flat-top operation dropping to 9 g at the end of the dwell phase.

The exhaust processing system shows inverse oscillation due to the engagement of the dwell bypass stream in which helium and plasma enhancement gases are absent. The resulting elevated tritium concentration in the volumes of the systems lead to an inventory increase to more than 8 g during the dwell phase in contrast to 6 g during flat-top.

The isotope rebalancing system represents the highest tritium inventory system of the fuel cycle with a total combined inventory of up to 492 g. The inventory shows an oscillating pattern, prompted by the periodic discharge and take up of gas. Up to 138 g of tritium are accumulated in the feed buffer vessel, of which 42 g are fed into the TSA columns once every cycle of the system. Their inventory is then shifted between the two columns, amounting to a maximum inventory of 236 g and 207 g in the first and second column respectively. The maximum inventory in each column is only reached if the other column is at a minimum of respectively 132 g and 133 g. Due to the use of the feed buffer vessel the systems inventory is not affected by the burn – dwell behavior of the Tokamak.

Tritium inventories in the systems of the outer fuel cycle are in a similar manner, but orders of magnitude lower, affected by the cyclic behavior of the inner fuel cycle. The exhaust detritiation system, interfacing to the exhaust processing system still shows minor oscillations in all components following the characteristic of the tritium flowrate across the interface. At any given time a maximum of 0.2 g tritium are present in the system, predominantly in the liquid hold-up of the saturator and wet scrubber column.

This pattern propagates dampened to the LPCE column in the water detritaition system in which 0.3 g of tritium are being held-up in liquid water. The majority of the systems inventory is present in the electrolyzer where tritium concentrations are highest, totaling a maximum system inventory of 2.1 g.

The isotope separation system buffers the intermittent flow received from the discharge of the isotope rebalancing system, inducing similar inventory oscillations between 16 g and 21 g in the buffer vessel. The inventory in the cryogenic distillation columns on the other hand is constant and is not affected by transients in any of the interfaces between inner and outer fuel cycle. Even though the size of the columns reduce with increasing tritium content, the third column still shows the highest inventory of 44 g, closely followed by the second column with 40 g. In total the system is able to operate with a maximum tritium inventory of 106 g.

Lastly, the gas distribution system is the central hub of the fuel cycle and experiences all transients of the burn-dwell behavior as well as the cyclic IRPR operation. As a consequence its tritium inventory, directly linked to the vessel pressure, fluctuates most heavily. During dwell phases gas moves from the torus and vacuum system to the buffer vessel while at the same time periodic discharges from IRPR arrive. Whenever these events coincide the inventory peaks, with a maximum observed case during eight pulses of 158 g. A lower limit of 84 g in the buffer vessel is enforced by the pressure control system by replenishing fuel from storage.

If looking at the combined operational tritium inventory off all fuel cycle systems, illustrated in Figure 6.5, over the duration of a single pulse no constant value is observed. The inventory is

depleted with time due to burn-up and increased once fuel is replenished. When also taking into account the storage, all oscillations cancel out and a constant total fuel cycle inventory is observed. This confirms the fully closed mass balances and negligible losses from the fuel cycle, guaranteeing the sufficient availability of tritium. In combination with the observed stability in the fuel composition and acceptable tritium discharges from the stack this operation point satisfies all requirements.

Tritium inventories present in the hold-ups of the system models and thus required for the operation of the fuel cycle are, with a total upper bound of less than one kilogram, very reasonable. It must, however, be pointed out that the inventories reported here are not directly representative of the total operational inventory of the fuel cycle to a level of detail as required from an accountancy perspective. The focus here is on the dynamic operation and behavior of the closed fuel cycle. Tritium extraction and coolant purification systems are not part of the simulation domain, and additionally only hold-ups in components are considered that impact the dynamic behavior. For example, the vapor phase in a gas – liquid contacting column generally does not limit the dynamics of composition changes and as such is not considered in respective models. However, especially at high tritium concentrations a non-negligible inventory can still be observed. Additionally, by virtue of the employed models, the absolute amount of hold-ups depend on the sizing of the individual components. While the here presented configuration achieves the overall requirements, no optimization towards lower tritium inventories by changing the physical component sizing is considered. Lastly, tritium may also sequestrate into structural material leading to a build-up of inventory which is not part of the operational fuel cycle inventory and as such not considered here.

The observed dynamic characteristics of tritium inventories and flowrates (acting also as surrogate for overall flowrates and inventories) warrant the conclusion that the employed configuration satisfies all requirements of the stated reference design point. Albeit minor shortcomings are observed in the amount of tritium discharged from the inner fuel cycle via the EPS – EDS interface, as well as in the achievable tritium enrichment in the fueling product of the outer fuel cycle, the overall operability of the fuel cycle is not impacted. The increased tritium flowrate towards tritium recovery systems leads to an increase of the tritium recovery fraction to $R_{\mathrm{R}} = 0.029$, as compared to the predicted $R_{\mathrm{R}} = 0.011$.

Regarding the transient behavior, both the inner and outer fuel cycle exhibit a pseudo steady state with any transients being periodic with the cyclic operation behavior of the Tokamak and Isotope Rebalancing Systems. No long term drifts or multi-cycle transients are observed within the evaluated time-frame of eight pulses. However, if cycling operations between both systems coincide their impact on the pressure in the central buffer vessel add to each other, leading to a pressure spike. Transients in the inner fuel cycle are driven by controlled gas flow servicing the torus (via fueling and pumping), whereas the outer fuel cycle still reflects the dynamics of the inner fuel cycle but no controlled shifting between states occurs, leading ultimately to a true steady state for the obtained fueling product. This provides an effective decoupling between the two loops. The flowrate of tritium discharged to stack is not fully dampened but average as well as maximum values are within applied release limits.

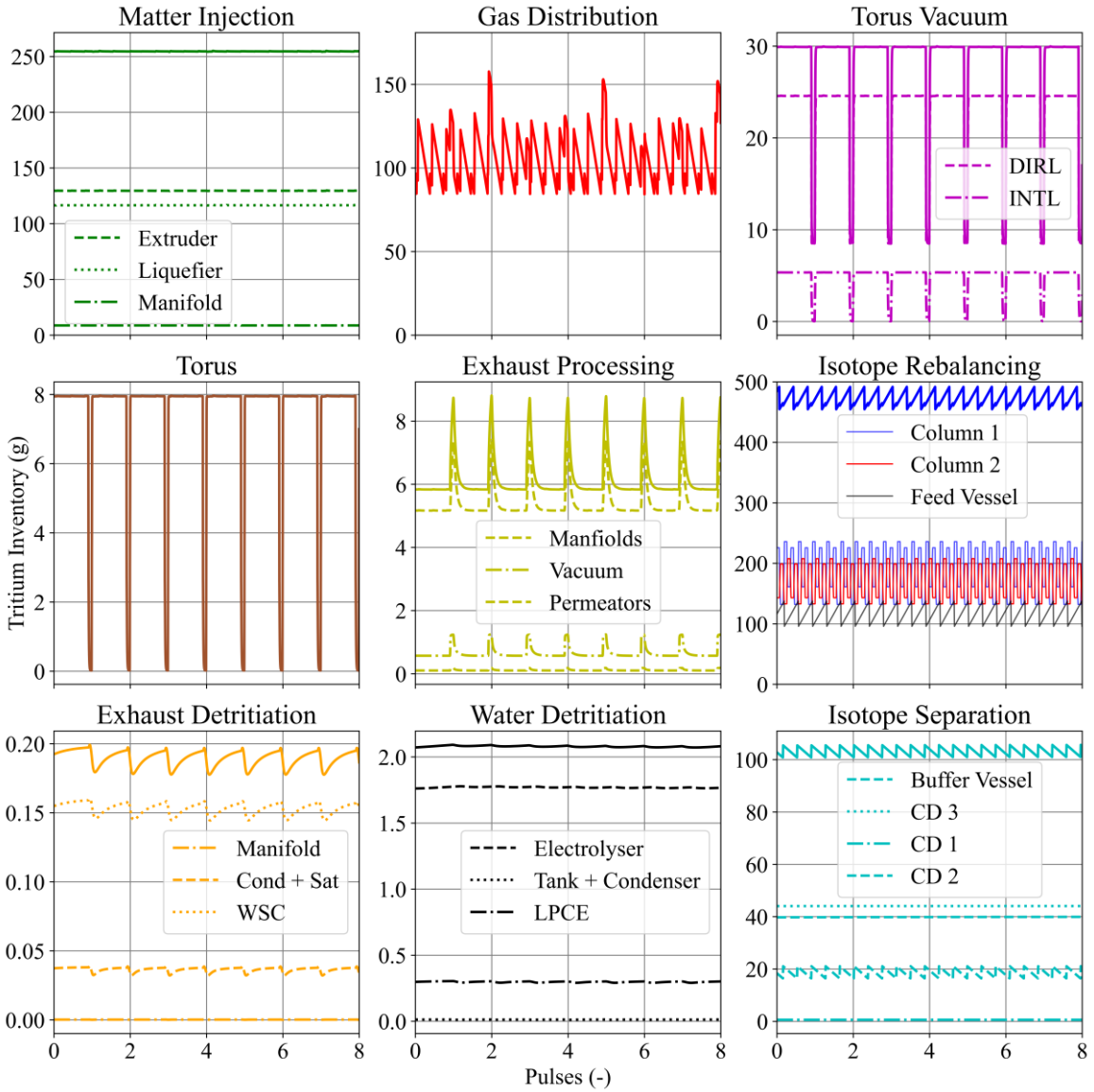

Figure 6.4: Tritium inventories in the hold-ups of the fuel cycle system models over the duration of eight pulses. Solid lines always indicate the sum of all individual hold-ups.

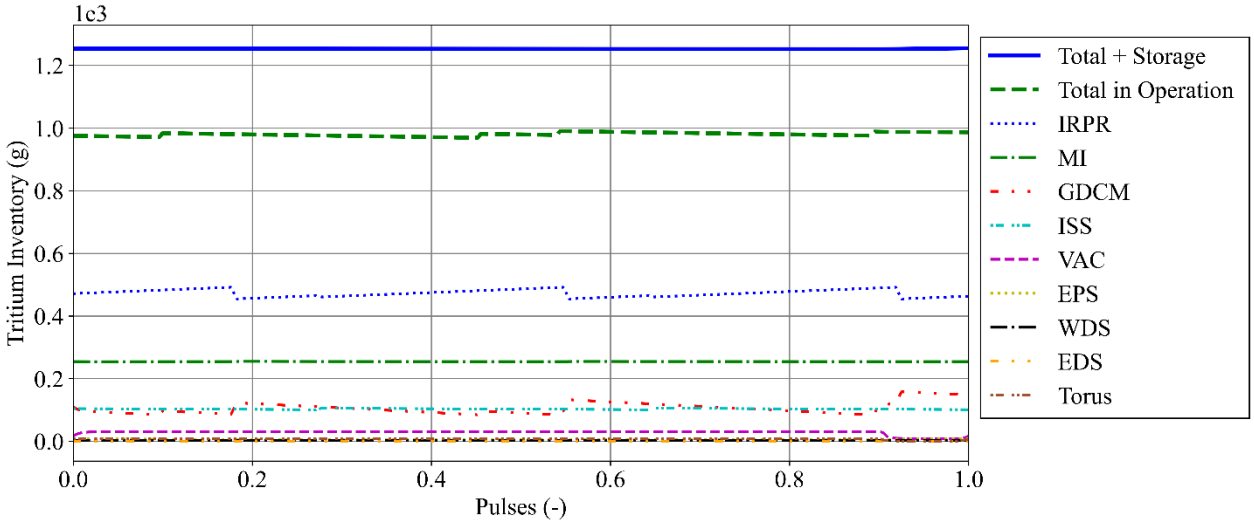

Figure 6.5: Tritium inventories in the fuel cycle systems over one pulse.

6.2 Sensitivity of Fuel Cycle Operation against Variations in Plant Boundary Conditions

While it has been established that the normal operation point fulfills all requirements and is stable, it is not guaranteed that the plant boundary conditions framing the operation of the fuel cycle will remain constant over the duration of the plant's life. The first boundary condition of the plasma chamber fuel throughput is closely coupled to the plasma scenario and design of the plant and tightly controlled by the fueling systems. Deviations thus mark a malfunction of the fuel cycle and do not constitute normal operation. Variations in the other plant boundary conditions on the other hand are expected due to aging of functional and structural materials such as the employed neutron multiplier or permeation barriers in the breeding blankets, directly impacting the associated tritium source terms. A fuel cycle design therefore has to be robust against such deviations. The following sections will discuss the origins of uncertainties associated with the plant boundary conditions and investigate the fuel cycle response to their variation.

6.2.1 Protium Source Term

Protium dilution of the fuel is one of the major concerns for the successful operation of the plant from a fuel cycle perspective, posing a high cost in terms of processing effort and associated tritium inventory to manage. Even though the design of the inner fuel cycle avoids the active use of protium as a processing medium (different from the ITER fuel cycle employing the PERMCAT process [95]), its presence in metals and tendency to outgas therefrom can nevertheless lead to unacceptable protium levels in the available fuel. At the same time reliable outgassing rates are hard to predict for any large scale system as for any material they depend on the exact geometry, temperatures, surface conditions, and ultimately history of the material in the machine as built [96][97]. A parameter study of the protium source term is conducted by adapting the torus protium outgassing rates of the simulation to $\Delta F_H = 2.0{\cdot}10^{-6}$, $5.0{\cdot}10^{-6}$, $1.0{\cdot}10^{-5}$ and $2.0{\cdot}10^{-5}$ mol.s^{-1}, corresponding to a 2 – 20 fold increase as compared to the reference operation point. During all cases an IRPR take-up fraction of $R_{H/D/T}$ = 2.5% of the circulated fuel is maintained. The changes are conducted as a step change on the simulation of the normal operation point and the transient

evolution of the protium content in the buffer vessel is recorded and the simulation results for a series of subsequent pulses are shown in Figure 6.6.

The observed underlying behavior is still that of the cyclic buffer vessel operation now superimposed with a limited growth. The rate of protium build-up increases proportional to the outgassing rate, while at the same time the amplitude of reductions caused by IRPR discharges grows larger until a new pseudo steady state is reached. The overall time constant of this process is one of the slowest in the fuel cycle, taking up to eleven pulses to reach a new steady state in the highest case. Even though the IRPR system achieves a general isotope separation, the D/T ratio in the buffer vessel is not impacted by the change in IRPR operating point.

The convergence to a new pseudo steady state allows the direct correlation of the final protium contamination and protium source term. Figure 6.7 shows the relationship between the maximum protium content observed in the buffer vessel and protium outgassing rate, both relative to the base case. A linear relationship between all points is observed with a proportionality coefficient of 0.45.

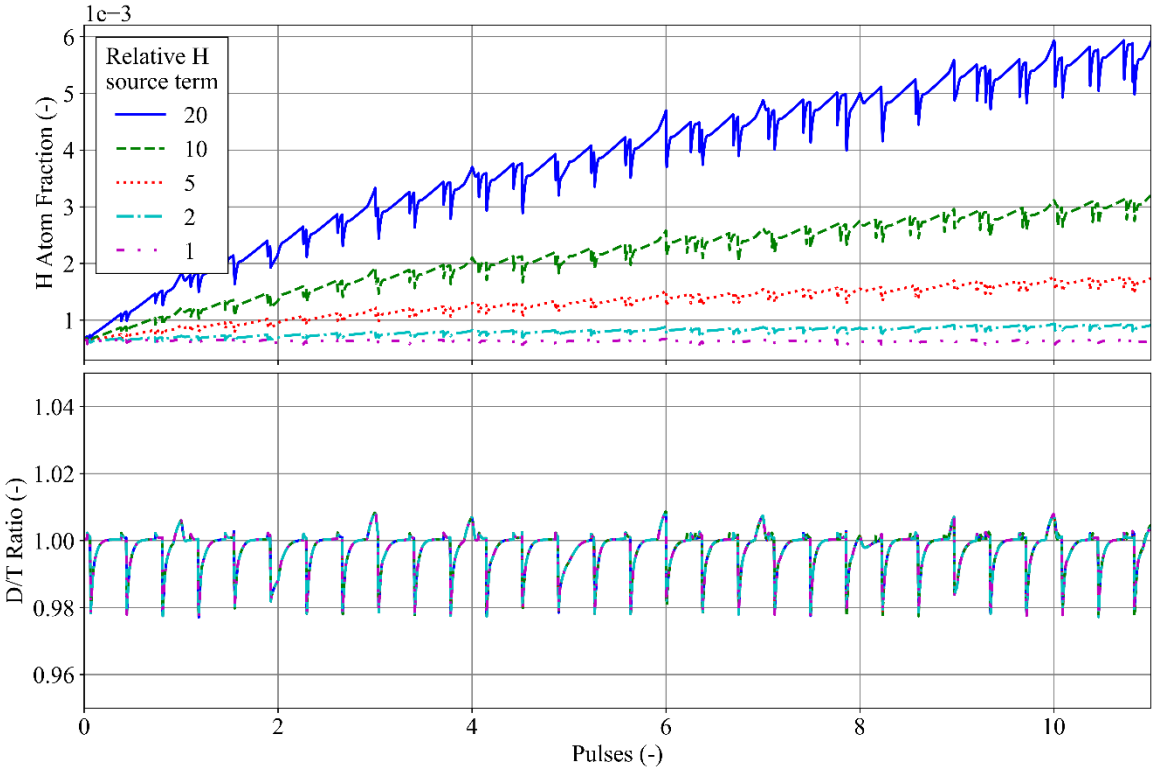

Figure 6.6: Top: Simulated evolution of the protium content in the central buffer vessel after a step change increase from the normal operation point. Bottom: D/T ratio in the buffer vessel for the same cases and duration.

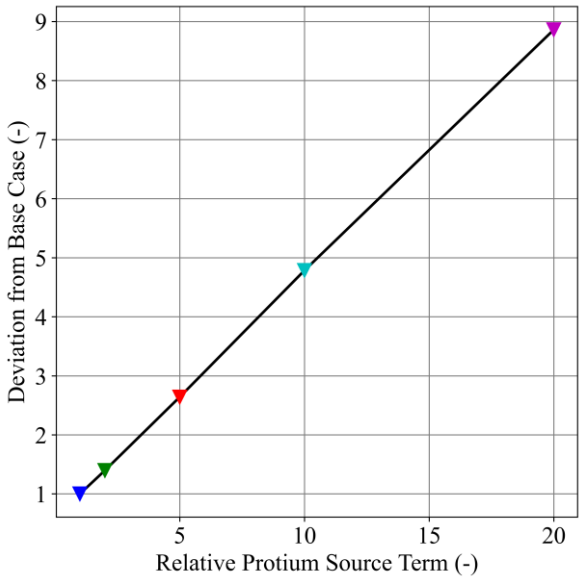

Figure 6.7: Evaluated correlation between the protium source term of the inner fuel cycle and time averaged steady state protium content in the buffer vessel of the gas distribution system.

This in turn allows to evaluate an integral protium removal efficiency of the inner fuel cycle by comparing the theoretical protium contamination level as obtained for the given bypass flowrate and outgassing rate (c.f equation 2.2) which assumes an ideal removal efficiency, to the values obtained from the simulation. Efficiencies ranging from 33% at the lowest protium level to 74% at the highest are observed as indicated in Table 6.1. The observed linear relationship between the protium source term and established protium content also allows for convenient interpolation of data points of (ΔF_{H}, $z_{\mathrm{H,real}}$) and in turn calculation of protium removal efficiencies without having to run further time intensive simulations. As a result the characteristic behaviour of the inner fuel cycle regarding protium management in the investigated range can be analytically assessed for the underlying fuel cycle configuration by applying η_{H} to equation 2.2.

Table 6.1: Comparison of obtained steady state protium levels for different protium outgassing rates. Ideal values are obtained from equation 2.2, real values evaluated from the simulation.

$\Delta F_{\mathrm{H}} \cdot 10^{6}$ (mol.s^{-1})	$z_{\mathrm{H,real}}$ (at.%)	$z_{\mathrm{H,ideal}}$ (at.%)	η_{H} (-)
1	0.06%	0.02%	33%
2	0.09%	0.04%	47%
5	0.16%	0.10%	63%
10	0.30%	0.21%	69%
20	0.56%	0.41%	74%

6.2.2 Tritium Extraction Rate

Tritium being extracted from the breeding blankets is the largest influx of tritium into the outer fuel cycle and as such a major design driver. While it is an integral design quantity of the overall plant derived from the fusion power and tritium breeding ratio there is still some uncertainty associated with the exact amount of tritium being generated and extracted. No experimental demonstration of tritium breeding on large scale in fusion relevant conditions has been performed to date, with the first planned experiments using fusion neutrons being the ITER test blanket module

program and the LIBRA experiment [98][99]. Any numerical predictions for achievable tritium breeding ratios feature significant uncertainty budgets arising also from experimental uncertainty in employed neutronic data [17].

At the same time there is only a narrow window that has to be met as a TBR < 1.025 is considered unfeasible to maintain tritium self-sufficiency [34], whereas a TBR > 1.1 can lead to excessive amounts of excess tritium being generated which poses additional challenges on tritium accountancy or even threaten the licensability of the plant. At the same time the achieved TBR can exhibit changes in time due to burn-up of functional materials.

A parametric study of the tritium extraction ratio employed in the simulation is performed by varying it from 1.025 to 1.1 in increments of 0.025 while keeping all other configurations constant. The parameter variations are enacted as a step change on the normal operation simulation. The case of TER = 1.05 coincides with the normal operation scenario and is computed again as reference.

Extracted tritium takes the shortest route through the outer fuel cycle, being fed to the isotope separation system from where it is then obtained in the fueling product. The isotope separation system also interfaces to the water detritiation system, rejecting light isotopes towards it. Figure 6.8 shows the transient evolution of the tritium flowrate obtained in the fueling product relative to the normal operating scenario as well as relative tritium inventory evolutions in ISS and WDS. As the ISS feed tank receiving gas from the IRPR is not affected by the interface to tritium breeding it is excluded from the evaluation to allow suppression of its fluctuations. All additional tritium being routed to the system is obtained in the fueling product after twelve pulses in the highest case following a logistic growth behavior with a delayed onset. The delay time arises from the need to first build-up tritium inventories and sufficient concentrations in the hold-up of the ISS cryogenic distillation columns following a first order limited growth behavior. The sole pathway of additional tritium towards the fueling product in turn leads to no significant change in the WDS tritium inventories meaning that the interface between ISS and WDS is not impacted by changes in tritium extraction ratio.

As the change in TER leads to a new steady state in the affected systems the overall impact can be correlated directly. Figure 6.9 shows the dependency of the ISS tritium inventory and tritium product flowrate relative to the normal operation scenario against the TER. Both show a linear dependency with a stronger sensitivity in the tritium inventory leading to a 5% increase in the tritium inventory of the ISS cryogenic distillation columns while only accounting for a 3% increase in the tritium product flowrate for the case of the highest TER.

The difference in sensitivity coefficient can be explained by the presence of other tritium feeds to the isotope separation system that remain unaffected, acting as a damping element. In the normal operating scenario tritium from breeding accounts for 67% of the total influx to the system. Additionally, as the stream is introduced higher up in the columns than the other major contribution from the inner fuel cycle its impact on the inventory is even more severe.

In summary, the interface to tritium extraction has very little impact on the outer fuel cycle only affecting the isotope separation system in the outer fuel cycle and none on the inner fuel cycle which is decoupled via the composition control system. The impact on the tritium inventories and flowrates of the affected systems and streams is linear over the full range of valid tritium production rates.

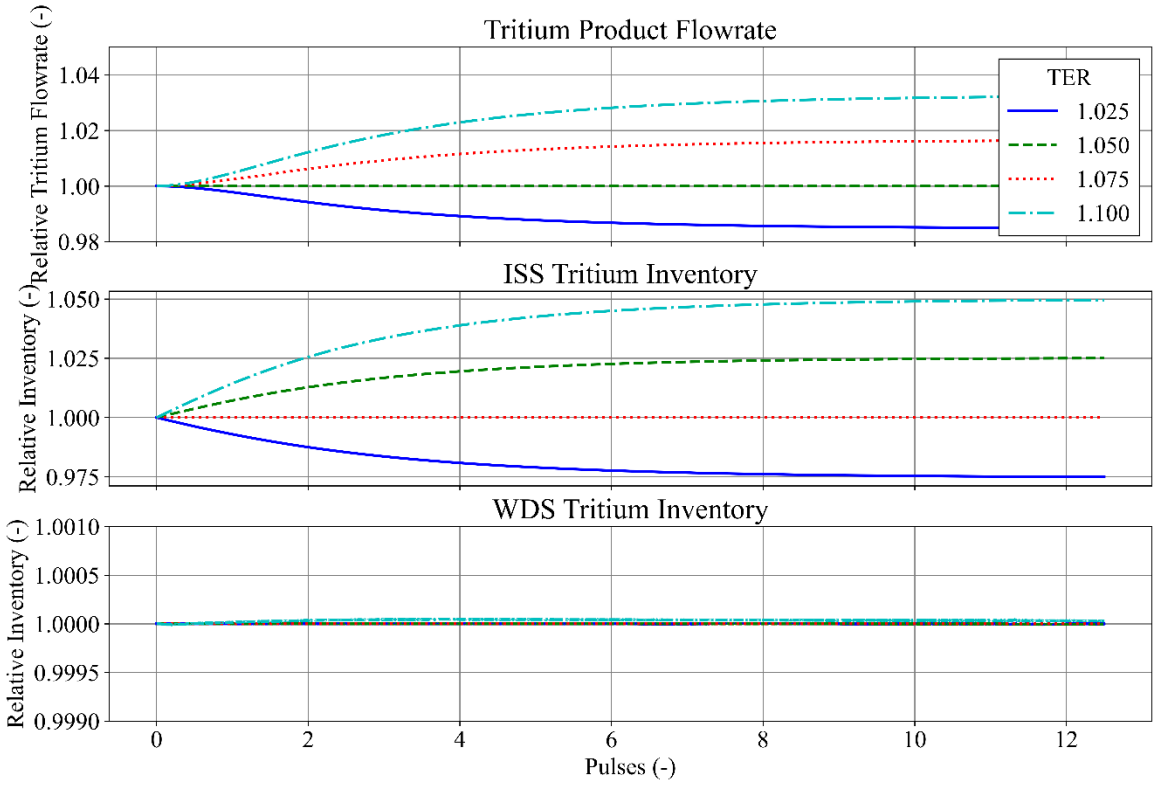

Figure 6.8: Top: Simulated evolution of tritium flowrate relative to the normal operation scenario in the fueling product of the isotope separation system after a step change in the tritium extraction ratio: Mid: Evolution of ISS relative tritium inventory. Bottom: Evolution of WDS relative tritium inventory.

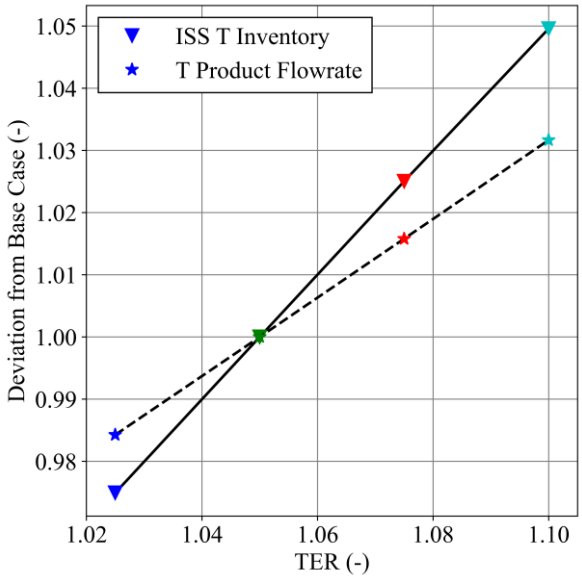

Figure 6.9: Evaluation of the correlation between the isotope separation system relative tritium inventory (triangles) and fueling product relative tritium flowrate (stars) as a function of tritium extraction ratio.

6.2.3 Tritium Recovery Rate

The amount of tritium received via the plant boundary condition of tritium recovery varies over the lifetime of the plant and is not easily predictable. While a stable steady state establishes for the tritium concentration in the coolant and consequently tritium flowrate to the fuel cycle over that part of the interface the tritium concentration in air and gases sent to the exhaust detritiation system from building rooms and gloveboxes is not controlled and varies. While expected to be at a stable level during routine operation, periods of elevated tritium concentration can occur during maintenance operations or as a result from increased leakages before they can be repaired. At the same time, excessive tritium concentrations in building air and glove-box atmospheres may, depending on severity, trigger the use of standby and safety detritiation systems interrupting the normal operation of the plant.

The impact of different tritium recovery loads on a given fuel cycle design point is investigated by scanning a range of tritium concentration in the gas stream sent to the exhaust detritiation system ranging from air tritium concentration of $1 \cdot 10^{8}$ Bq.m^{-3} for the normal operation point to $1 \cdot 10^{9}$ Bq.m^{-3} yielding a tritium flowrate of 0.08 g.day^{-1} to 0.8 g.day^{-1}. The changes are enacted as a step-change on the simulation of the normal operation point allowing to also observe the transient response of the fuel cycle.

The exhaust detritiation system is the first link in the chain of systems for tritium recovery and enrichment, with the water detritiation system and isotope separation system downstream being also affected. The exhaust detritiation system is also the draw-off location of one of the fuel cycles products, releasing a stream through the stack to the environment. Figure 6.10 shows the simulated time evolution of tritium flow rates to the stack and inventories of the affected systems. As demonstrated, the tritium releases to stack do not significantly reflect the cyclic behavior of the inner fuel cycle (inherited from the interface between EPS and EDS). This behavior continuous to be observed in all cases showing a smooth growth with delayed onset until a new steady state is reached after eight pulses in the highest case. In steady state the increase in tritium discharge from the stack correlates linearly with the increase in the received tritium flow rate, as shown in Figure 6.11, with a proportionality coefficient of 0.23. A tenfold increase in tritium influx to the EDS system via the tritium recovery interface thus leads to an increase in annual tritium releases from 0.17 gram tritium per year to 0.53 gram tritium per year.

The tritium inventories of the EDS and WDS system retain their fluctuating behavior and grow to new pseudo steady states increasing by an average 8% and 11% respectively for a tenfold increase in tritium flowrate routed to EDS. The tritium inventory of the isotope separation increases significantly slower, being delayed by its upstream systems and housing the overall largest tritium inventory, requiring in excess of twelve pulses for the highest case to converge towards a new steady state and exceeding the time horizon of the simulation. For the case of a doubling in the interface tritium flowrate the isotope separation systems tritium inventory increases by 0.02%. It must, however, be noted that the tritium influx over this interface accounts only for 0.02% of the overall isotope separation system tritium throughputs in the normal operation scenario.

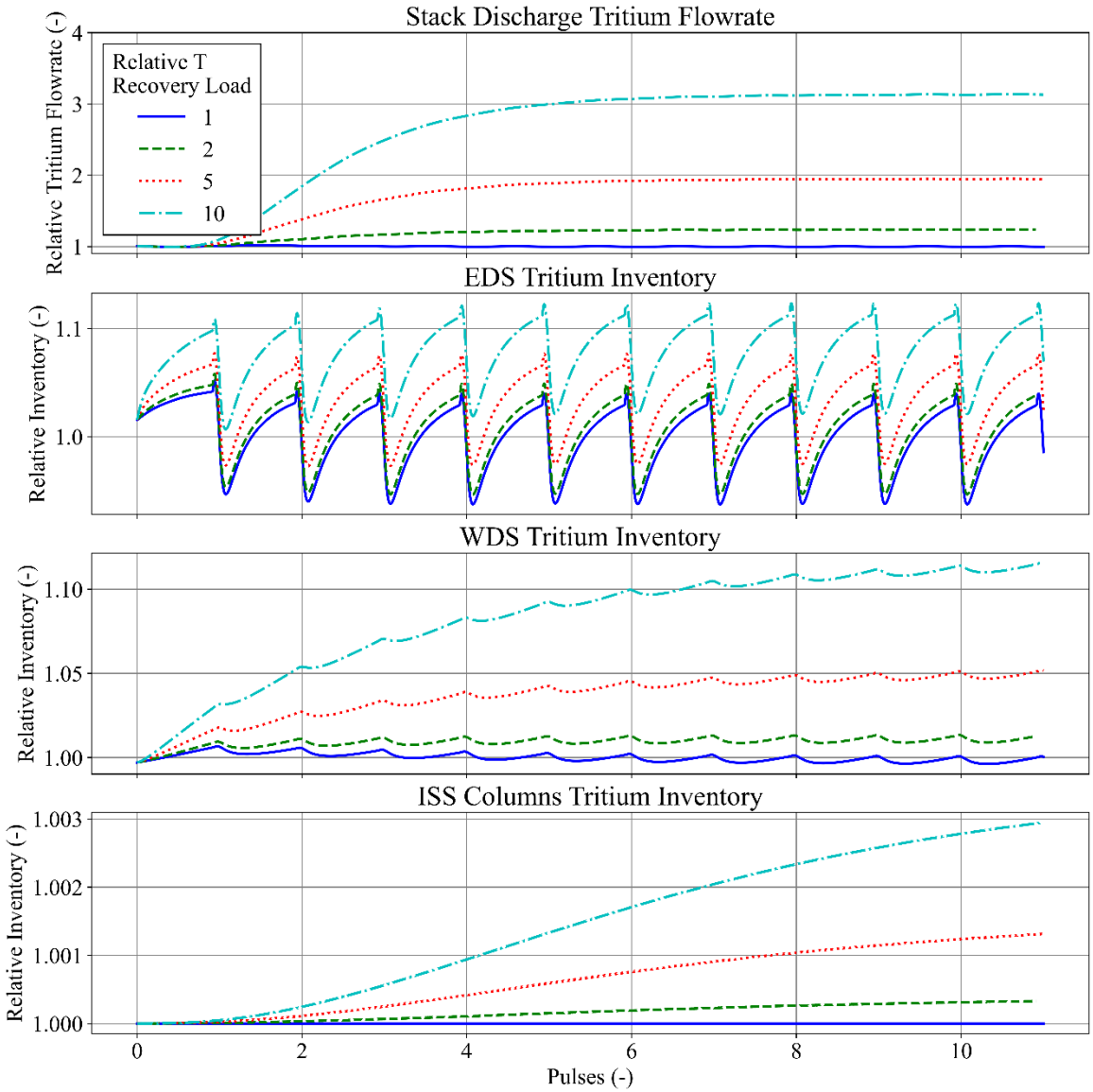

Figure 6.10: Calculated response of the fuel cycle to a step change in tritium recovery load sent to the exhaust detritiation system relative to normal operation. From top to bottom: tritium discharge from the stack, tritium inventory in the exhaust detritiation system, tritium inventory in the water detritiation system, tritium inventory in the cryogenic distillation column of the isotope separation system.

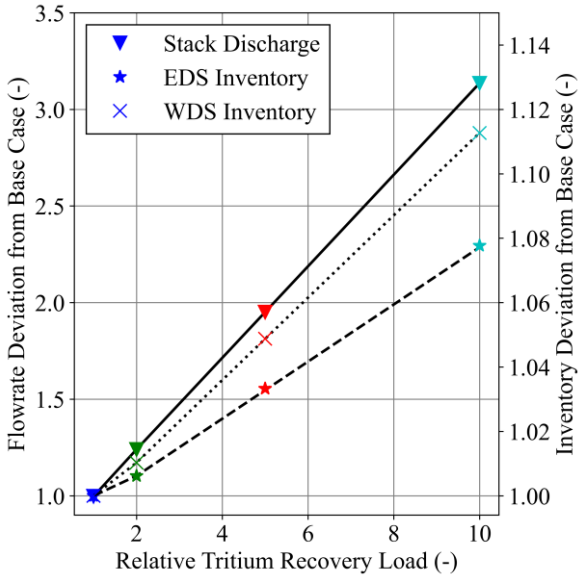

Figure 6.11: Evaluated correlation between tritium recovery load on EDS and tritium flowrate of the stack (left axis, triangles) and tritium inventories in affected systems (right axis, stars and crosses).

6.3 Sensitivity of Fuel Cycle Operation against Deviating Technology Performance

Next to variations and uncertainties in the boundary conditions and interfaces of the fuel cycle, its successful operation may also be affected by variations in the performance of its systems and technologies employed therein. While any uncertainties are largely addressed in the design stage and do not reflect on the operational characteristics of the fuel cycle once built, some deviations of performance due to failure of components or degradation of active materials in separation systems can be reasonably expected. Fuel cycle systems in the tritium plant are comparatively easily accessible allowing for routine maintenance and immediate repairs while also having sufficient space available to keep stand-by components of critical equipment thus enabling operation of the fuel cycle with all systems performing within their intended operation point. Components installed close to the Tokamak and within the bioshield on the other hand are not easily accessible, having to be served by remote maintenance systems and requiring a shutdown of the machine for their replacement or repair.

The metal foil pumps of the fuel separation system provide the separation between the direct recycling and inner tritium plant loop and are located directly in the lower ports of the vacuum vessel while at the same time being composed of an assembly of a large number of individual pumps working in parallel. In order to not jeopardize the operational availability of the integral plant upon failure of individual units operation with a reduced number of metal foil pumps in service is a requirement. From a fuel cycle perspective this directly translates to operation at different achievable direct internal recycling ratios.

Changes to the DIR-ratio affect all systems of the direct internal recycling loop and inner tritium plant loop altering their flow rates with exception of the isotope rebalancing system which takes up a controlled constant feed rate. In order to investigate the impact of varying DIR-ratios on

the operation of the fuel cycle three simulation cases are set-up specifying varying hydrogen separation efficiencies in the model of the metal foil pump of 60% and 70%, as well as a case of higher DIR-ratio of 90%. The parameter variation is enacted as a step-change on the simulation of the normal operation scenario with a DIR-ratio of 80% which is computed in parallel to serve as reference.

The most critical points for the performance of the inner fuel cycle is the stability of the fuel composition in the buffer vessel, as well as the amount of tritium that is routed to the outer fuel cycle over the interface between the exhaust processing system and exhaust detritiation system. As demonstrated in section 6.1 the normal operation of the fuel cycle is characterized by a decoupling between the inner fuel and outer fuel cycle, as well as only minor fluctuations of the D/T ratio in the central buffer vessel of the latter. The impact of changes in the DIR ratio on these properties is therefore investigated.

Figure 6.11(a) shows the simulated temporal evolution of the tritium flowrate between the exhaust processing system and exhaust detritiation system over four pulses after the step-change. During the flat-top phase a new steady state establishes within the first pulse. The flowrate then follows the normal characteristic of the burn-dwell cycling. However, a peak at the start of each flat-top phase is observed which declines over the first half of each pulse. This leads to an overall increase in the average amount of tritium being routed to the outer fuel cycle, amounting to 4% and 7% compared to normal operation (corresponding to $6.41 \cdot 10^{-5}$ $g.s^{-1}$) for the cases of 70% and 60% DIR-ratio, respectively. No reduction is observed in case of 90% DIR-ratio due to the lower pressure set-point control of the system now triggering the engagement of the dwell bypass stream during all times.

The changes in inner fuel cycle flowrate are also reflected in the tritium inventory of the exhaust processing system, as illustrated in Figure 6.11(b). Increased flowrates at lower DIR-ratios lead to a pressure build up in the first permeator stage, consequently increasing the systems tritium inventory. During burn-dwell cycling this excess pressure diminishes rapidly and all cases converge towards the normal operation scenario driven by the engagement of the pressure control system ensuring a minimum feed side pressure. On average, a 23% and 66% higher inventory as in the normal operation scenario (average of 6.2 g) is observed for case of 70% and 60% DIR-ratio respectively. No impact on the system tritium inventory is observed for the case of higher than normal DIR-ratio.

No significant deviations are observed in the D/T ratio of the central buffer vessel, as depicted in Figure 6.11(c), maintaining the operability of the inner fuel cycle in all cases, while its pressure, shown in Figure 6.11(d), experiences small shifts and offsets, as well as an increase in the peak pressure incurred during the burn/dwell transition for cases of lower than normal DIR-ratio. This is caused by the presence of excess inventory in the exhaust processing system which is transferred to the buffer vessel during the dwell phase, amounting to an overall maximum pressure increase of 0.9% and 2.1% for cases of 70% and 60% DIR ratio as compared to the normal operation case.

Overall the integral operation of the fuel cycle is not impacted by changes in the DIR ratio, even if taking no adaptive measures. While a change in the DIR-ratio from 80% to 60% leads to a doubling in the hydrogen throughput of the inner tritium plant loop systems, the operational stability of the inner fuel cycle is still preserved at the cost of increased tritium inventories in the exhaust processing systems and increased tritium propagation to the outer fuel cycle.

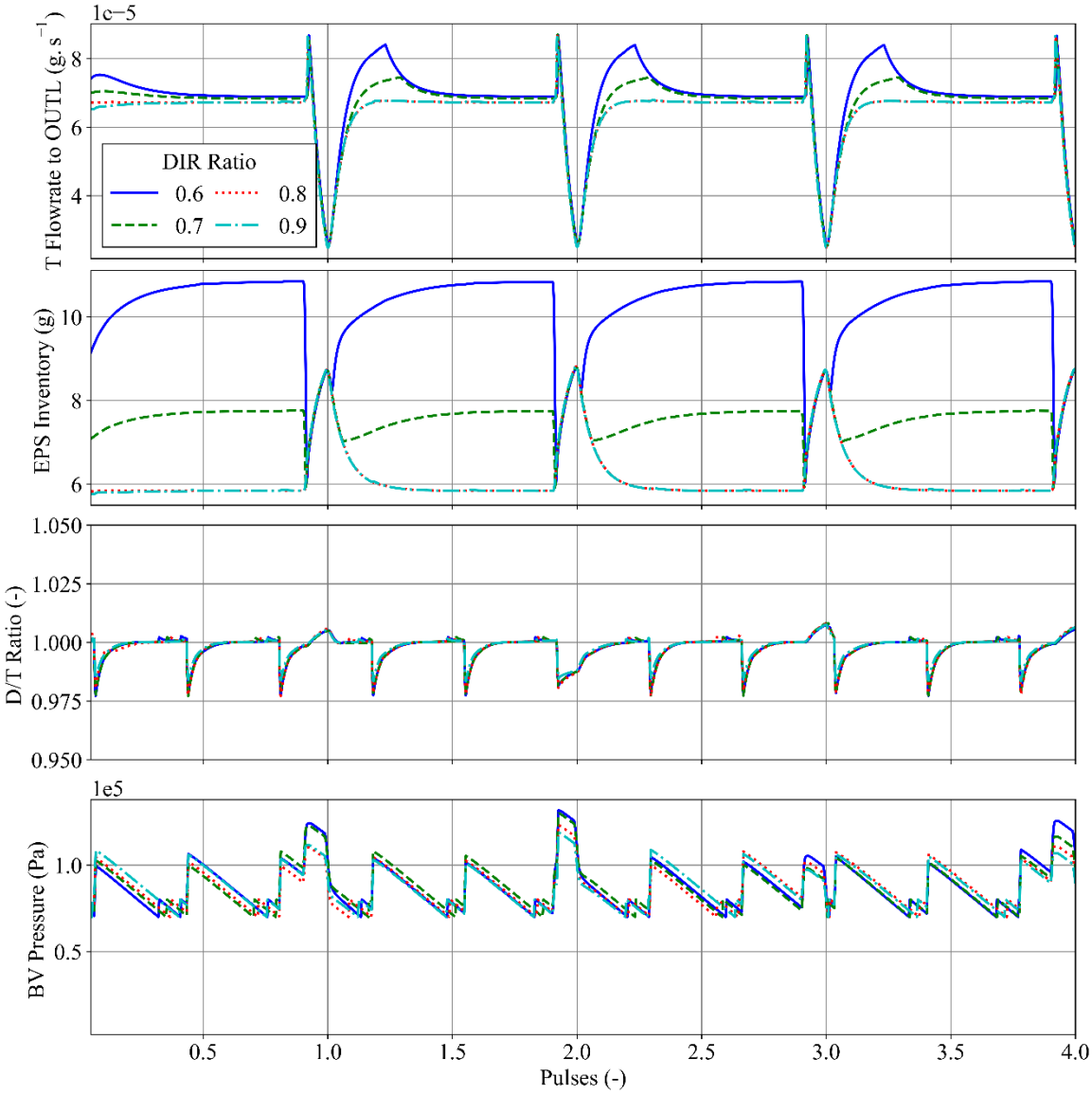

Figure 6.11: Computed impact of operation with different DIR-ratios as a function if time for various fuel cycle metrics. From top to bottom: (a): Tritium flowrate between the EPS – EDS interface,(b) tritium inventory in the exhaust processing system, (c) D/T ratio obtained in the central buffer vessel, (d) pressure in the central buffer vessel.

6.4 Reduced Order Model of the Fuel Cycle

Building on the observations that

- tritium throughputs in fuel cycle system directly scale with applying plant boundary conditions,
- fuel cycle systems exhibit a linear response on changes in tritium throughputs,
- and the overall fuel cycle tritium inventory required for operation is constant,

the formulation of a reduced order model that correlates tritium throughputs in all regions of the fuel cycle with the expected inventory of tritium in systems required for operation is possible. Figure 6.12 shows the architecture of the EU-DEMO fuel cycle with systems re-grouped according to their principal processing functionality. The tritium throughputs in the indicated groups can be derived by directly applying the fundamental relationships developed in section 2.1.

The overall dependency of the operational tritium inventory $m_{\mathrm{T}}^{\mathrm{op}}$ of the fuel cycle is then given by weighting the ratio of tritium inventory to boundary condition parameter (R_{i}) values for the evaluated normal operation scenario (indicated with *) in each functional loop with an actual parameter value and summing the individual terms.

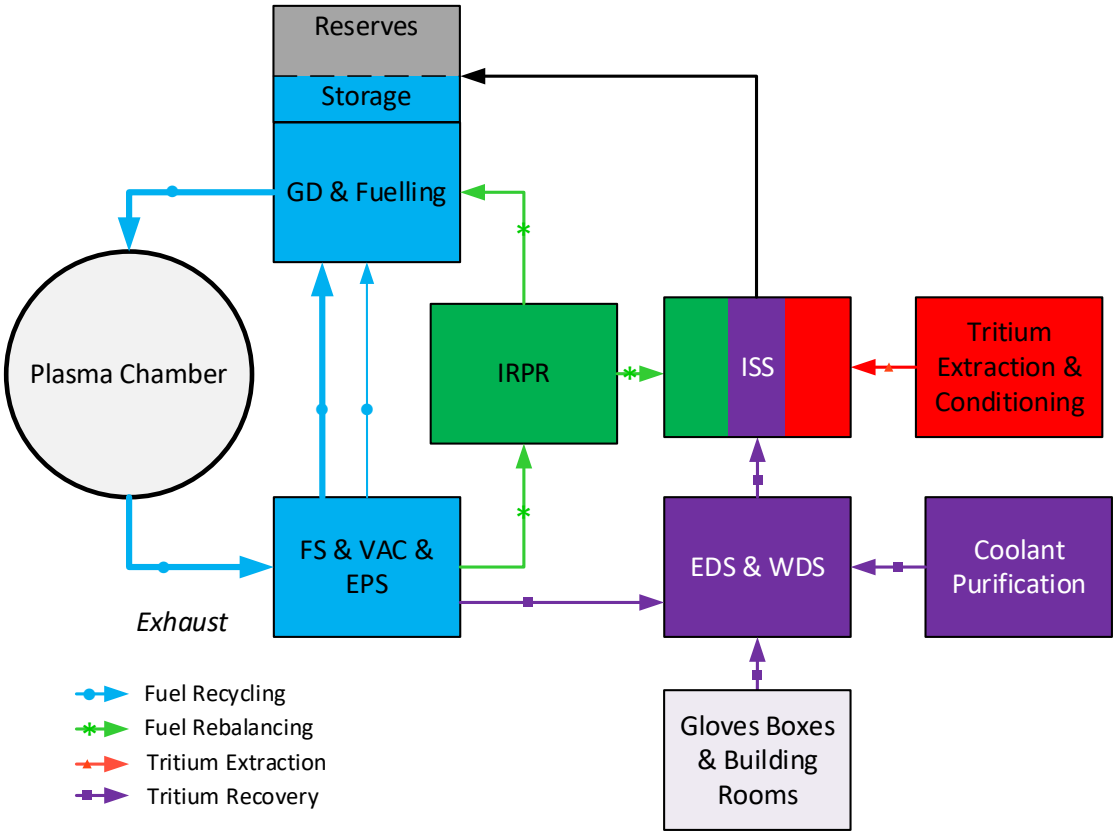

Figure 6.12: Systems of EU-DEMO fuel cycle grouped according to the principal processing functionalities they serve.

$$m_{\mathrm{T}}^{\mathrm{op}} = \frac{1}{R_{\mathrm{F}}}\frac{R_{\mathrm{F}}^{*}}{m_{\mathrm{T,F}}^{*}} + R_{\mathrm{H}}\frac{m_{\mathrm{T,H}}^{*}}{R_{\mathrm{H}}^{*}} + R_{\mathrm{E}}\frac{m_{\mathrm{T,E}}^{*}}{R_{\mathrm{E}}^{*}} + R_{\mathrm{R}}\frac{m_{\mathrm{T,R}}^{*}}{R_{\mathrm{R}}^{*}} + m_{\mathrm{T,reserves}}^{*} \tag{6.1}$$

The set of reference values is then given in Table 6.2. Reported inventory values only refer to systems of the closed loop fuel cycle, as evaluated in section 6.1. However, systems part of the breeding blanket infrastructure (tritium extraction, tritium conditioning, coolant purification), can also be included in their respective functional area if their tritium inventories are evaluated for the same reference design point.

This formulation neglects the dynamic shift of inventory between the individual systems and is thus only applicable for the integral fuel cycle where the overall inventory has been shown to be constant. Reference inventory group values are obtained by taking the time average group inventory values. The storage inventory is distributed between reserves and operational inventories with the maximum amplitude of fluctuations accounting for operational inventories and the remainder being reserves that do not scale with the fuel cycle boundary conditions.

As the isotope separation system processes tritium streams arising from multiple functionalities the total inventory of its cryogenic distillation columns is distributed proportional to the tritium flowrates for the reference design point, with 67% of the ISS tritium throughput arising from tritium extraction, 31% from fuel rebalancing and 2.1% from tritium recovery. The inventory of the feed buffer is accounted solely towards fuel rebalancing.

By directly combining inventories of exhaust detritiation and water detritiation systems without differentiating the location of their various feed streams, all liquid feeds are potentially overweighed by the EDS inventory. Liquid tritium recovery loads however only account for 7% of the total tritium recovery load while the EDS inventory only accounts for 10% of the combined EDS and WDS inventory, yielding an overall error of 0.7% which is deemed acceptable when considering the overall low sensitivity of tritium recovery inventories (4 g) on the total inventory of 1017 g.

Table 6.2: Reference values in plant boundary conditions and related tritium inventories.

i	**Fuel recirculation**	**Fuel rebalancing**	**Tritium extraction**	**Tritium recovery**	**Total**
R_{i}^{*} (-)	0.06	0.025	1.05	0.029	-
$m_{\mathrm{T,i}}^{*}$ (g)	438	518	57	4	1017
$m_{\mathrm{T,i}}^{*}/\sum_{\mathrm{i}} m_{\mathrm{T,i}}^{*}$ (-)	0.43	0.51	0.06	0.004	1.00

7 Summary of Results and Outlook

7.1 Summary

Future deuterium – tritium fusion power plants will be required to employ a closed fuel cycle in order to be able to operate tritium self-sufficiently while minimizing chronic radiological releases to the environment. As such the fuel cycle of the European DEMO reactor is representative, featuring all elements projected to be present also in a commercial power plant. It is based around the novel concept of direct internal recycling, aiming to fuel the reactor with a deuterium-tritium mixture instead of separating out individual hydrogen isotopes, greatly reducing its projected tritium inventories.

This type of fuel cycle can be subdivided in the inner and outer fuel cycle. The inner fuel cycle processes deuterium and tritium from the reactor exhaust and is responsible for the fueling of the machine while also maintaining the isotopic balance and purity of the fuel. The outer fuel cycle processes tritium streams arising from tritium breeding in the machines blankets and tritium recovered from secondary media and volumes. These mark the four principal processing functionalities of a generic advanced DT fuel cycle. These functionalities have to be achieved under the constraints of minimizing the tritium inventories held up in the processing systems required for operation, minimizing radiological releases to the environment, while ideally also minimizing the energy consumption and plant footprint of the process.

In order to achieve these processing functionalities the EU-DEMO fuel cycle is based on a three loop architecture employing dedicated systems for each functionality in the inner fuel cycle and combining separation tasks according to the employed technologies in the outer fuel cycle, each serving multiple clients. The EU-DEMO fuel cycle receives tritium carrying streams via its interfaces to other plant systems, with the *plasma chamber* being the sole interface in the inner fuel cycle and *tritium extraction*, and *coolant purification* systems, as well as *building* and *glove box volumes* in the outer fuel cycle. The outer fuel cycle then produces two product streams, a pure hydrogen stream enriched in tritium and depleted of protium to be used to make up burned fuel and for composition control in the fueling systems, as well as a detritiated air and gas stream discharged to the environment.

The technical implementation of the EU-DEMO fuel cycle relies on five principal types of separation operations: Removal of inert species and impurities from hydrogen isotopes, isotopic separation of hydrogen, recovery of hydrogen isotopes from inert carrier gases, tritium removal and recovery from water, and finally tritium removal from humid gases and air. These are achieved by the use of hydrogen permeable membranes, temperature swing absorption as well as cryogenic distillation, combined electrolysis and catalytic exchange, and wet scrubber columns.

As Tokamaks are operated in a series of burn-dwell cycles the operation of the fuel cycle is inherently transient, having to provide fuel and receiving exhaust streams from the reactor during the burn phase and evacuating the plasma chamber during the dwell phase. On the other hand, the design, sizing, and optimization of the employed technologies and systems is typically performed against steady-state design cases from which the valid operation window of each system is obtained. It is thus also valuable to investigate early on in the design phase the integration of all system forming closed loops and their transient behavior. To investigate these interactions a first of its kind

flowsheet based dynamic process simulation tool using physics based mass transfer models has been developed.

The centerpiece of the simulation tool are numeric implementations of state of the art rate based or equilibrium 1-D mass transfer models of all employed separation technologies (with exception of the metal foil pump, which is still in an earlier development stage). These are supplemented by simple models for auxiliary components. Each model features fully closed mass balances for all present species as well as dynamic treatment of hold-ups in all areas where they impact the transient behavior. All models are supported by a library of thermophysical property data and thermodynamic equilibrium states.

Mass transfer and auxiliary models are assembled to capture the architecture of each fuel cycle system, which are characterized for their dynamic behavior and performance. System models are then integrated with each other and the fuel cycle interfaces to mirror the high level system block architecture of the EU-DEMO fuel cycle, accommodating all tritium carrying streams and systems forming the closed fuel cycle. All models are configured to present a viable operation point marking the first fully closed loop, physics based dynamic simulation of a fusion fuel cycle. The simulation is built on the Aspen Custom Modeler® platform utilizing its flowsheet capabilities and powerful numerical solvers. The simulation features more than 4400 mass and species balances, computing more than 32000 linked equations in each timestep.

The simulation tool has been employed to characterize the normal operation behavior of the EU-DEMO fuel cycle. Transients are strongest in the inner fuel cycle with flowrates directly governed by the burn-dwell cycling behavior of the Tokamak. It could be shown that the use of dwell bypass streams enables critical systems to maintain a stable operation point reducing inventory oscillations between systems and minimizing the impact on buffer vessels. This further provides an effective decoupling of the inner and outer fuel cycle with any remaining transient in the interfaces not propagating to the obtained fueling product stream. The isotopic composition of fuel in the inner fuel cycle is stable and can be effectively controlled for its deuterium - tritium ratio and protium content. Tritium discharges to the stack show minor periodic oscillations reflecting the burn-dwell behavior of the inner fuel cycle with the total time average as well as maximum values within release objectives.

It could further be shown that the fuel cycle is robust against variations in all external interfaces converging to always linear responses and no feedback loops were found. The simulation thus confirms the robustness of the fuel cycle architecture as well as the suitability of employed technologies, their configuration, and selection of design parameters.

7.2 Outlook and Recommendations for Future Work

The developed simulation tool for the very first time establishes a self-consistent platform that allows to describe the integral and block specific dynamic behavior and performance of a novel deuterium – tritium fuel cycle. Next to the presented results its applications also allows shaping of further work and progression in three distinct directions.

Firstly, the fundamental working principle of the developed simulation tool is such that it can also be employed to other fuel cycles and similar projects as it provides a centralized implementation of dynamic models for all common technologies in tritium processing and fuel cycle applications. Any given continuous D/T fuel cycle may be simulated by adapting the architecture, model configuration, and boundary conditions of the simulation. This capability is especially useful with more demonstration reactors and fusion power plant projects progressing their fuel cycle designs and seeking to analyze and ultimately validate integrated systems. The framework further allows for the easy implementation of new models, already providing a suite of thermophysical property data and thermodynamic models for hydrogen isotopologues and their molecules.

Secondly, the obtained results offer valuable insights for the continuation of the EU-DEMO fuel cycle development and design. The observed decoupling of the inner and outer fuel cycle allows for largely independent design and optimization, allowing to speed up design iterations. The dynamic of the inner fuel cycle is primarily driven by gas flow controllers governing the fueling pattern and dwell bypass streams across multiple systems whereas such integrated control loops are absent in the outer fuel cycle. The fidelity and time resolution of the inner fuel cycle simulation can be further increased, expanding on pressure drop relations, implementing pipe geometries once available, and adding valve characteristics to allow the synthesis of advanced control systems. The outer fuel cycle on the other hand can be optimized largely independently from the inner fuel cycle, enabling the use of steady state tools to be applied in rigorous large scale parameter scans for further optimization.

Thirdly, the developed reduced order model of the fuel cycle allows implementation in plant-wide system codes, capturing dependencies of key metrics such as tritium inventories on the performance of other plant systems, especially tritium migration behavior through the breeding blankets.

8 References

[1] National Academies of Sciences, Engineering, and Medicine: *Bringing Fusion to the U.S. Grid*, The National Academies Press, Washington, DC, (2021). DOI: 10.17226/25991

[2] Department for Energy Security and Net Zero: *The ten point plant for a green industrial revolution*, (2020). Available at https://www.gov.uk/government/publications/the-ten-point-plan-for-a-green-industrial-revolution (last accessed 09.05.2023).

[3] Department for Business, Energy & Industrial Strategy: *Towards fusion energy the UK government's fusion strategy*, 2021. Available at https://www.gov.uk/government/publications/towards-fusion-energy-the-uk-fusion-strategy, (last accessed 09.05.2023).

[4] J. Zheng, J. Qin, K. Lu, M. Xu, X. Duan, G. Xu, J. Hu, X. Gong, Q. Zang, Z. Liu, L. Wang, R. Ding, J. Cen, P. Li, L. Xue, L. Cai and Y. Song: *Recent progress in Chinese fusion research based on superconducting tokamak configuration.* The Innovation, Volume 3, Issue 4, 100269, (2022). DOI: /10.1016/j.xinn.2022.100269.

[5] The Integrated Innovation Strategy Promotion Council: *Fusion Energy Innovation Strategy*, 2023. Available at https://www8.cao.go.jp/cstp/fusion/230426_strategy.pdf (last accessed 09.05.2023).

[6] K. Kim, K. Im, H.C. Kim, S. Oh, J.S. Park, S. Kwon, Y.S. Lee, J.H. Yeom, C. Lee, G-S. Lee, G. Neilson, C. Kessel, T. Brown, P. Titus, D. Mikkelsen and Y. Zha: *Design concept of K-DEMO for near-term Implementation.* Nuclear Fusion, Volume 55, Number 5, 053027, (2015). DOI: 10.1088/0029-5515/55/5/053027

[7] EUROfusion: *European research roadmap for the realisation of fusion energy,* (2018). Available at https://euro-fusion.org/eurofusion/roadmap/ (last accessed 09.05.2023).

[8] H.-S Bosch and G.M. Hale: *Improved formulas for fusion cross-sections and thermal reactivities*, Nuclear Fusion, Volume 32, Number 4, 611, (1993). DOI: 10.1088/0029-5515/32/4/I07

[9] L. L. Lucas and M. P. Unterweger: *Comprehensive Review and Critical Evaluation of the Half-Life of Tritium*, Journal of Research of the National Institute of Standards and Technology, Volume 105, Number 4, 541, (2000). DOI: 10.6028/jres.105.043

[10] S. Kaufman and W. F. Libby, *The Natural Distribution of Tritium*, Physical Review, Volume 93, Issue 6, 1337, (1994). DOI: 10.1103/PhysRev.93.1337

[11] G. L. Jackson, V. S. Chan and R. D. Stambaugh: *An Analytic Expression for the Tritium Burnup Fraction in Burning-Plasma Devices.* Fusion Science and Technology, Volume 64, Issue 1, 8, (2013). DOI: 10.13182/FST13-A17042

[12] B. Plöckl, P.T. Lang, G. Sellmair, J.K. Stober, W. Treutterer and I. Vinyar: The enhanced high speed inboard pellet fuelling system at ASDEX Upgrade. Fusion Engineering and Design, Volume 88, Issues 6–8, 1059, (2013). DOI: 10.1016/j.fusengdes.2012.12.025

[13] D. J. Wilson, L. R. Baylor, P. Bennett, D. Ciric, R. Eagle, I. Hayward, A. Geraud, T. T. C. Jones, P. T. Lang, A. Lorenz, J.-L. Marechal, R. Mooney, K. Nicholls, J. Ongena, W. Spensley, A. Thomas and M. J. Watson: *Recent developments in pellet fuelling at JET*. 20th IEEE/NPSS Symposium on Fusion Engineering, San Diego, CA, USA, 2003, pp. 86-91, DOI: 10.1109/FUSION.2003.1426594

[14] L. R. Baylor, T. C. Jernigan, S. K. Combs, W. A. Houlberg, M. Murakami, P. Gohil, K. H. Burrell, C. M. Greenfield, R. J. Groebner, C.-L. Hsieh, R. J. La Haye, P. B. Parks, G. M. Staebler, The DIII-D Team, G. L. Schmidt, D. R. Ernst, E. J. Synakowski and M. Porkolab: *Improved core fueling with high field side pellet injection in the DIII-D tokamak.* Physics of Plasmas Volume 7, Issue 5, 1878, (2000). DOI: 10.1063/1.874011

[15] L.R Baylor, T.C Jernigan, C.J Lasnier, R Maingi and M.A Mahdavi: *Fueling efficiency of pellet injection on DIII-D.* Journal of Nuclear Materials, Volumes 266–269, 457, (1999). DOI: 10.1016/S0022-3115(98)00585-6

[16] A. Geraud, B. Pegourie,and IPADBASE Collaboration: *Analysis of pellet fuelling efficiency from the international pellet ablation database.* 23. European physical society conference on controlled fusion and plasma physics, Kyiv (Ukraine), 24-28 June 1996, INIS-UA-043.

[17] U. Fischer, L.V. Boccaccini, F. Cismondi, M. Coleman, C. Day, Y. Hörstensmeyer, F. Moro and P. Pereslavtsev: *Required, achievable and target TBR for the European DEMO*. Fusion Engineering and Design, Volume 155, 111553, (2020). DOI: 10.1016/j.fusengdes.2020.111553

[18] German Federal Office of Justice: *Notfall-Dosiswerte-Verordnung vom 29. November 2018* (BGBl. I S. 2034, 2172; 2021 I S. 5261) (2018). Available at: https://www.gesetze-im-internet.de/ndwv/BJNR217200018.html (last accessed 10.05.2023).

[19] Chr. Day, K. Battes, B. Butler, S. Davies, L. Farina, A. Frattolillo, R. George, T. Giegerich, S. Hanke, T. Härtl, Y. Igitkhanov, T. Jackson, N. Jayasekera, Y. Kathage, P.T. Lang, R. Lawless, X. Luo, C. Neugebauer, B. Ploeckl, A. Santucci, J. Schwenzer, T. Teichmann, T. Tijssen, S. Tosti, S. Varoutis and A. Vazquez Cortes: *The pre-concept design of the DEMO tritium, matter injection and vacuum systems*. Fusion Engineering and Design, Volume 179, 113139, (2022). DOI: 10.1016/j.fusengdes.2022.113139

[20] A.C. Bell, C.A. Gentile, R.L.K. Lässer and J.P. Coad: Tritium inventory control—the experience with DT tokamaks and its relevance for future machines. Fusion Engineering and Design, Volumes 66–68, 91, (2003). DOI: 10.1016/S0920-3796(03)00137-6

[21] J. R. Bartlit: *The tritium systems test assembly at Los Alamos National Laboratory*. Fusion Engineering and Design, Volume 12, Issue 3, 393, (1990). DOI: 10.1016/0920-3796(90)90012-U

[22] F. Priester, D. Hillesheimer, A. Marsteller, M. Röllig and Michael Sturm: *Tritium Processing Systems and First Tritium Operation of the KATRIN Experiment*, Fusion Science and Technology, Volume 76, Issue 4, 600, (2020). DOI: 10.1080/15361055.2020.1730118

[23] R. Lässer, A.C Bell, N. Bainbridge, P.D. Brennan, B. Grieveson, J.L. Hemmerich, G. Jones, D. Kennedy, S. Knipe, J. Lupo, J. Mart, A. Perevezentsev, N. Skinner, R. Stagg, J. Yorkshades, G.V. Atkins, L. Dörr, N. Green, M. Stead and K Wilson: *Overview of the performance of the JET Active Gas Handling System during and after DTE1*. Fusion Engineering and Design, Volume 47, Issues 2–3, 173, (1999). DOI: 10.1016/S0920-3796(99)00082-4

[24] M. Glugla, D.K. Murdoch, A. Antipenkov, S. Beloglazov, I. Cristescu, I.-R. Cristescu, C. Day, R. Laesser and A. Mack: *ITER fuel cycle R&D: Consequences for the design*. Fusion Engineering and Design, Volume 81, Issues 1–7, Pages 733-744, (2006). DOI: 10.1016/j.fusengdes.2005.07.038

[25] S. Maruyama, Y. Yang, R.A. Pitts, M. Sugihara, S. Putvinski, B. Li, W. Li, L.R. Baylor, S.J. Meitner, C. Day, B. LaBombard and M. & Reinke: *ITER Fuelling System Design and Challenges - Gas and Pellet Injection and Disruption Mitigation*. 23. Fusion Energy Conference, Daejeon, Korea, 11-16 Oct 2010, ITR/P1-28.

[26] C. Day and T. Giegerich, *The Direct Internal Recycling concept to simplify the fuel cycle of a fusion power plant*. Fusion Engineering and Design, Volume 88, Issues 6–8, Pages 616-620, (2013). DOI: 10.1016/j.fusengdes.2013.05.026

[27] M. Siccinio, J.P. Graves, R. Kembleton, H. Lux, F. Maviglia, A.W. Morris, J. Morris and H. Zohm. *Development of the plasma scenario for EU-DEMO: Status and plans*, Fusion Engineering and Design, Volume 176, 113047, (2022). DOI: 10.1016/j.fusengdes.2022.113047

[28] L. Barucca, W. Hering, S. Perez Martin, E. Bubelis, A. Del Nevo, M. Di Prinzio, M. Caramello, A. D'Alessandro, A Tarallo, E. Vallone, I. Moscato, A. Quartararo, S D'amico, F. Giannetti, P. Lorusso, V. Narcisi, C. Ciurluini, M.J. Montes Pita, C. Sánchez, A. Rovira, D. Santana, P. Gonzales, R. Barbero, M. Zaupa, M. Szogradi, S. Normann, M. Vaananen, J. Ylatalo, M. Lewandowska, L. Malinowski, E. Martelli, A. Froio, P. Arena and A. Tincani: *Maturation of critical technologies for the DEMO balance of plant systems*. Fusion Engineering and Design, Volume 179, 113096, (2022). DOI: .1016/j.fusengdes.2022.113096

[29] M. Siccinio, W. Biel, E. Fable, T. Franke, F. Janky, P.T. Lang, M. Mattei, F. Maviglia, F. Palermo, O. Sauter, M.Q. Tran, S. Van Mulders and H. Zohm: *Impact of the plasma operation on the technical requirements in EU-DEMO*, Fusion Engineering and Design, Volume 179, 113123, (2022). DOI; 10.1016/j.fusengdes.2022.113123

[30] A. Del Nevo, P. Arena, G. Caruso, P. Chiovaro, P.A. Di Maio, M. Eboli, F. Edemetti, N. Forgione, R. Forte, A. Froio, F. Giannetti, G. Di Gironimo, K. Jiang, S. Liu, F. Moro, R. Mozzillo, L. Savoldi, A. Tarallo, M. Tarantino, A. Tassone, M. Utili, R. Villari, R. Zanino and E. Martelli: *Recent progress in developing a feasible and integrated conceptual design of the WCLL BB in EUROfusion project*. Fusion Engineering and Design, Volume 146, Part B, 1805, (2019). DOI: 10.1016/j.fusengdes.2019.03.040

[31] F. A. Hernández, P. Pereslavtsev, G. Zhou, Q. Kang, S. D'Amico, H. Neuberger, L. V. Boccaccini, B. Kiss, G. Nádasi, L. Maqueda, I. Cristescu, I. Moscato, I. Ricapito and F. Cismondi: *Consolidated design of the HCPB Breeding Blanket for the pre-Conceptual Design Phase of the EU DEMO and harmonization with the ITER HCPB TBM program*. Fusion Engineering and Design, Volume 157, 111614, (2020), DOI: 10.1016/j.fusengdes.2020.111614

[32] G. Federici, L. Boccaccini, F. Cismondi, M. Gasparotto, Y. Poitevin and I. Ricapito: *An overview of the EU breeding blanket design strategy as an integral part of the DEMO design effort.* Fusion Engineering and Design, Volume 141, 30, (2019). DOI: 10.1016/j.fusengdes.2019.01.141

[33] L.V. Boccaccini, F. Arbeiter, P. Arena, J. Aubert, L. Bühler, I. Cristescu, A. Del Nevo, M. Eboli, L. Forest, C. Harrington, F. Hernandez, R. Knitter, H. Neuberger, D. Rapisarda, P. Sardain, G.A. Spagnuolo, M. Utili, L. Vala, A. Venturini, P. Vladimirov and G. Zhou: *Status of maturation of critical technologies and systems design: Breeding blanket*, Fusion Engineering and Design, Volume 179, 113116, (2022). DOI: 10.1016/j.fusengdes.2022.113116

[34] I. Cristescu and M. Draghia: *Developments on the tritium extraction and recovery system for HCPB*, Fusion Engineering and Design, Volume 158, 111558, (2020). DOI: 10.1016/j.fusengdes.2020.111558

[35] G.A. Spagnuolo, R. Arredondo, L.V. Boccaccini, P. Chiovaro, S. Ciattaglia, F. Cismondi, M. Coleman, I. Cristescu, S. D'Amico, C. Day, A. Del Nevo, P.A. Di Maio, M. D'Onorio, G. Federici, F. Franza, A. Froio, C. Gliss, F.A. Hernández, A. Li Puma, C. Moreno, I. Moscato, P. Pereslavtsev, M.T. Porfiri, D. Rapisarda, M. Rieth, A. Santucci, J.C. Schwenzer, R. Stieglitz, S. Tosti, F.R. Urgorri, M. Utili and E. Vallone: *Integrated design of breeding blanket and ancillary systems related to the use of helium or water as a coolant and impact on the overall plant design*, Fusion Engineering and Design, Volume 173, 112933, (2021). DOI: 10.1016/j.fusengdes.2021.112933

[36] F. Vasut, M. Zamfirache, A. Bornea, C. Pearsica and N. Bidica: *Experimental study about hydrogen isotopes storage on titanium bed*. Fusion Engineering and Design, Volume 69, Issues 1–4, Pages 87-90, (2003) DOI: 10.1016/S0920-3796(03)00256-4

[37] V. Narcisi, A. Quartararo, I. Moscato and A. Santucci: *Analysis of Coolant Purification Strategies for Tritium Control in DEMO Water Primary Coolant*. Energies, Volume 16, Issue 2, 617, (2023). DOI: 10.3390/en16020617

[38] G. Caruso, S. Ciattaglia, B. Colling, L. Di Pace, D.N. Dongiovanni, M. D'Onorio, M. Garcia, X.Z. Jin, J. Johnston, D. Leichtle, T. Pinna, M.T. Porfiri, W. Raskob, N. Taylor, N. Terranova and R. Vale: *DEMO – The main achievements of the Pre – Concept phase of the safety and environmental work package and the development of the GSSR*. Fusion Engineering and Design, Volume 176, 113025, (2022). DOI: 10.1016/j.fusengdes.2022.113025

[39] T. Haertl, C. Day, T. Giegerich, S. Hanke, V. Hauer, Y. Kathage, J. Lilburne, W. Morris and S. Tosti: *Design and feasibility of a pumping concept based on tritium direct recycling*. Fusion Engineering and Design, Volume 174, 112969, (2022). DOI: 10.1016/j.fusengdes.2021.112969

[40] S. Hanke, C. Day, T. Giegerich, J. Igitkhanov, Y. Kathage, X. Luo, S. Varoutis, A. V. Cortes, T. Härtl, A. Busniuk, A. Livshits, S. Merli, A. Schulz, M. Walker, K. Baumgärtner and J. Hofmann: *Progress of the R&D programme to develop a metal foil pump for DEMO*. Fusion Engineering and Design, Volume 161, 111890, (2020) DOI: 10.1016/j.fusengdes.2020.111890

[41] T. Giegerich, N. Bekris, P. Camp, Chr. Day, M. Gethins, S. Lesnoy, X. Luo, R. Müller, S. Ochoa, P. Pfeil, R. Smith, H. Strobel and H. Stump: *Advanced design of the Mechanical Tritium Pumping System for JET DTE2*, Fusion Engineering and Design, Volumes 109–111, Part A, 359, (2016). DOI: 10.1016/j.fusengdes.2016.02.098

[42] T. Giegerich and C. Day: *The KALPUREX-process – A new vacuum pumping process for exhaust gases in fusion power plants*, Fusion Engineering and Design, Volume 89, Issues 7–8, 1476, (2014). DOI: 10.1016/j.fusengdes.2014.03.082

[43] Y. Hörstensmeyer: *Holistic fuel cycle modelling of a future fusion reactor*. Doctoral Thesis, Karlsruhe Institute of Technology, Faculty of Mechanical Engineering, KIT Open, (2022). DOI: 10.5445/IR/1000148749

[44] R. Penzhorn, U. Berndt, E. Kirste and J. Chabot: *Performance Tests of Palladium/Silver Permeators with Tritium at the Tritium Laboratory Karlsruhe*, Fusion Technology, Volume 32, Issue 2, Pages 232-245, (1997). DOI: 10.13182/FST97-A19893

[45] A. Santucci, L. Farina, S. Tosti and A. Frattolillo: *Novel Non-Evaporable Getter Materials and Their Possible Use in Fusion Application for Tritium Recovery*. Molecules, Volume 25, 5675, (2020). DOI: 10.3390/molecules25235675

[46] C. Neugebauer, Y. Hörstensmeyer and C. Day: *Technology Development for Isotope Rebalancing and Protium Removal in the EU-DEMO Fuel Cycle*, Fusion Science and Technology, Volume 76, Issue 3, Pages 215-220, (2020). DOI: 10.1080/15361055.2019.1704139

[47] A. N. Perevezentsev, A. C. Bell, B. M. Andreev, M. B. Rozenkevich, Yu. S. Pak and A. V. Ovcharov: *Wet Scrubber Column for Air Detritiation*. Fusion Science and Technology, Volume 56, Issue 4, 1455, (2009). DOI: 10.13182/FST56-1455

[48] M. Rabbani, A. Busigin, H. Mao, N. Halsey and D. La Barbera: *Comparison of AWD to CECE for ITER-Scale Water Detritiation*, Fusion Science and Technology, Selected Papers from the 13th International Conference on Tritium Science and Technology, (2023). DOI: 10.1080/15361055.2023.2232227

[49] D. R. Stull: *Vapor Pressure of Pure Substances. Organic and Inorganic Compounds.* Industrial & Engineering Chemistry Research, Volume 39, Issue 4, 517, (1947). DOI: 10.1021/ie50448a022

[50] Aspen Technology Inc: *Aspen Plus*® [Online], 2023, Available at: https://www.aspentech.com/en/products/engineering/aspen-plus (last accessed 06.11.2023).

[51] Aspen Technology Inc: *Aspen HYSYS*®. [Online], 2023, Available at: https://www.aspentech.com/en/products/engineering/aspen-hysys (last accessed 06.11.2023).

[52] Siemens AG: *gPROMS - Digital Process Design and Operations.* [Online], 2023, Available at: https://www.siemens.com/global/en/products/automation/industry-software/gproms-digital-process-design-and-operations.html (last accessed 06.11.2023).

[53] DWSIM: *DWSIM – The Open Source Chemical Process Simulator*. [Online], 2023, Available at: https://dwsim.org/index.php/about/ (last accessed 06.11.2023).

[54] A. Busigin, S.K. Sood and O.K. Kveton: *Dynamic Simulation of the ITER Fuel Cycle.* Fusion Technology, Volume 21, Issue 2P2, 915, (1992), DOI: 10.13182/FST92-A29867

[55] A. Busigin and P. Gierszewski: *CFTSIM-ITER dynamic fuel cycle model.* Fusion Engineering and Design, Volumes 39–40, 909, (1998). DOI: 10.1016/S0920-3796(98)00222-1

[56] I.-R. Cristescu, L. Dörr, A. Busigin and D. Murdoch: *ITER Dynamic Tritium Inventory Modeling Code.* Fusion Science and Technology, Volume 48, Issue 1, 343, (2005). DOI: 10.13182/FST05-A939

[57] C. Tesch, R. Carlson, R. Michelotti, M. Rogers and S. Willms: *Tritium Systems Test Assembly (TSTA) Stabilization.* Fusion Science and Technology, Volume 48, Issue 1, 258, (2005). DOI: 10.13182/FST05-A923

[58] P.J. Linstrom and W.G. Mallard (Editors): *NIST Chemistry WebBook, NIST Standard Reference Database Number 69.* National Institute of Standards and Technology, Gaithersburg MD, 20899, DOI: 10.18434/T4D303

[59] E. W. Lemmon, I.H. Bell, M.L. Huber and M.O. McLinden: *NIST Standard Reference Database 23: Reference Fluid Thermodynamic and Transport Properties-REFPROP, Version 10.0*. National Institute of Standards and Technology, Standard Reference Data Program, Gaithersburg, (2018). DOI: 10.18434/T4/1502528

[60] J. D. Cox, D. D. Wagman and V.A. Medvedev: *CODATA Key Values for Thermodynamics*. Hemisphere Publishing Corp., New York, ISBN: 0891167587, 284 pages, (1989).

[61] DDBST GmbH: *Dortmund Data Bank.* [Online], 2023, Available at: www.ddbst.com. (last accessed 10.05.2023).

[62] Y.Y. Milenko, R.M. Sibileva, and M.A. Strzhemechny: *Natural ortho-para conversion rate in liquid and gaseous hydrogen*. Journal of Low Temperature Physics, Volume 107, 77, (1997). DOI: 10.1007/BF02396837

[63] P.C Souers: *Cryogenic hydrogen data pertinent to magnetic fusion energy*. Lawrence Livermore National Laboratory Report UCRL-52628, United States. (1979). DOI: 10.2172/6205719

[64] W. A. Van Hook: Vapor pressures of the isotopic waters and ices. The Journal of Physical Chemistry, Volume 72, Issue 4, 1234, (1968). DOI: 10.1021/j100850a028.

[65] E. R. Grilly: The Vapor Pressures of Hydrogen, Deuterium and Tritium up to Three Atmospheres. Journal of the American Chemical Society, Volume 73, Issue 2, 843, (1951). DOI: 10.1021/ja01146a103

[66] P. C. Souers*: Hydrogen Properties for Fusion Energy.* University of California Press (1986). DOI: 10.1525/9780520338401

[67] A. E. Sherwood: *Vapor pressure of HD, HT, and DT.* Fluid Phase Equilibria, Volume 51, 327, (1989). DOI: 10.1016/0378-3812(89)80374-7

[68] B.J. Peters: *Development of a Hydrogen-Selective Vacuum Pump on the Basis of Superpermeation.* Doctoral Thesis, Karlsruhe Institute of Technology, Faculty of Mechanical Engineering, KIT Open, (2020). DOI: 10.5445/IR/1000122305

[69] H.C. Urey: *The thermodynamic properties of isotopic substances.* Journal of the Chemical Society, Issue 0, 562 (1947). DOI: 10.1039/JR9470000562

[70] A. E. Sherwood and P. C. Souers: *Thermodynamics of Liquid Hydrogen Solutions.* Nuclear Technology - Fusion, Volume 5 Issue 3, 350, (1984). DOI: 10.13182/FST84-A23110

[71] J. B. Hunter: *Silver-palladium film for separation and purification of hydrogen*. U.S. Patent US505563A, Washington D.C., United States Patent Office. (1956).

[72] R.-D. Penzhorn, U. Berndt, E. Kirste and J. Chabot: *Performance Tests of Palladium/Silver Permeators with Tritium at the Tritium Laboratory Karlsruhe*, Fusion Technology, Volume 32 Issue 2, 232, (1997). DOI: 10.13182/FST97-A19893

[73] H. Yoshida, S. Konishi and Y. Naruse: *Preliminary Design of a Fusion Reactor Fuel Cleanup System By The Palladium-Alloy Membrane Method*, Nuclear Technology - Fusion, Volume 3, issue 3, 471, (1983). DOI: 10.13182/FST83-A20869

[74] M. Glugla, I. R. Cristescu, I. Cristescu and D. Demange: *Hydrogen isotope separation by permeation through palladium membranes*. Journal of Nuclear Materials, Volume 355, Issues 1–3, 47, (2006). DOI: 10.1016/j.jnucmat.2006.04.003

[75] E. Serra, M. Kemali, A. Perujo, and D. K. Ross: *Hydrogen and deuterium in Pd-25 pct Ag alloy: Permeation, diffusion, solubilization, and surface reaction*. Metallurgical and Materials Transactions A, Volume 29, 1023, (1998). DOI: 10.1007/s11661-998-1011-3

[76] H. Fujita, S. Okada, K. Fujita, H. Sakamoto, K. Higashi and T. Hyodo: *Ratio of Permeabilities of Tritium to Protium through Palladium-Alloy Membrane*, Journal of Nuclear Science and Technology, Volume 17, Issue 6, 436, (1980). DOI: 10.1080/18811248.1980.9732607

[77] D. Ducret, A. Ballanger, J. Steimetz, C. Laquerbe, O. Baudouin and P. Sere Peyrigain: *Hydrogen isotopes separation by thermal cycling absorption process.* Fusion Engineering and Design, Volumes 58–59, 417, (2001). DOI: 10.1016/S0920-3796(01)00475-6

[78] J. Zhou, X. Zhang, S. Hao and W. Huang: *Dynamic simulation of Thermal Cycling Absorption Process with twin columns for hydrogen isotopes separation*. International Journal of Hydrogen Energy, Volume 39, Issue 25, 13873, (2014). DOI: 10.1016/j.ijhydene.2014.04.025

[79] J. Kozeny: *Ueber kapillare Leitung des Wassers im Boden.* Sitzungsberichte der Kaiserlichen Akademie der Wissenschaften., Band 136(2a), Seiten 271-306, (1927).

[80] A. Busigin: *Rigorous Tritium Wet Scrubber Column Modeling and Design*, Fusion Science and Technology, Volume 76, Issue 3, 252, (2020). DOI: 10.1080/15361055.2019.1705747

[81] A.N. Perevezentsev, B.M. Andreev, M.B. Rozenkevich, Yu.S. Pak, A.V. Ovcharov and S.A. Marunich: *Wet scrubber technology for tritium confinement at ITER*. Fusion Engineering and Design, Volume 85, Issues 7–9, 1206, (2010). DOI: 10.1016/j.fusengdes.2010.03.005

[82] D. A. Spagnolo and A. I. Miller: *The CECE Alternative for Upgrading/Detritiation in Heavy Water Nuclear Reactors and for Tritium Recovery in Fusion Reactors*, Fusion Technology, Volume 28, Issue 3P1, 748, (1995). DOI: 10.13182/FST95-A30494

[83] A. V. Ovcharov, M. B. Rozenkevich and A. N. Perevezentsev: *Simulation of CECE Facility for Water Detritiation*, Fusion Science and Technology, Volume 56, Issue 4, 1462, (2009). DOI: 10.13182/FST56-1462

[84] A. Busigin: *Rigorous Two-Fluid and Three-Fluid Liquid Phase Catalytic Exchange Models and Their Application*, Fusion Science and Technology, Volume 71, Issue 3, 438, (2017). DOI: 10.1080/15361055.2017.1293411

[85] A. Busigin: *Mass Transfer Model Liquid Phase Catalytic Exchange Column Simulation Applicable to any Column Composition Profile*, Fusion Science and Technology, Volume 67, Issue 2, 286, (2015). DOI: 10.13182/FST14-T12

[86] A. M. Bornea, M. Zamfirache, G. Ana, L. Stefan, O. Balteanu and C. Bucur: *The Study of CECE Process for Low-Tritiated Liquid Waste Prior to Experimental Phase*, Fusion Science and Technology, Volume 76, Issue 4, 384, (2020), DOI: 10.1080/15361055.2020.1712991

[87] A. M. Bornea, M. Zamfirache and I. Stefanescu: *Theoretical Analysis for Setting Up a Catalyst-Packing Mixture that Equips a Catalytic Isotopic Exchange Column*, Fusion Science and Technology, Volume 71, Issue 4, 532, (2017). DOI: 10.1080/15361055.2017.1290973

[88] M. R. Fenske: *Fractionation of straight-run Pennsylvania gasoline.* Industrial & Engineering Chemistry, Volume 24, Issue 5, 482, (1932)

[89] W.L. McCabe and E.W. Thiele. *Graphical Design Of Fractionating Columns.* Industrial and Engineering Chemistry, Volume 17, Issue 6, 605, (1925). DOI: 10.1021/ie50186a023

[90] A. Busigin and S. K. Sood: *FLOSHEET--A Computer Program for Simulating Hydrogen Isotope Separation Systems.* Fusion Technology, Volume 14, 529, (1988). DOI: 10.13182/FST88-A25187

[91] A. Busigin and S.K. Sood: *Steady State and Dynamic Simulation of the ITER Hydrogen Isotope Separation System*. Fusion Technology, Volume 28, Issue 3P1, 544, (1995). DOI: 10.13182/FST95-A30459

[92] W. L. Pillinger, J. J. Hentges, and J. A. Blair: *Tritium Decay Energy.* Physical Review, Volume 121, 232, (1961). DOI: 10.1103/PhysRev.121.232

[93] L. P. Roy: *Influence of Temperature on the Electrolytic Separation Factor of hydrogen Isotopes.* Canadian Journal of Chemistry. Volume 40, Issue 7, 1452, (2011). DOI: 10.1139/v62-219

[94] I. S. Duff and J. K. Reid: *The design of MA48: a code for the direct solution of sparse unsymmetric linear systems of equations*. ACM Transactions on Mathematical Software, Volume 22, Issue 2, 187 (1996). DOI: 10.1145/229473.229476

[95] B. Bornschein, M. Glugla, K. Günther, R. Lässer, T.L. Le, K.H. Simon and S. Welte: *Tritium tests with a technical PERMCAT for final clean-up of ITER exhaust gases*, Fusion Engineering and Design, Volume 69, Issues 1–4, 51, (2003). DOI: 10.1016/S0920-3796(03)00234-5

[96] K. Battes, C. Day and V. Rohde: *Basic considerations on the pump-down time in the dwell phase of a pulsed fusion DEMO*. Fusion Engineering and Design, Volume 100, 431, (2015). DOI: 10.1016/j.fusengdes.2015.07.011

[97] K. Battes, C. Day and V. Hauer: *Outgassing rate measurements of stainless steel and polymers using the difference method*. Journal of Vacuum Science & Technology A, Volume 33, Issue 2, 021603, 2015. DOI: 10.1116/1.4905099

[98] L.M. Giancarli, M. Abdou, D.J. Campbell, V.A. Chuyanov, M.Y. Ahn, M. Enoeda, C. Pan, Y. Poitevin, E. Rajendra Kumar, I. Ricapito, Y. Strebkov, S. Suzuki, P.C. Wong and M. Zmitko: *Overview of the ITER TBM Program*, Fusion Engineering and Design, Volume 87, Issues 5–6, 395, (2012), DOI: 10.1016/j.fusengdes.2011.11.005

[99] S. E. Ferry, K. B. Woller, E. E. Peterson, C. Sorensen and D. G. Whyte: *The LIBRA Experiment: Investigating Robust Tritium Accountancy in Molten FLiBe Exposed to a D-T Fusion Neutron Spectrum*, Fusion Science and Technology, Volume 79, Issue 1, 13, (2023). DOI: 10.1080/15361055.2022.2078136

[100] R. Lässer, P. Meuffels and R. Feenstra: *Datenbank der Löslichkeit der Waserstoffisotope Protium (H), Deuterium (D) und Tritium (T) in den Metallen V, Nb, Ta, Pd und den Legierungen V1-x Nbx, V1-xTax, Nb1-x Mox, Pd1-xAgx*. Report Jül-2183 (in German), Kernforschungsanlage Jülich GmbH, Jülich, (1988).

[101] F. Siviero, L. Caruso, T. Porcelli, M. Mura, E. Maccallini, P. Manini, E. Sartori, M. Siragusa, C. Day and P. Sonato: *Characterization of ZAO® sintered getter material for use in fusion applications.* Fusion Engineering and Design, Volume 146, Part B, 1729, (2019). DOI: 10.1016/j.fusengdes.2019.03.026

[102] A. D. Shugard, C. R. Tewell, D. F. Cowgill and R. D. Kolasinski: *Uranium for hydrogen storage applications: a materials science perspective*. Sandia National Laboratories Report SAND2010-5195, (2010). DOI: 10.2172/993617

[103] R. Lässer, K.-H. Klatt, P. Mecking, H. Wenzl: *Eigenschaften von Tritium in Vanadium, Niob, Tantal und Palladium.* Report JüI-1800 (in German), Kernforschungsanlage Jülich GmbH, Jülich, (1982).

9 Appendix

A) Reference Case Configuration

The fuel cycle simulator is set-up to establish parity between a given fuel cycle design and its representation in the simulator. For this purpose each technology model can be configured by a set of parameters representing its dimensioning and performance. They are derived for each model in section 4.3 and Table A.1 summarizes all design parameter values used in the evaluation of the reference case of the EU-DEMO fuel cycle.

Table A.1: List of all parameters and their reference values employed in the simulation of the EU-DEMO fuel cycle.

Gas Distribution	Value	Unit
Buffer vessel p_{low}	700	mbar
Buffer vessel p_{high}	1500	mbar
Buffer vessel volume	1.0	m^3
Buffer vessel make-up flowrate	0.05	$mol.s^{-1}$
Buffer vessel discharge flowrate	0.1	$mol.s^{-1}$
System operation temperature	300	K
Fuel mixture D/T ratio set-point	1.0	-
Fuel mixer 1 PEG content (Xe)	$4.5 \cdot 10^{-4}$	-
Fuel mixer 2 PEG content (Ar)	0.009	-
Fueling and Torus		
Pellet injection system inlet manifold volume	0.1	m^3
Pellet injection system inlet manifold pressure	600	mbar
Pellet injection system inlet manifold temperature	300	K
Liquefier volume	2.0	liter
Extruder volume	2.0	liter
Recoverable pellet loss fraction	20%	$mol.s^{-1}$
Torus total volume	6000	m^3
Torus gas temperature in divertor	573	K
Torus fuel implantation rate (during burn)	1e-4	$mol.s^{-1}$
Torus total outgassing rate	1e-4	$mol.s^{-1}$
Torus outgassing composition	1.0% H2	-
	99% DT	-
Fuel Separation and Torus Vacuum		
Metal foil pump Q_2 separation efficiency (for all Q_2)	0.8	-
Metal foil pump lower operation pressure	1	Pa
Ring line volume (DIRL)	52.5	m^3
Ring line lower pressure (DIRL)	100	Pa
Ring line volume (INTL)	21.4	m^3
LDP pump stage effective pumping speed	31.14	$m^3.s^{-1}$
Transfer line volume (DIRL)	5.4	m^3
Transfer line volume (INTL)	2.3	m^3
LRP stage 1-3 effective pumping speed (DIRL)	1.197	$m^3.s^{-1}$
LRP stage 4-6 effective pumping speed (DIRL)	0.532	$m^3.s^{-1}$
LRP stage 1-3 effective pumping speed (INTL)	0.532	$m^3.s^{-1}$
LRP stage 4-6 effective pumping speed (INTL)	0.266	$m^3.s^{-1}$
Exhaust Processing		
Inlet manifold volume	0.005	m^3

Inlet manifold lower pressure threshold	2.0	bar	
Inlet manifold temperature	300	K	
Permeator tube diameter	0.01	m	
Permeator tube length	0.5	m	
Permeator operating temperature	723.15	K	
Permeator stage 1 number of tubes	40	-	
Permeator stage 2 number of tubes	6	-	
Permeator stage 1 bleed flowrate	0.00105	$mol.s^{-1}$	
Permeator stage 2 pressure set-point	2.0	bar	
Total converter volume	0.01	m^3	
Reactor impurity conversion efficiency	100%	%	
Total permeate volume	1.0	m^3	
Permeate vacuum system pumping speed	0.21	m^3s^{-1}	
Gas detritiation system hydrogen recovery efficiency	90%	%	
PEG separation system PEG recovery efficiency	90%	%	
Isotope Rebalancing	Col. 1	Col. 2	
Column length	2.0	2.0	m
Column diameter	0.1	0.1	m
Number of parallel columns	100	100	
Packing porosity	0.8	0.8	-
Particle diameter	0.0012	0.0012	m
Active material amount	2.1	2.1	mol
Hot temperature	350	280	K
Cold temperature	273	230	K
Heat transfer coefficient	50	50	$W.m^{-2}s^{-1}$
Feed flowrate	$2.81 \cdot 10^{-3}$	0	$mol.s^{-1}$
Extraction flowrate	$2.39 \cdot 10^{-3}$	$4.23 \cdot 10^{-4}$	$mol.s^{-1}$
Exhaust Detritiation			
Inlet manifold volume	10	m^3	
Inlet manifold temperature	300	K	
Inlet manifold pressure	1.01	bar	
Condenser one liquid hold-up	100	mol	
Condenser one temperature	275	K	
Condenser one operating pressure	1.01	bar	
Recombiner conversion efficiency	100%	%	
Saturator liquid hold-up	100	mol	
Saturator temperature	320	K	
Saturator operating pressure	1.01	bar	
WSC number of stages	80	-	
WSC operating temperature	320	K	
WSC operating pressure	1.01	bar	
WSC liquid hold-up per stage	76	mol	
WSC vapor to liquid ratio	1.0	-	
Condenser two liquid hold-up	100	mol	
Condenser two temperature	300	K	
Condenser two operating pressure	1.0	bar	
Water Detritiation			
Electrolyzer operating temperature	343	K	
Electrolyzer liquid hold-up	6490	mol	
LPCE & saturators operating temperature	320	K	
LPCE & saturators operating pressure	1.2	bar	
LPCE vapor to liquid ratio (top segment)	1.75	-	
LPCE segments cross section area	0.78	m^2	

	Segment			
	1	2	3	
LPCE segment length	30	25	2.0	m
LPCE k_s	50		$mol.s^{-1}m^{-3}$	
LPCE k_d	50		$mol.s^{-1}m^{-3}$	
LPCE relative liquid hold-up	4320		$mol.m^{-1}$	
LPCE relative gas hold-up	29.0		$mol.m^{-1}$	
LPCE relative vapor hold-up	2.84		$mol.m^{-1}$	
Permeator draw-off flowrate	1.085		$mol.s^{-1}$	
Saturators liquid hold-up	550		mol	
Condenser liquid hold-up	553		mol	
Condenser temperature	300		K	
Condenser operating pressure	1.2		bar	
Oxygen detritiation system efficiency	100%		%	

Isotope Separation	Column			
	1	2	3	
Number of equilibrium stages	42	50	35	-
Distillate to feed ratio	0.9895	0.94	0.92	-
Reflux ratio	4.0	4.0	10	-
Feed stage	29	38	24	-
Operating pressure	100000	95000	90000	Pa
Stage liquid hold-up	9.4	2.7	0.33	mol
Reboiler liquid hold-up	112	32.6	3.90	mol
Equilibrator temperature		300		K

B) Property Data Parameter

The employed mass transfer models require a wide range of thermodynamic property and equilibrium data. In order to express these, algebraic formulations are presented in section 4.1 and 4.2. Parameter values for fit parameter of resulting expression are reported in the following Tables B.1 – B.9.

Table B.1: Parameter values in the expressions for the calculation of the isotopic water vapor pressure from [49], [64**].**

Parameter	H_2O	HDO	HTO	D_2O	DTO	T_2O
A	4.6543	26398.8 K²	37813.2 K²	49314.9 K²	59313.4 K²	68702.3 K²
B	1435.264 K	-89.6065 K	-136.751 K	-164.266 K	-204.941 K	-244.687 K
C	-64.848 K	0.075802	0.124096	0.140049	0.182686	0.224388

Table B.2: Parameter in the hydrogen vapor pressure expression of Souers [63].

	H2	HD	HT	D2	DT	T2
C_1 (-)	9.64596	11.5827	12.7295	12.6317	14.2203	15.8148
C_2 (K)	83.5177	109.419	123.995	130.249	147.349	164.486
C_3 (-)	1.98042	1.57756	1.3444	1.38962	1.0495	0.707997

Table B.3: Parameter in the Arrhenius expression for the hydrogen isotopic equilibrium constant. From [68]

Reaction	A (-)	B (K)
$H2 + D2 \rightleftharpoons 2HD$	4.075	19.456
$H2 + T2 \rightleftharpoons 2HT$	4.207	75.316
$D2 + T2 \rightleftharpoons 2DT$	4.518	166.588

Table B.4: Reactions between isotopic water and hydrogen isotopologues as well as the formulation for the associated equilibrium constant. Fitted from [69].

#	Reaction	Equilibrium	R^2
1	$H2O + HD \rightleftharpoons HDO + H2$	$K_1 = \frac{[HDO][H2]}{[H2O][HD]} = 2.763 \cdot 10^{-5}\left(\frac{T}{K}\right)^2 - 3.176 \cdot 10^{-2}\left(\frac{T}{K}\right) + 10.81$	0.993
2	$HDO + D2 \rightleftharpoons D2O + HD$	$K_2 = \frac{[D2O][HD]}{[HDO][D2]} = 1.951 \cdot 10^{-5}\left(\frac{T}{K}\right)^2 - 2.270 \cdot 10^{-2}\left(\frac{T}{K}\right) + 8.139$	0.994
3	$H2O + HT \rightleftharpoons HTO + H2$	$K_3 = \frac{[H2O][HT]}{[HTO][H2]} = 6.686 \cdot 10^{-5}\left(\frac{T}{K}\right)^2 - 7.451 \cdot 10^{-2}\left(\frac{T}{K}\right) + 22.73$	0.989
4	$HTO + T2 \rightleftharpoons T2O + HT$	$K_4 = \frac{[T2O][HT]}{[HTO][T2]} = 4.225 \cdot 10^{-5}\left(\frac{T}{K}\right)^2 - 4.764 \cdot 10^{-2}\left(\frac{T}{K}\right) + 15.24$	0.991
5	$D2O + DT \rightleftharpoons DTO + D2$	$K_5 = \frac{[DTO][D2]}{[D2O][DT]} = 3.779 \cdot 10^{-6}\left(\frac{T}{K}\right)^2 - 4.698 \cdot 10^{-3}\left(\frac{T}{K}\right) + 2.622$	0.998
6	$DTO + T2 \rightleftharpoons T2O + DT$	$K_6 = \frac{[T2O][DT]}{[DTO][T2]} = 4.907 \cdot 10^{-6}\left(\frac{T}{K}\right)^2 - 5.882 \cdot 10^{-2}\left(\frac{T}{K}\right) + 2.978$	0.997

Table B.5: Parameter for the temperature dependent calculation of the second virial coefficient for hydrogen isotopologues. From [70].

	H2	HD	HT	D2	DT	T2
B_0 ($cm^3.mol^{-1}$)	-151	-167	-172	-184	-190	-197
b	1.44	1.52	1.58	1.64	1.70	1.77

Table B.6: Parameter for the calculation of binary interaction parameters for hydrogen isotopologues. From [70].

	H_2	HD	HT	D_2	DT	T_2
κ	1.731	1.471	1.354	1.224	1.111	1.000

Table B.7: Sievert's parameter for the solution of hydrogen isotopes on metals and alloys.

$K_s = a \cdot \exp\left(\frac{b}{RT}\right)$		a ($mol.m^{-3}Pa^{-0.5}$)			b (eV)		
		H	D	T	H	D	T
PdAg	[100]	0.45	0.49	0.58	-0.175	-0.153	-0.134
V	[100]	0.26	0.26	0.24	-0.330	-0.333	-0.349
Nb	[100]	0.27	0.27	0.33	-0.366	-0.403	-0.351
$\log(p) = a + 2\log(c) - \frac{b}{T}$		(log(Pa))			(log(Pa).K)		
ZaO	[101]	9.64	9.71	-	7290	7337	-

Table B.8: Isotherm parameters for metal hydride systems employed in the fuel cycle. From [61][62]. TiMn values for tritium are extrapolated using square root ratio of the atomic weight.

	a ($kJ.mol^{-1}$)			b ($J.mol^{-1}K^{-1}$)		
	H	D	T	H	D	T
U [102]		35.05			92.12	
Pd [103]	39.0	35.3	33.3	92.5	93.4	91.6
TiMn‡	23.16	27.02	29.95	99.93	109.04	115.96

‡ The TiMn alloy has been characterized in cooperation with Fraunhofer-IFAM using thermogravimetric analyis and results are not yet published. They are therefore reprinted in Figure B.1.

Table B.9: Parameter in the calculation of hydrogen permeability in Pd-Ag. The tritium permeability is extrapolated from protium according to the square root mass ratio according to [76].

$Pe = \mathrm{a} \cdot \exp(\frac{\mathrm{b}}{RT})$	a ($\mathrm{mol.m^{-1}s^{-1}Pa^{-0.5}}$)	b ($\mathrm{J.mol^{-1}}$)
H	$5.58 \cdot 10^{-8}$	-6304
D	$3.43 \cdot 10^{-8}$	-6156
T	$Pe_T = \frac{1}{2.1} Pe_H$	

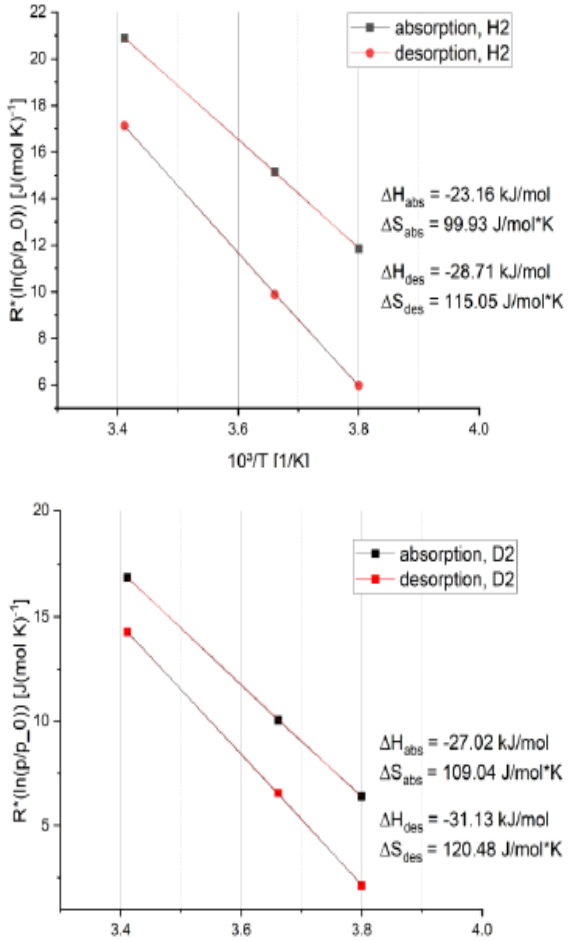

Figure B.1: Van't Hoff plots of protium and deuterium absorption in TiMn alloy as measured by Fraunhofer-IFAM.